ELECTRICAL AND THERMAL BEHAVIOR OF ALUMINA-BASED NANOCOMPOSITES

BY

IBRAHIM MOMOHJIMOH

A Thesis Presented to the
DEANSHIP OF GRADUATE STUDIES

KING FAHD UNIVERSITY OF PETROLEUM & MINERALS

DHAHRAN, SAUDI ARABIA

In Partial Fulfillment of the
Requirements for the Degree of

MASTER OF SCIENCE

In

MATERIAL SCIENCE AND ENGINEERING

MAY 2016

KING FAHD UNIVERSITY OF PETROLEUM & MINERALS

DHAHRAN- 31261, SAUDI ARABIA

DEANSHIP OF GRADUATE STUDIES

This thesis, written by **Ibrahim Momohjimoh** under the direction his thesis advisor and approved by his thesis committee, has been presented and accepted by the Dean of Graduate Studies, in partial fulfillment of the requirements for the degree of **MASTER OF SCIENCE IN MATERIALS SCIENCE & ENGINEERING.**

Dr. Zuhair M. Gasem
Department Chairman

Dr. Nasser M. Al-Aqeeli
(Advisor)

Dr. Salam A. Zummo
Dean of Graduate Studies

Dr. Saheb Nouari
(Member)

9/6/16

Date

Dr. Tahar Laoui
(Member

To my beloved Mother

ACKNOWLEDGMENTS

I would like to thank the Kingdom of Saudi Arabia through the ministry of higher education for providing me scholarship for my MSC study in the prestigious King Fahd University of Petroleum and Minerals, Dhahran, Saudi Arabia.

To my scholarly advisor: **Professor Nasser M. Al-Aqeeli** for his intellectual guidance, mentorship and wisdom from the beginning to the end of this thesis. I really appreciate your words of wisdom and I am grateful to have carry out my thesis research under your tutelage. I could not have imagined having a better advisor and mentor for my MSc study in KFUPM.

To my committee members: **Dr. Saheb Nouari** and **Dr. Tahar Louai** for their criticism to ensure quality and standard both in the experiment and write-up of this thesis. May Allah continues to bless them and their household. I would like to acknowledge and thank the Chairman of Mechanical Engineering Department Dr. Zuhair M. Gasem and the Dean of graduate studies: Professor Salam Zummo.

My sincere appreciation goes to my research team member: Mr. Umer Hayat and Mr. Muhammad Khawaja for their unconditional supports during the experimental work of this thesis. My profound gratitude goes to the KACST project for providing funds for this research through the grant number: AR-34-3.

I really thank the effort of the following people for their contributions: Mr. Latif, Dr. Khaled Mazen, Engr. Abbas, Mr. Haider Ali, Mr. Muhammed Khan, Mr. Azeez, Mr. M.J Adinoyi and all my friends in the Department of Mechanical Engineering, KFUPM. Finally, to my beloved family for their prayers and moral support.

TABLE OF CONTENTS

LIST OF TABLES

LIST OF FIGURES

LIST OF ABBREVIATIONS

CNT	:	Carbon Nanotube
SiC	:	Silicon Carbide
SWCNT	:	Single-walled Carbon Nanotubes
MWCNT	:	Multi-walled Carbon Nanotubes
SPS	:	Spark Plasma Sintering
HIP	:	Hot Isostatic Pressing
HP	:	Hot Pressing
CIP	:	Cold Isostatic Pressing
MW	:	Microwave Sintering
XRF	:	X-ray Fluorescence
XRD	:	X-ray Diffraction
SEM	:	Scanning Electron Microscopy
TEM	:	Transmission Electron Microscopy
FE-SEM	:	Field Emission Scanning Electron Microscopy
DC	:	Direct Current

ABSTRACT

Full Name : IBRAHIM MOMOHJIMOH

Thesis Title : Electrical and thermal behavior of Alumina-based nanocomposites

Major Field : Material Science and Engineering

Date of Degree : May, 2016

Alumina is an interesting ceramic material due to its excellent mechanical high temperature strength, high hardness, high creep resistance, thermal and chemical stability. However, its low fracture toughness, low thermal and electrical conductivities are the major limitations of the utilization of alumina for structural and functional applications. Several efforts have been devoted to the improvement of the fracture toughness of alumina but little work have been done on the effect of addition of second nanophase SiC and carbon nanotubes (CNTs) on its electrical and thermal performance.

In this current work, alumina was reinforced with 5wt% and 10wt%SiC nanoparticles by spark plasma sintering process to produce Alumina-SiC nanocomposites. At the same time alumina was reinforced with 1wt% and 2wt% functionalized multi-walled carbon nanotubes (MWCNTs) which was also consolidated by SPS at the same conditions to produce alumina-MWCNT nanocomposites. Densifications, thermal and electrical properties of the nanocomposites were studied and the relative density of the nanocomposites was found to decrease with the addition of the nanophase to alumina but

increase with SPS temperature. The thermal properties of alumina decreased with the addition of SiC nanoparticles and functionalized MWCNT although, electrical properties of alumina increased tremendously with the inclusion of SiC nanoparticles and MWCNTs. Thermal properties (thermal diffusivity, specific heat capacity and thermal conductivity) at elevated temperature were evaluated in the temperature range (25-250°C) and the value of thermal diffusivity and thermal conductivity decreased with the measuring temperature while that of specific heat capacity increased with the increasing measuring temperature. The microstructure of the nanocomposites confirmed the reduction in the thermal properties of the nanocomposites with the increasing contents of the nanophase.

ملخص الرسالة

الاسم الكامل: **ابراهيم مومهج يموه**

عنوان الرسالة: السلوك الحراري و الكهربائي لـ ركبات الألمونيا النانوية

التخصص: علم و هندسة المواد

تاريخ الدرجة العلمية: **مايو 2016**

الألومينا هي احد مواد السيراميك المثيرة للاهتمام بسبب امتلاكها خواص ميكانيكية متميزة عند درجات حرارة مرتفعة و كذك لديها قوة كبيرة الميكانيكية، صلابة عالية، مقاومة عالية للزحف، واستقرار حراري وكيميائي. ومع ذلك، فإن متانة الكسر المنخفضة و انخفاض الموصلية الحرارية والكهربائية للألومينا، هما من القيود الرئيسية للإستفادة من الألومينا في التطبيقات الهيكلية والوظيفية. تم تكريس العديد الجهود لتحسين متانة كسر الألومينا، لكن قليل من الدراسات عنيت بدراسة تأثير إضافة طور ثانوي بحجم النانو من كربيد السيليكون وأنابيب الكربون النانوية (الأنابيب النانوية الكربونية) علي الأداء الكهربائي والحراري للألومنيا.

في هذا العمل الحالي، تم تعزيز مادة الألومينا بإضافة 5٪ و10٪ نسبة حجم من جزيئات كربيد السيلكون النانوية بواسطة عملية التلبيد عن طريق شرارة البلازما لإنتاج مركب ألومينا– كربيد السيلكون. في نفس الوقت، تم تعزيز مادة الألومينا بإضافة 1٪ و 2٪ نسبة حجم من أنابيب الكربون النانوية الفعالة متعددة الجدران و ايضا تم استخدام شرارة البلازما لتلبيد المركب في نفس الظروف لإنتاج مركب الألومينا- أنابيب الكربون متعددة الجدران النانوي. تم دراسة التكثيف، الخواص الحرارية، و الخواص الكهربائية للمركب النانوي الجديد و قد وجد أن الكثافة النسبية للمركب تقل مع إضافة طور ثانوي الألومينا، ولكن تزيد مع زيادة درجة حرارة عملية التلبيد. و قد تقرر أيضا أن الخواص الحرارية للألومينا تنخفض مع إضافة جزيئات كربيد السيلكون و جزيئات أنابيب الكربون متعددة الجدران

النانوية، على الرغم من أن الخواص الكهربائية تزيد بشكل عالي مع إدراج جسيمات كربيد السيلكون و جزيئات أنابيب الكربون متعددة الجدران النانوية. تم تقييم الخواص الحرارية (الإنتشارية الحرارية، السعة الحرارية النوعية، والموصلية الحرارية) عند درجة حرارة مرتفعة في نطاق درجات الحرارة (25 – 250 درجة مئوية)، و قد تقرر أن قيمة الأنتشارية الحرارية والموصلية الحرارية تنخفض مع قياس درجة الحرارة في حين أن الحرارة النوعية تزيد مع زيادة قياس درجة الحرارة. أكدت البنية المجهرية للمركب الإنخفاض في الخواص الحرارية للمركب مع إزدياد محتوي الطور النانوي.

CHAPTER 1

INTRODUCTION

The processing and fabrication of nanocomposite materials is a developing field refer to as nanotechnology which involves the production of bulk material with crystalline size less than 100nm with superior mechanical and functional properties as compared to microcrystalline or bulk composites[1]. Ceramics generally have high hardness, high stiffness and excellent thermal stability but its inherent brittleness hampers its use in structural applications[2]. Several techniques have been deployed to improve the mechanical properties of Nanocrystalline ceramic by homogenous dispersion of second phase nanoparticles into the ceramics matrix to achieve nanocomposite ceramic material[3].

Alumina is one of the most commonly used ceramics in the industry due to its excellent mechanical hardness, chemically inert and good thermal/electrical insulation properties. Various industrial applications of alumina include dental implants, wear resistant parts and high-speed cutting tools[4,5]. The advanced structural and aerospace space utilization of alumina such as aircraft engine parts, rocket material and high-temperature cutting tools require not only the mechanical properties but appreciable thermal and electrical performance are also necessary. Despites high hardness and compressive strength of alumina, its intrinsic low fracture toughness and low thermal or electrical properties have limited its usage in structural and functional applications. Cracks easily propagate in ceramics and as such unexpected failure usually occur when placed in service and sometimes the failure could happen catastrophically on the application of

small impact load even though the load is lower than the yield strength of ceramic material. It was Niihara in 1991 who first reported that the fracture toughness of alumina could be improved by the addition of nanoparticles of SiC to alumina matrix[6]. Significant improvement in the mechanical strength of 1.05GPa and fracture toughness of 4.7MPam$^{1/2}$ were reported by Niihara. These exceptional mechanical properties of Alumina-SiC nanocomposites according to Niihara was attributed to the reduction in processing flaws and the overall refinement of the microstructure. However, these results reported by Niihara have not been reproduced by other researchers[6].

Continuous improvement in fracture toughness and thermal properties of alumina is vital in the field of high speed cutting tools applications. Specifically speaking, there are certain properties which any ideal cutting tools material should possess so as to perform its functions. These properties include: high hardness, toughness, hot strength and appreciable thermal conductivity. The low fracture toughness and low thermal conductivity of alumina increases its susceptibility of the alumina cutting tools to damage by thermal shock related failure. Several researchers have confirmed that addition of second phase nanoparticles of titanium carbide (TiC), Silicon nitride (Si_3N_4), Titanium boride (TiB), Titanium carbonitride (Ti(C,N)), silicon carbide (SiC) and carbon nanotubes (CNT) to alumina has significant improvement on the fracture toughness as well as its thermal conductivity[7]. Among the nanoparticles and fibers reported; SiC[8] and CNT[2] have proven to be better candidates in improving the thermal conductivity of alumina because of their intrinsic high thermal conductivity. Besides, the addition of SiC and CNT to alumina was found to increase the electrical conductivity of the alumina due to the formation of interconnected continuous conducting networks in the nanocomposite.

SiC addition to Al_2O_3 matrix enhance the fracture toughness as well as its thermal shock resistance[9,10]. Al_2O_3-SiC composites display higher strength and hardness than unreinforced alumina matrix[11]. The significant improvement in strength and fracture toughness of Alumina-SiC composites was attributed to reduction in the processing flaws, change in fracture mode from intergranular to transgranular, crack bridging and crack deflection due to SiC addition. Besides, the thermal coefficient expansion and elastic modulus mismatch between SiC and alumina matrix which result in the generation of dislocations also contributed to the enhancement in the mechanical properties[12,13].

The cutting performance of commercial tools and alumina-SiC composites have been studied by Ko et al[14]. According to Ko et al. alumina containing 10wt%SiC has the best cutting performance for machining heat treated AISI4140, while alumina containing 5wt% SiC composite exhibit the best cutting performance for machining grey cast iron. Thus, tool life of alumina containing 10wt%SiC and 5wt% SiC was 7times and 1.5times longer than that of commercial tools (Al_2O_3-TiC and Al_2O_3-TiB) on machining heat treated AISI and grey cast iron respectively. Again, when the SiC content increase beyond 10wt% in alumina, the cutting performance reduce and Ko et al. concluded that the decrease in cutting performance with increasing SiC content was due to the chemical reaction which occur between SiC and Fe during machining at high speed.

The need for cutting tool material with high mechanical and functional performance has spurred the scientists and researchers to develop and improve on exist known cutting tool materials. addition of nanoparticles of SiC can improve significantly on the mechanical properties of alumina matrix[15,16]. The discovery of carbon nanotube by Iijima in 1991 has created opportunity to improve the mechanical and functional properties of ceramics

materials. The mechanical properties of alumina/SiC and alumina/CNT nanocomposites have been reported in literatures but little has been done in the area of thermal and electrical properties of alumina/SiC and alumina/CNT nanocomposites even though thermal conductivity is essential for maintaining the integrity of alumina in cutting tool application so as to reduce thermal shock related failure. To the best of our knowledge, limited works have been done on the thermal and electrical behavior Al_2O_3/SiC and Al_2O_3/CNT nanocomposites with low percolation threshold of reinforcement phase. For instance, Parchoviansky et al.[17] reported appreciable improvement in thermal conductivity of Al_2O_3/SiC nanocomposite with 20vol% SiC nanoparticles. Also, Borrell et al.[18] reported improvement in electrical conductivity at 17vol% SiC while Kumari et al.[19], revealed significant improvement in thermal properties of CNT/Al_2O_3 nanocomposite with 7.3wt%CNT.

1.1 Problem Definition

Ceramics cutting tools have been identified as the right candidate tools for machining of various metallic materials for about 50 years ago however, there low fracture toughness and low thermal shock resistance have limited their widespread use. Among the prominent mechanical properties, strength and hardness are vital for the machining performance of cutting tools. As the strength of material is increased, larger cutting force is required and this raise the temperature within the cutting zone thereby making the material more difficult to cut. The conventional cutting tools such as high-speed steel (HSS) and carbide tool were considered ideal cutting tool materials[20]. The inability of HSS tool to maintained its mechanical hardness and strength at elevated temperature and

the chemical affinity of carbide tool material for the workpiece have made them unsuitable for the development of cutting tool operating at high speed[21]. Polycrystalline diamond (PCD)[22] polycrystalline cubic boron nitride (PCBN)[23] which are the hardest and the second hardest materials respectively on earth with outstanding high hot hardness and high temperature strength are primarily used for machining hard-to-cut materials. They are capable of operating at high speed without losing their mechanical integrity but their high tooling cost have made them economically inefficient and widespread application. Ceramics tools which are mainly alumina (Al_2O_3) silicon nitride (Si_3N_4) and sialon-based are capable of retaining their hardness at elevated temperature although their low fracture toughness and low thermal conductivity are the current limitations of their wide applications[24]. However, the possibility of adding high thermal conductivity materials to ceramics can significantly improve the fracture toughness and thermal conductivity by careful control of the microstructures and compositions leading to creation of ceramic tools capable of machining various materials at high speed[25].

1.2 Motivation/Objectives

The need to develop cutting tool materials with high mechanical and functional performances with relatively low cost has been goal of manufacturing engineers and scientists. The advent of nanotechnology has provided opportunities to increase the performance of existing devices through the use of nano-size particles. The mechanical performance of nanostructured ceramic materials has been studied over the years but little work has been done on its thermal and electrical behavior even though these properties are vital in some specific applications such as high speed cutting tools. Nanocrystalline

structures contain large grain boundaries and the interaction of the grain boundaries with dislocations could improve the mechanical properties of the material. However, the effect of this large grain boundaries have not been investigated in terms of the functional performance of the material. Again, spark plasma sintering of ceramics nanocomposites have been proved to be effective in the microstructural control of the final product through the formation of fine microstructures. Taken the advantages of the use of nanoparticle addition to ceramics based matrix; SPS consolidation is expected to fabricate a component of better performance. The goal of this research is to study the thermal and electrical properties of Alumina-SiC and alumina-carbon nanotubes nanocomposites. The main objectives of the investigation were to process and fabricate nanocomposites from the starting nanopowders and study the influence of spark plasma sintering on electrical and thermal behavior of the sintered nanocomposites. The main application of the fabricated nanocomposites is in the development of cutting tool for high speed machining.

1.3 Outline

Chapter two provides detailed literature review on the processing of nanocomposites, mechanical properties, thermal and electrical properties of Alumina-SiC and Alumina-CNTs nanocomposites. Chapter three is devoted to the materials and methodology used in carrying out the experimental parts of this work. Results and discussion is presented in chapter four starting from the relative density of the monolithic and nanocomposites down to the microstructural evaluation.

Chapter five deals with the conclusion and recommendations, and that ends the thesis.

CHAPTER 2

LITERATURE REVIEW

Nanocomposite is defined as a type of composite system which consists of a matrix and homogenous disperse phase with at least one dimension less than 100nm[26]. Ceramic matrix nanocomposites (CMNC) are widely used both in academia and industry due to their unique properties offer by the high surface area to volume ratio of their nano-disperse phases. The exceptional properties (mechanical, electrical or thermal properties) of ceramic nanocomposites are highly influenced by the dispersion state and the quality of the interface formed between nanoparticles or nanofibers and the ceramic matrices[7].

Synthesis and fabrication of nanocomposite is still a major challenge facing the development of nanotechnology. As the size of the particles become reduce the surface area of the particles increases and this in turn increases the surface energy of the particles thereby leading to agglomeration[27]. The agglomeration of nanoparticles usually results in inhomogeneous distribution of the reinforcement phase which can significantly affect the performance of the resulting nanocomposites[28]. Several methods such as shear mixing, mechanical alloying/mechanical milling, sonication and in situ polymerization have been device to reduce agglomeration of nanoparticle during powder processing. Combinations of the above techniques are usually employed in the dispersion of nanoparticles in the ceramic matrix to achieve homogenous powder prior to consolidation.

Consolidation of nanocomposites is an important stage in the nanocomposites processing. Conventional consolidation techniques which include hot isostatic

pressing, hot pressing, cold isostatic pressing, have been used over the years for the sintering of nanocomposite powders. These techniques have some limitations such as longer sintering time and higher sintering temperature that leads to grain growth which result in degradation of mechanical properties. Nonconventional consolidation methods such as spark plasma sintering (SPS) which is also known as field assisted sintering (FAST) and microwave sintering are novel sintering techniques that combine the advantages of high heating rate and relatively low sintering temperature. SPS due to its high heating rates, relatively low sintering temperature for shorter time, high densification and lack of pre-compaction has made it an ideal technique for nanopowders consolidation. SPS technique has offered a means of controlling the microstructure of nanocomposites and retains their nanofeatures[29].

2.1 Synthesis and Processing of Ceramic Nanocomposites

2.1.1 Powder Processing

Powder processing is the first step in the ceramic nanocomposite processing and it is the most common manufacturing technologies due its ability to economically produce and fabricate complex components of high quality from many materials. High surface area to volume ratio of nanopowders is one of the important characteristics which lead to behavior that lies between solid and that of fluid. There are various techniques used in the preparation of nanopowders and this includes: sol-gel processing, reactive synthesis, mechanical alloying, chemical precipitation and gas atomization. Among the techniques, mechanical alloying is the mostly widely used for ceramic nanopowders processing.

2.1.2 Mechanical Alloying

The technique of Mechanical alloying or mechanical milling is used for homogenous production of materials from elemental powders. This technique which was invented and developed by John Benjamin and his colleague in 1966 at the research laboratory of the International Nickel Company (INC) as a result of their search for nickel-based superalloy for high-temperature strength, corrosion and oxidation resistance application in gas turbine engine[30] Mechanical alloying mechanism for powder processing involves repeated fracturing, cold welding, and rewelding of powder particles in a high-energy ball mill. In literature, Mechanical Alloying (MA) and Mechanical Milling (MM) are two different terms normally used to describe powder processing in high-energy ball mills. MA involves milling of powder mixture which includes transfer of material to obtain a homogenous powder mixture while mechanical milling describes the milling process that does not involve transfer material for homogenization of powder mixture[31]. The procedure of MA begins with mixing of the powders in the correct composition and then packing the powder mixture in the milling container in addition with the grinding medium (milling balls). The mixture is ground for a given period of time until a steady state is attained when the powder composition is almost the same as in the starting powder mixture. The most paramount components of MA thus include the raw materials (elemental powders), the mill and the process variables. Planetary ball mill (figure 1a) is a popular mill for mechanical alloying experiments in which certain amount of powder is milled for a given time. The mill owed its name due to the planetary-like movement of its vials. The grinding vials as well as the balls exists in eight different

materials- agate, nitride, silicon carbide, sintered corundum, zirconia, chromate steel, Cr-Ni steel (stainless steel), tungsten carbide and plastic polyamide[30].

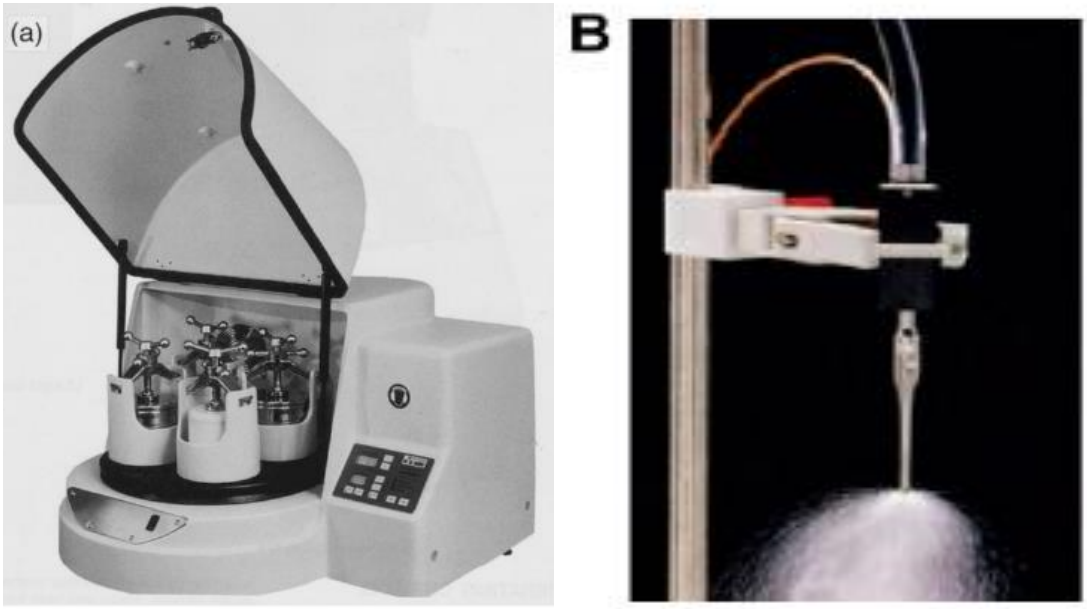

Figure 1 (a) Planetary ball mill (b) Probe sonicators [30,32]

2.1.3 Ultrasonication

Ultrasonication involves application of ultrasound energy to stir particles of powder in a particular solution. This is achieved in laboratory using an ultrasonic probe as shown in figure 1b. Ultrasonication is the most frequently used techniques for the dispersion of nanoparticles. During ultrasonication, ultrasound is propagated through a series of compression and attenuated waves which are transferred in the molecules of the medium through which it is propagated. The shock waves produced assist in the de-agglomeration of individual nanoparticles and this result in detaching of individualized nanoparticles from the bundles or agglomerates[33]. To avoid damage to CNTs particularly when using probe type sonicators, dispersion of CNTs should be carefully done and proper selection

of sonication parameters are necessary as extreme sonication result in destruction of graphene layers of CNTs. Eventually CNTs are transformed into amorphous carbon. As such, the damaged CNTs result in deterioration of mechanical alongside electrical properties of CNT nanocomposites[34].

2.2 Powder consolidations

Consolidation of powders consists of assembly of powder particles in a monolithic product so as to obtain a desired geometry, structure or property. Consolidation processes depend on the application of energy (mechanical, chemical and thermal) to effect bonding of powder particles. Nanopowders consolidation is an essential ingredient of densification with minimal microstructural transformation. In most cases, densification usually results in either grain coarsening or undesirable small specimen size and insufficient bonding. This has detrimental effect on the nanomaterial properties especially the mechanical properties. Several researches have been done on the subject of nanopowders consolidation to find suitable methods for the sintering and consolidation of nanopowders particles s into sizable parts and retain their nanofeatures[35,36]. Densification of nanopowders has several challenges and in attempt to achieve higher densification will result into grain coarsening and loss of nanostructures. Again, inability to produce sizable and dense parts has led engineers and scientists to search for efficient and better consolidation process to overcome these challenges. Consolidation is broadly classified into two which are conventional and nonconventional consolidation.

In conventional consolidation, heat is produced externally and conveyed to the material by heat transfer processes such as conduction, convection and radiation. Conventional

consolidation processes include: pressureless sintering, hot pressing (HP), hot isostatic pressing (HIP), cold isostatic pressing (CIP), sintering forging, extrusion and ultrahigh pressure sintering. Conventional consolidation processes have some drawback such as grain coarsening, high consolidation time, requirement for pre-compaction, high sintering temperature and this has led to the search for novel methods for nanopowders consolidation. Nonconventional consolidation is a novel techniques developed to overcome consolidation challenges of undesirable grain growth and loss of nanostructures. In this technique, the materials absorb energy which is converted into heat within their bodies. Nonconventional consolidation includes spark plasma sintering and microwave sintering[37].

Spark Plasma Sintering (SPS) which is also known as Plasma activated sintering (PAS), Field assisted sintering is a sintering techniques that utilizes uniaxial force (pressure) and pulsed (on-off) direct electrical current at low temperature and pressure for powder consolidation. High heating, high cooling rates and enhanced densification with low grain growth allow the powders to maintain their nanofeatures in the fully dense products. SPS offers several advantages over conventional systems and high densification, shorter sintering time, relatively low sintering temperature and absence of pre-compaction are the common features of SPS. The mechanism of SPS (figure 2) involves generation of high energy from the low voltage supply due to electrical spark discharge phenomenon that exists between the powder particles which result in thermal and electrolytic diffusion. Most SPS temperature usually span from low to over 2000^{o}C which are 200 and 500^{o}C lower than those of conventional sintering furnaces[38].

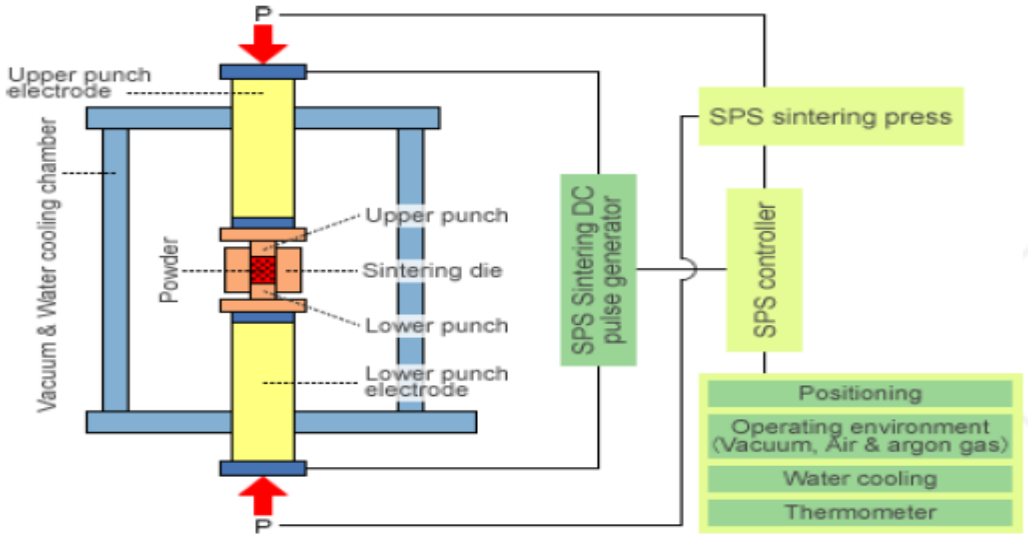

Figure 2 SPS configuration and vacuum chamber [37].

Hardy and Green[39], investigated the mechanical properties of porous alumina by sintering and holding at temperature below 1050°C to avoid grain growth which could occur beyond 1050°C. This is because longer holding time leads to an increase in neck growth formation through surface diffusion; thus enhance mechanical resistance.

Li et al.[13] reinforced porous alumina with 2wt% alumina nanophase particles for the improvement in strength and toughness. Increment of 50% in fracture strength and toughness was reported and when nanoscale alumina particles were entirely used for the reinforcement of alumina, only minor enhancement in fracture toughness was achieved. Also Lee et al.[40] studied the effect of microwave sintering on the full densification and hardness of alumina and they reported that full densification was achieved but average fracture toughness of 2.7MPam1/2 was measured which is comparatively lower than the values reported in the literature. This clearly showed that microwave sintering is inimical to the fracture toughness of alumina monolithic. Continuous improvement in the fracture

toughness of alumina could be achieved by coarsening the grain of high aspect ratio powder particles. Moreover, fracture toughness enhancement through grain coarsening is a trade-off as this usually results in degradation of hardness and strength. High aspect ratio second phase particles of SiC, TiC, ZrO_2, Si_3N_4 etc. have been used to reinforced alumina[41]. Meanwhile Al_2O_3-SiC nanocomposite system was found to have the best mechanical and functional properties.

2.3 ALUMINA BASED NANOCOMPOSITES

2.3.1 Alumina/SiC Nanocomposites

Aluimna/SiC nanocomposites which consist of alumina matrix and a reinforced nano-size silicon carbide particle has become an interesting field since the concept of structural ceramics proposed by Niihara in 1991. Several attentions of other researchers have been focused on the processing and improvement on the mechanical properties of this nanocomposite. Niihara and his co-workers[6], reported that addition of 5vol% SiC nanopowders to alumina matrix significantly improved the fracture strength of Al_2O_3 to over 1GPa while the fracture toughness increased to 4.7MPam$^{1/2}$ however, the results has not been reproduced by other researchers and they concluded that the significant results achieved by Niihara could be due to the method of processing employed in the preparation of the nanocomposite which was not explicitly stated. As stated by Niihara and Nakahira[42], Ohji[43] and Deng[44], when alumina is reinforced with 5-7vol% SiC particles, creep resistance was improved as compared to monolithic alumina. Many researches have been done on the improvement of mechanical properties (strength, hardness, fracture toughness) of Al_2O_3-SiC nanocomposites however, few research

papers have been published[17,18,45] on the thermal and electrical properties of this nanocomposite even though these functional properties are very important in cutting tools applications. In nanocomposite materials, the paramount factors that control the properties consist among other things; the positioning of the second particles in the matrix (intergranular, intragranular or both), the grain sizes of both reinforcement and the matrix and the chemical composition of nano-reinforcement phase.

2.3.2 Alumina-Carbon Nanotubes Nanocomposites

Carbon nanotube (CNT) which was discovered by Iijima in 1991 has been identified as key ingredient in the reinforcement of alumina due to its excellent mechanical and functional properties. The structure of CNT can be imagined as rolled up of graphene sheet with planar-hexagonal arrangement of carbon atoms distributed in a honey lattice.

CNTs are classified into single-walled carbon nanotube (SWCNT) and multi-walled carbon nanotube (MWCNT) according to the rolling layers of graphene sheets. Although SWCNT has higher thermal and electrical conductivity as well as high purity however, its high cost and clustering which hinder dispersibility limit its application in the fabrication of ceramic-CNT nanocomposites. There are several techniques for the production of CNT which includes arc discharge[46], laser ablation[47], and chemical vapor deposition[48]. CNTs by their design in pristine form are chemically inert, which is not always desirable for some applications. To overcome this difficulty, is to functionalize CNT. Functionalization improves their properties and consequently their application potential.

2.3.2.1 Functionalization of Carbon Nanotubes

The addition of oxygen-containing species on the surface of CNTs promotes their solubility in aqueous or organic solvents and decreases the van der Waals associations between different CNTs, enhancing the dissociation of nanotube bundles into individual tubes. Basically, there are two methods of functionalizing CNTs which include chemical functionalization and physical functionalization[49,50]. Chemical functionalization occurred as a result of the covalent linkage of functional entities onto carbon scaffold of CNTs. Chemical functionalization is usually done using strong acids such as HNO_3, H_2SO_4 or a mixture of them[51] or with strong oxidants such as $KMnO_4$[49]. The treatment process involved a mixture of CNT, nitric acid and sulfuric acid of high concentration followed by sonication for 3hrs. It is thereafter stirred for 24hrs and then washed and rinsed with distilled water until the PH is 7. The CNT is sieved and dried for overnight at 100^{o}C[52]. The defects created by the oxidation agents are neutralized by bonding with carboxylic acid (-COOH) or hydroxyl (-OH) groups. These functional groups have sufficient chemistry and the CNTs can be used as a precursor for further chemical reaction. Mansoor et al.[53], investigated the two chemical methods of functionalization using nitric acid and hydrogen peroxide and they concluded that hydrogen peroxide based functionalization is more effective than nitric acid functionalization. The MWCNT was found to be completely de-roped in hydrogen peroxide process and the better dispersion was observed in the epoxy resulting in high mechanical properties of MWCNT-epoxy nanocomposites.

Physical functionalization of carbon nanotubes involves adsorption of surfactant molecules on the surface of CNTs so as to ensure that agglomeration does not occur.

Several factors such as the characteristic properties of surfactant, the chemistry of the medium and the nature of the ceramic matrix determine the efficiency of physical functionalization of CNTs. However, the two major drawback of chemical and physical functionalization of CNTs include damaging due to ultrasonication or ball milling [32] process. In some cases, this damage could occur on the sidewalls of CNTs which might result in severe degradation in both mechanical and functional performances of CNTs [50]. The benefit of CNTs functionalization includes removal of impurities such as catalyst remnants, the addition of hydroxyl or carboxyl group for bonding with the matrix and high level of dispersion in water[54].

2.3.3 Alumina-SiC Nanopowders Preparation

There are several ways of processing Al_2O_3-SiC nanocomposites which include MA alloying or MM, sol-gel processing and polymer processing. All these methods of processing aimed at homogenous dispersion of the nano-SiC particles into the alumina matrix. In their work, Gao et al.[55], prepared 5vol% SiC-Al_2O_3 powder using Nano-SiC particles, aluminum chloride and ammonia. The nano-SiC particles were ultrasonically dispersed to break the agglomerate and the PH was carefully adjusted between 9 and 10. The suspended aqueous nano-SiC was continuously stirred at room temperature and then solution of aluminum chloride and ammonia were added and continuously stirred until complete precipitation occurred. The SiC-Al_2O_3 gel formed was washed with distilled water until it was free of chloride ions and then dried at 100^{o}C. Thereafter, the gel was calcined at 700^{o}C and then sieved through a 200 mesh sieve to obtain the final SiC-Al_2O_3 powder.

Wang et al.[56], prepared 5vol% and 10vol% SiC-Al_2O_3 powder using a combination of sol-gel and wet-ball milling. In this preparation, $AlCl_3$ was added to SiC particles and the mixture was stirred. Ammonium hydroxide (NH_4OH) was then added until precipitation occurred. The resulting SiC-Al_2O_3 powder was obtained after drying, calcining and attrition milling of the slurry. Chao et al.[57], in their work prepared SiC-Al_2O_3 powder by ball milling 17vol%SiC-Al_2O_3 powder mixture in ethanol for 12hrs using alumina balls. 20vol% SiC was then added and ball milled for another 6 hrs. The slurry was dried completely in a microwave oven and the agglomerate was ball milled for six hours to achieve the final powder for consolidation.

Al_2O_3-SiC powder preparations by a combination of sonication and mechanical ball milling using zirconia balls and media have been reported by several authors [58–60]. In these preparations, SiC powder was dispersed in distilled water together with alumina powder and the mixture was sonicated for 20minutes. The slurry was thereafter transferred to attritor mill with zirconia balls and media and then ball milled for 2hrs at a speed of 500rpm. PH of 9 was maintained for the dispersion and the slurry was dried for 24hrs and finally ball milled for 1hrs. Al_2O_3-SiC powder was obtained by sieving through a 150μm sieve.

Parchoviansky et al.[17] in their work prepared Al_2O_3/SiC nanopowders containing different fraction of SiC by convention mixing of alumina powder with nano-sized SiC powder particles. Here the homogenization of powder mixtures was done by mechanical milling in isopropyl alcohol for 24hrs in a polymer flask using high purity Al_2O_3 balls. The slurry was dried in oven and the soft agglomerated powders after drying were crushed with the aid of pestle in agate mortar. Detailed preparation of Al_2O_3-SiC powder

was reported by Borrell et al.[18]. Powder mixture containing 17vol% nano-SiC was ball milled using ethanol as solvent. High purity (99.5%) alpha alumina balls of diameter 2mm were used and powder to ball ratio of 4:1 was maintained. Milling was performed at a speed of 100rpm for 48hrs and the slurry was dried at 60°C to obtain soft agglomerate. The agglomerate was crushed in a pestle and sieved through a 60μm sieve.

Preparation of Al_2O_3-SiC nanopowders using alumina milling balls and milling vials have been reported in several papers[13,61–65]. The powder mixture in an isopropyl ethanol was ball milled using alumina balls in alumina media for 24hrs at a speed of 100rpm. The powder mixture was dried in an oven for 24hrs and the agglomerates dried powder formed was ball milled for 12hrs and sieved through appropriate sieve sizes to obtain the powder for consolidation. As reported by Liu et al.[65], Watanabe and Kimura[66], a combination of sonication and planetary ball milling using alumina balls and vials was found to be very effective in the dispersion of SiC nano-particles into alumina matrix. In their work, mixture of SiC and alumina powder in ethanol was sonicated for 45 minutes and the slurry was transferred into alumina vials containing alumina balls and then ball milled for 2hrs. The powder mixture was dried and crushes in a mortar using pestle and sieved prior to consolidation. The use of ultrasonication and magnetic stirring for the preparation of Al_2O_3-SiC powder was reported by Sciti et al.[67] Here the powder mixture containing Al_2O_3-SiC powder was magnetically stirred followed by sonication for 2hrs. The slurry was dried and sieved to obtain Al_2O_3-SiC powder. Al_2O_3-SiC powder was reported to have been prepared by Ko et al.[14] using SiC balls and SiC media. In their work, mixture of alumina and SiC in ethanol was ball milled for 24hrs using SiC balls in polyethylene jar. The slurry was dried and sieved

through 60μm mesh. It is paramount to know that the objective of the Alumina-SiC powder processing methods highlighted above is to ensure homogenous distribution of the SiC nanoparticles in alumina.

2.3.4 Alumina-CNT Powder Preparation

Dispersion of CNT in alumina matrix is crucial in the processing and fabrication of alumina-CNT nanocomposites. Mechanical method such as sonication and ball milling have been used to effectively dispersed CNT in alumina matrix. For instance, Zhang et al.[68] and Kumari et al.[19] dispersed CNT in alumina directly by growing CNT on alumina nanoparticles using $Co(NO_3)_2.6H_2O$ as catalyst and the mixture of alumina and CNT in ethanol is sonicated for 15mins. Sonication and planetary ball milling process for the dispersion of CNT in alumina have been reported by some authors[69–71]. In this process, CNT is dispersed in Dimethylformadie (DMF) using high power sonicators for 2hrs and thereafter hand mixed with alumina nanopowders. The mixture was ball milled for 8hrs and then dried for 12hrs at 75^{o}C on a heating plate in air, followed by oven drying at 100^{o}C for 3 days.

2.3.5 Al_2O_3-SiC Nanopowders Consolidation

Wang et al.[56] consolidated Alumina/SiC nanopowders by hot pressing at pressure of 35MPa and sintering temperature of 1650^{o}C and 1750^{o}C. Higher densification was achieved at 1650^{o}C at 35MPa however, further increase in temperature to 1750^{o}C do not lead to change in densification although, the microstructural analysis showed significant grain growth and loss of nanostructures (grain size >100nm).

Spark plasma sintering of Al_2O_3-SiC nanopowders containing 17vol% SiC was performed by Borrell et al.[18]. In their study, the composite powder was inserted into graphite mold of diameter 20mm and then unixially cold pressed at 30MPa. The compressed powders were sintered at 1400 and 1550^{o}C for dwelling time of 1min and heating rate of 100^{o}C/min. the sintering pressure was kept at 16MPa which was raised while heating to 80MPa sintering pressure within the next 100^{o}C and maintained throughout the holding time. The grain size of the alumina was found to be smaller at 1400^{o}C sintering temperature (430nm) than the composite sintered at 1550^{o}C sintering temperature (590nm) although; there is significant change in the densification of the composites sintered at two different temperatures. In their work, Parchoviansky et al.[17] studied the thermal and electrical behaviour of Al_2O_3/SiC nanocomposites by hot pressing the nanopowders of SiC-Al_2O_3 containing 3-20vol% SiC. The powders were inserted in a graphite die of inner diameter 20mm and uniaxially compressed at 30MPa. The compressed powder was hot pressed at 1740^{o}C and 1hr dwell time and pressure of 30MPa. For the consolidation of monolithic reference material (Alumina), the sintering was reduced to 1350^{o}C so as to produce alumina of comparable grains size as that of Al_2O_3/SiC nanocomposites. Greater than 98% densification was achieved on the nanocomposites sintered at 1740^{o}C.

Spark Plasma Sintering (SPS) of Al_2O_3-SiC powder consolidation has been studied by several researchers[13,55,63,65,72,73] under different conditions of sintering temperature, dwelling time, heating rate and applied pressure. Conventional consolidation techniques such as hot pressing (HP) [6,42,61,67,74–77], cold isostatic pressing (CIP) [59,60,78] and hot isostatic pressing (HIP)[64,79]have equally been used in the

consolidation of Al_2O_3-SiC powder. High sintering temperature, long sintering time and lack of proper control over the grain size limit the application of conventional sintering in processing of Al_2O_3/SiC nanocomposites.

2.3.6 Alumina-CNT Powder Consolidations

As reported in the previous studies[80], densification of ceramics can be inhibited by the presence of inclusions such as CNTs in the matrix. As such most of Al_2O_3-CNT nanocomposites reported so far has been fabricated by hot pressing [81–84] or Spark plasma sintering[85,86]. Hot pressing involves application of heat and uniaxial pressure to enhance densification of the powders. This method is more preferable to pressureless sintering of alumina-CNT nanopowders[87] as excessive grain growth occurs during sintering which result in the degradation of mechanical and functional properties. To preserve structural integrity of CNTs, Spark plasma sintering (SPS) is a better technique used to sinter alumina-carbon nanopowders as the technique offers high heating rate, short sintering time and high cooling rate which provide an avenue to have better control over the microstructures of the nanocomposites.

Spark Plasma sintering of alumina-CNT nanopowders has been reported in several papers [19,68,69,71,85]. Kumari et al.[19], and Zhang et al.[68], consolidated alumina-CNT nanopowders in a graphite of 15mm diameter by SPS at 100MPa, 1150 or 1450^{o}C sintering temperature, heating rate of 100^{o}C/min and 10min holding time. Hot pressing (HP) of alumina–CNT powders has been investigated by Ahmad et al.[5] by hot pressing alumina-CNT powders at 40MPa and 1600^{o}C sintering temperature for 60 mins. It has been established by few researchers that SPS temperature for fabricating CNT/Al_2O_3 nanocomposite should be in the range of 1150^{o}C to 1250^{o}C while the pressure should

vary from 20-100MPa to retain structural integrity of nanotubes[88,89]. Similar to SPS, for hot pressing of CNT/Al_2O_3 nanocomposites researchers used wide range of temperature (1350-1850^oC) and pressure (20-40MPa) as far as pressureless sintering is concern, only limited group of researchers have tried the techniques.

2.3.7 Densification of Al_2O_3-SiC Nanocomposites

The pressureless sintering techniques which are used in the consolidation of Al_2O_3-SiC nanopowders do not give higher densification. Usually, the SiC particles as a result of the composite powder preparation are located at the interfaces between the grains of alumina matrix and this serves as obstacle to densification that restrict the grain boundary motion through pinning effect. The advent of pressure assisted sintering techniques such as hot pressing, hot isostatic pressing, spark plasma sintering etc. can produce composites of full densification. To achieve higher densification in pressureless sintering, high sintering temperature is required and this promote grain growth that impairs the mechanical and functional properties of the nanocomposites[90]. To reduce the sintering temperature during pressureless sintering, additives are usually added to aid sintering at relatively lower temperature. For pressureless sintering of Al_2O_3-SiC, powder is doped with 0.1wt MgO and Y_2O_3 and this reduce sintering temperature from 1800^oC to 1300^oC[91], although the coarse microstructure is obtained.

The successful densification of nanocomposite by pressureless sintering is limited to the content of SiC nanoparticles which normally do not exceed 10vol%. Full densification of composite with relatively higher SiC content (>20vol%) can be obtain by the combination of pressureless sintering and hot isostatic pressure[92].

2.3.8 Densification of Al_2O_3-CNT Nanocomposites

The CNTs just like SiC particles has pinning effect on the alumina matrix which resist densification. Specifically speaking, the high aspect ratio, high specific surface and their incompatibility with the surrounding matrix has made CNTs to behave in two distinct ways: (1) reduction in the sintered density (2) decrease in the size of alumina due to reduction in grain boundary migration through efficient pinning[93][94]. Besides, the presence of CNT clusters at the grain boundaries due to imperfect de-agglomeration also contributed to the reduction in densities. The agglomerates act as obstacles at the boundary interfaces that resist densification. Thus, increasing the content of CNT in the nanocomposite increase the difficulty in the densification of the CNTs-containing nanocomposites. Several attempt have been made to sinter CNT-alumina nanopowders although it is always unsuccessful as high sintering temperature cause oxidation of CNT in the ceramics. Zhang et al.[95] and Rice[96] discovered that the relative density decrease from 98.5% to 95% when the CNT contents in alumina increase from 1wt% to 3wt%. Again, to avoid oxidation of CNT, the maximum sintering temperature of CNT-alumina nanopowders is usually kept below 1550^{o}C[96]. To accomplish this, more attention has been paid to pressure assisted sintering techniques. SPS has been considered by researchers to be an idea sintering techniques in the consolidation of alumina-CNT nanopowders dues to its high heating rate, relatively low sintering temperature and shorter sintering time. This result in fine microstructure and enhance mechanical and functional performance.

2.4 Mechanical Properties of Alumina-Based Nanocomposites

2.4.1 Mechanical Properties of Al2O3-SiC Nanocomposites

Gao et al.[55] investigated mechanical behavior and microstructure of alumina-SiC composite containing 5%vol SiC nanopowders. The mechanical properties were evaluated after SPS consolidation at 1450^{o}C and 40MPa. The maximum bending strength of 980MPa was achieved as compared to monolithic alumina of 350MPa while, 19GPa hardness was achieved at 1400^{o}C which was the maximum hardness evaluated. There was no significance difference in hardness value between 1400^{o}C and 1500^{o}C. Again, the fracture toughness was found to be improved (4.5MPam$^{1/2}$) while the alumina ceramics was 3.5MPam$^{1/2}$. Maximum densification was attained at 1450^{o}C (99.8%). The mechanical behaviors of Al_2O_3/SiC nanocomposites are stated in table1. The overall enhancement of the mechanical behavior was attributed to the effective distribution of SiC nanoparticles in the matrix of alumina grains and at the boundaries of the alumina. The SiC particles at the boundary inhibit grain boundary movement and decrease the grain size of alumina that results into fine microstructure and better mechanical properties.

Table 1 Mechanical properties of Al2O3/SiC Nanocomposites.

Al_2O_3-SiC Nanocomposites	Consolidation Type	Hardness (GPa)	Strength (MPa)	Fracture toughness ($MPam^{1/2}$)	Ref.
Al_2O_3-5SiC	SPS	19	980	4.5	[55]
Al_2O_3-5SiC Al_2O_3-10SiC	HP	- -	467 415	4.7 3.8	[56]
Al_2O_3-17SiC	HP	22	400	4.6	[97]
Al_2O_3-5SiC	HP	21.2	760	4.4	[74]
Al_2O_3-10SiC	SPS	20.7	-	3.3	[73]

2.4.2 Mechanical Properties of Alumina-CNT Nanocomposites

It has been established that the range of CNT content in CNT/Al_2O_3 nanocomposites varied over a wide span from 0.01wt% to35wt%[98]. Yamamto et al.[99], Sarkar and Das[100], Cha et al.[101]and Zhang et al.[68] discovered that MWCNT started to form agglomerate beyond 0.9, 0.6, 0.18 and 1vol% respectively. The agglomeration of carbon nanotubes between 2 to 7.39wt% MWCNT in alumina matrix have been reported in literatures[98,99,102]. The concentration of SWCNT with much better morphological precision, properties and high clustering tendency than MCNT is expected to be lower

than MWCNT so as to achieve the same effects[103]. The hardness of Al_2O_3/CNT nanocomposites varies significantly with various factors which include CNT content and extent of dispersion, CNT purity, sintering temperature, extent of densification, nature of interface formed matrix grain size and applied indentation load. Zhang et al.[68] studied the mechanical properties of Al_2O_3/MWCNT nanocomposites consolidated by SPS between 1150 and 1450°C. The maximum properties of nanocomposites were achieved at 7.39wt%MWCNT. For instance, the hardness (9.98GPa) was achieved on the nanocomposites sintered at 1450°C while pure monolithic alumina was 9.21GPa measured under the same conditions. Maximum fracture toughness of 4.7MPam$^{1/2}$ was achieved on the nanocomposite containing 7.39wt%MWCNT sintered at 1450°C. The mechanical properties of the Alumina monolithic and nanocomposites were found to be lower at low sintering temperature (1150°C). Also the densification of the nanocomposites was all lower than the monolithic sintered at the same conditions. 98.2% and 79.1% densification was achieved on monolithic alumina and 7.39wt%MWCNT/Al_2O_3 nanocomposite respectively. Some of the mechanical properties of Al_2O_3-CNT nanocomposites are presented in the table 2 below. As presented in the table 2, high fracture toughness (4.7MPam$^{1/2}$) was obtained on the nanocomposites sintered by SPS as compared to other sintering techniques shown in the table 2.

Table 2 Mechanical Properties of Alumina-CNT Nanocomposites.

Al_2O_3-CNT Nanocomposite	Consolidation Type	Hardness (GPa)	Strength (MPa)	Fracture toughness ($MPam^{1/2}$)	Ref.
Al_2O_3-7.39wt%MWCNT	SPS	9.98	-	4.7	[68]
Al_2O_3-0.3wt%MWCNT	HP	21.4	-	4.47	[99]
Al_2O_3-2wt%MWCNT	HP	18	-	4.2	[104]

2.5 Thermal Properties of Alumina-Based Nanocomposites

It is well established that the heat transport properties of any materials strongly rely upon the purity condition of the crystal lattice of the grains. Therefore, careful control of the impurities emanating from the starting raw materials and processing conditions has to be achieved in order to enhance the thermal properties of the material. Thermal properties which include thermal diffusivity, specific heat capacity, the coefficient of thermal expansion and thermal conductivity are important parameters in many applications of alumina based nanocomposites[105].

2.5.1 Heat Capacity

The heat capacity of a given material is the ability of the material to absorb thermal energy. Thermal energy comprises of kinetic of atomic motion and potential energy of distortion of interatomic bonds. Heat capacity C is express by the equation 2.1

$$C = \frac{\Delta Q}{\Delta T} = \frac{dQ}{dT} \quad \text{(2.1)}$$

Where Q is the heat amount of heat absorb, T is the temperature. The unit of heat capacity is J/K. Heat capacity can be measured under conditions of constant temperature or constant volume[106].

2.5.2 Thermal diffusivity

Thermal diffusivity is a thermophysical characteristic of materials that defines the velocity of heat transmission by conduction through the material during a change of temperature. The thermal diffusivity is related to the thermal conductivity, specific heat capacity and the density of the material. Among the methods of measuring thermal diffusivity, a flash method is considered to be the most effective method as this method requires short measuring time, completely non-destructive and give an accurate result which is reproducible. Flash method of thermal diffusivity measurement involves uniform radiation of the small specimen over its front face with a short pulse of energy [107]. Thermal diffusivity is expressed as;

$$\alpha = \frac{\lambda}{\rho C_p} \quad \text{(2.2)}$$

Where α is the thermal diffusivity, λ is the thermal conductivity, ρ is the density and C_p is the heat capacity of the material.

2.5.3 Thermal conductivity

Thermal conductivity as a mechanism of heat transfer can be defined as the property of a material which indicates its ability to conduct or transfer heat. The first general statement relating to heat flow and temperature gradient was made by Fourier in 1822. According to Fourier, for a material under steady state heat flow, the quantity of heat (q) is related to the temperature gradient ($\frac{dT}{dx}$) by the expression; $q = -\lambda \frac{dT}{dx}$..... (2.3).

Where λ is the proportionality called thermal conductivity with unit W/mK[108].

The mechanism of heat conduction in dielectric solids can be model with the aid of Debye kinetic equation $\lambda = 1/3Cvl$..... (2.4).

In the equation (2.4) above, C is the specific heat per unit volume, v is the mean sound velocity and l represents the average free path of phonon. It is important to know that the average free path decrease with rising in temperature. The product of velocity and mean free path of the phonon is called thermal diffusivity D; $D = v.l$

Thus, the thermal conductivity; $\lambda = 1/3C_P \rho D$..... (2.5)

The mechanism of heat transfers by conduction through solid requires thermal energy. The carriers for heat transfer by conduction include electrons, phonons or photons. For nonmetallic materials, phonon is the carrier of heat by thermal vibrations of the atoms. However, in metals, heat conduction is by electrons but in alloys and semiconductors, both phonons and electrons contribute to their thermal conduction[109].

Thermal conductivity of materials can be determined either by indirect method or direct method. In indirect method also known as laser flash method, the thermal diffusivity is

measured by the transmission of the laser pulse through the sample specimen. The thermal conductivity is therefore determined from the values of specific heat capacity, density of the bulk material and the thermal diffusivity as shown in equation (2.5). The direct measurement of thermal conductivity gives the actual value of the material thermal conductivity as evaluated by the thermal conductivity equipment.

2.5.4 Thermal Properties of Al_2O_3-SiC Nanocomposites

The thermal conductivity of SiC containing compound is difficult to model as only room temperature thermal conductivity data are available for SiC materials. The thermal conductivity of SiC vary from 40-100W/mK[110,111] however, higher values in the range of 150-325W/mK[112–114] have been reported for SiC evaluated from heat conduction model. Barea et al.[45], studied the thermal diffusivity of Al_2O_3-SiC nanocomposites containing 30vol% SiC after hot pressing at 1550^{o}C for 60mins and sintering pressure of 50MPa. The thermal diffusivity Vs temperature (figure 3) of the composites was evaluated. The ambient temperature thermal diffusivity increases with SiC platelet concentration from 0.092cm^2/s for the alumina monolithic to 0.153cm^2/s for the 30vol% SiC-Al_2O_3 composite. Again, for each nanocomposite, thermal diffusivity decrease with increase in temperature and at 1000 ^{o}C, the values of 0.015cm^2/s and 0.028cm^2/s were achieved for 0 and 30 vol% of SiCpl, respectively. It was also confirmed that the thermal diffusivity measured in perpendicular configuration is higher than the parallel one at all temperatures. In addition to the thermal diffusivity, thermal conductivity, λ Vs temperature was also evaluated (figure 4) and a maximum λ value of 42 W/mK was attained at room temperature for the 30 vol.% SiC platelet content tested in the parallel direction which 52% more than monolithic alumina (28-35W/mK)[105],

while λ value in the perpendicular direction is 49K/mK. The decrease in thermal conductivity with temperature was due to increasing in crystal lattice vibration with temperature which results in increasing scattering of the phonon. Barea et al thus concluded that the thermal conductivity is independent of the shape and size of the dispersing phase.

Parchoviansky et al.[17] hot pressed Al_2O_3-SiC powder containing 20vol%SiC and reported 0.093cm^2/s and 0.135cm^2/s as the room temperature thermal diffusivity for alumina and Al_2O_3-20SiC nanocomposite respectively. The maximum value of λ at room temperature was achieved in the composites at $AS_{20}c$ and AS_{20f} (38W/mK) but the alumina monolithic thermal conductivity was only 28W/mK. This measured thermal conductivity is lower than the expected value based on the intrinsic thermal conductivity of SiC (490W/mK for single crystal and 270W/mK for polycrystalline SiC). This is because the most paramount factor affecting the thermal conductivity is phonon scattering and SiC addition act as scattering sites. Besides, phonons could also interact with lattice defects, impurities, interfacial resistance, grain boundaries, triple junctions and other microstructural defects which all contributed to the lower value of thermal conductivity of the composites. It is important to note that in nanocomposites materials, the thermal properties such as thermal conductivity is affected by many critical factors which includes composition of the starting powder mixtures, the level of impurities of other materials, the microstructure of the composites (matrix grain size and the grain boundaries) and the distribution of the reinforcement phase (intergranular, intragranular or both).

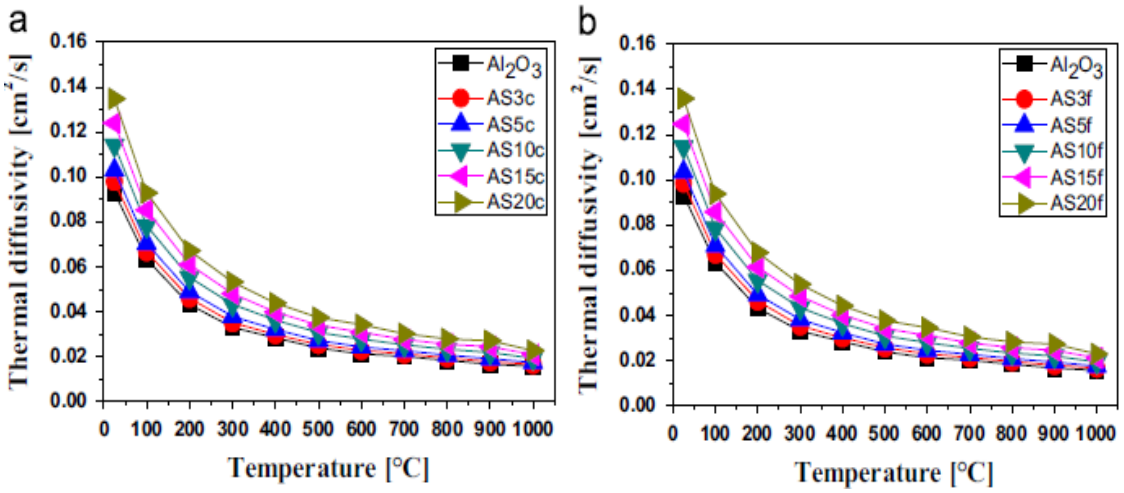

Figure 3 The response of thermal diffusivity with measuring temperature for (a) coarse grains and (b) fine grain [17].

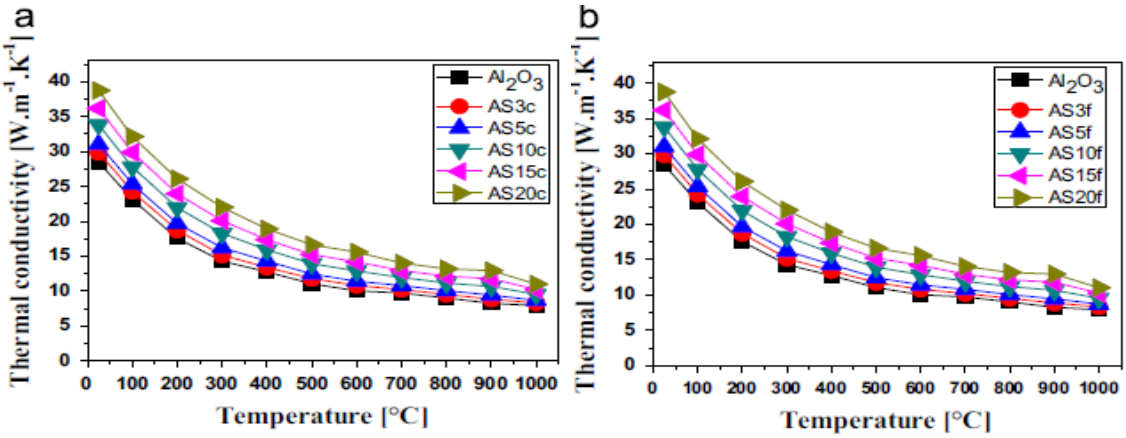

Figure 4 Variation of thermal conductivity with the measuring temperature for (a) coarse grains and (b) fine grain [17].

Table 3 Thermal Property of Al2O3-SiC Composites.

Nanocomposites	Consolidation type	Densification (%)	Thermal Conductivity (W/mK)	Ref.
Al_2O_3-20SiC	HP	99.3	38	[17]
Al_2O_3-60SiCw	HP	---	42.1	[105]
Al_2O_3-30SiCp	HP	99	49	[45]
Al_2O_3-20SiCw	HP	98.3	34.25	[111]

2.5.5 Thermal Properties of Al_2O_3-CNT Nanocomposites

Limited work has been done on thermal conductivity of alumina-CNT nanocomposites as presented in table 5.0. Substantive increase in thermal conductivity (90.44W/mK) of Al_2O_3/CNT nanocomposites was reported by Kumari et al.[19] for 7.39wt% MWCNT/Al_2O_3 nanocomposites over alumina, after consolidating at 1550^{o}C. Further loading of MWCNT to 19.1wt% could result in decreasing thermal conductivity of Al_2O_3/MWCNT nanocomposite even at higher sintering temperatures. The thermal diffusivity and thermal conductivity of Al_2O_3-SWCNT were investigated by Zhan and Mukherjee[71] and the thermal conductivity of 11.4W/mK was achieved on 10%wtSWCNT and this decrease to 7.3W/mK as the CNT content increased to 15wt%. Also Sivakumar et al.[115] reported improvement in thermal conductivity SiO_2-MWCNT

nanocomposites containing 10vol% MWCNT and maximum thermal conductivity of 4.08W/mK was obtained at room temperature. Both thermal diffusivity and thermal conductivity decrease with measured temperature. This decrease in thermal conductivity with measured temperature was as a result of increase scattering of phonons due to increase in crystal vibration as temperature increase[19]. Table 4 shows the thermal conductivity of alumina-CNT nanocomposites densified by various sintering techniques. It is evidence in the table that densification alone is not sufficient to give appreciable thermal conductivities. High densification was achieved by Sarkar and Das[87], but the thermal conductivity is relatively low as compared to the values reported by SPS process; thus implies that pressureless sintering is not ideal technique for the consolidation of alumina-CNT nanocomposites.

Scattering of phonons by the residual pores, low thermal conductivity of highly clustered CNT, scattering of phonon by the interfacial thermal resistance and blocking of the phonon by kinks or twists are the factors affecting the thermal conductivity of CNT-Al_2O_3 nanocomposites. The interfacial resistance between the CNT and ceramic matrix can limit the heat transportation in CNT nanocomposites. It is evidence in the literatures that SWCNT with high thermal conductivity (6600W/mK)[50] cannot produce significant enhancement in thermal conductivity of composites as does MWCNT even though the thermal conductivity of MWCNT (2000-3000W/mK)[116] is lower than the SWCNT. Tube-tube interaction is another factor affecting thermal conductivity of CNT-ceramics nanocomposites. CNTs tend to agglomerate as a result of their Vander Waals forces between them and this contributes to the scattering of the phonons. Besides, high pressure during sintering process can create kinks or twists in the length of CNTs which

reduce the phonon mean free path. As the phonons travel along the length and meet the kink or twist, they are blocked and this reduce the thermal conductivity of CNT-ceramics nanocomposites. To enhance thermal conductivity of ceramic-CNT nanocomposites, effective dispersion of CNT free of agglomerations, high interfacial bonding and relatively low sintering temperature offer by SPS are necessary.

Table 4 Thermal property of Al2O3-CNT Nanocomposites.

Nanocomposites	Consolidation type	Densification (%)	Thermal conductivity (W/mK)	Ref.
Al_2O_3-10SWCNT	SPS	95.2	11.4	[71]
Al_2O_3-7.39MWCNT	SPS	84.2	90.44	[19]
Al2O3-1.2MWCNT	Pressureless	92.32	13.37	[87]

2.6 Electrical Properties of Alumina-based Nanocomposites

Electrical resistivity which is inverse of electrical conductivity is an important physical property of materials. it describes the extent that material resist the flow of electricity. It is measure in the unit of ohm-meters (Ωm). Low electrical resistivity implies that electricity can easily flow through the material otherwise means that the material has high

resistivity. For example, aluminum and copper have low resistivity and this is why they are good conductors of electricity while plastics and most monolithic ceramics have high resistivity and thus use as insulating materials. Electrical conductivity is therefore defined as the inverse of the resistivity which measure how easy or difficult electricity can flow in a material. It is an intrinsic property of a material which is independent of the size, shape or geometry of the material. Proper understanding of the electrical conductivity of nanomaterials requires deep understanding of quantum mechanics. Microscopically, electricity can be conceptualized as the movement of electrons through a material as indicated in figure 5.0. The thermal energy of semi-conducting material set them on constant mechanical vibration and as such the valence electrons emanate from its shell and exist as free electron in the crystal. At the same time, hole is created on the parent atom. The electron-hole pair created in the crystal under the influence of applied voltage move with drift velocity. This constitutes the flow of electricity in a semi-conducting material. For a pure semi-conductor (intrinsic semi-conductor), the number of holes equal to the number of free electrons at any particular point in time. The electron moves from left to right under the influence of the external force acting on it. As the electron move through the material, it collides with the atoms of the material and this collision tends to slow down the movement of the electron. The number of collisions electron encounter can vary from material to material. If a material produces a lot of collisions as the electron flows through it, then it is termed as high-resistivity material. Also, the resistivity of a material changes with temperatures and applied magnetic field.

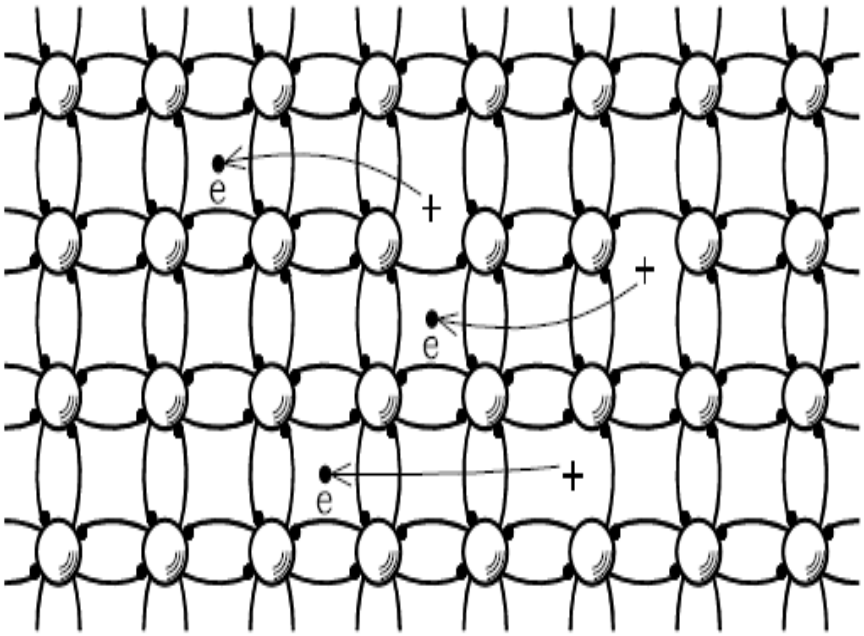

Figure 5 Model showing the flow of electron through a semi-conducting material under the influence of applied voltage [117].

2.6.1 Methods of Measuring Electrical Resistivity

2.6.1.1 Two-Point Technique

Two-point method is used for measuring the electrical resistance of a material taken into consideration the physical dimension of the sample specimen. In this method, the sample is cut into the shape of rectangular bar of length l, height h, and width w. electrical voltage V, is applied at the ends of the bar with the aid of copper wire as shown in figure 6a. The amount of current I, flowing through the bar is measured by the ammeter. Thus, the resistance of the bar is given as

$R = \frac{V}{I}$.....(2.6)

The two-point electrical resistivity of the bar can be calculated from the dimension of the bar as:

$$\rho \equiv \frac{Rwh}{l} \quad \text{.....(2.7)}$$

Two-point technique do not give accurate result as there is usually some resistance between the contact wires and the sample material even in the measuring equipment itself. Thus two-point technique gives higher electrical resistivity than the true value. Also, modulation of the sample resistivity as a result of applied current and the problem of contacts between semi-conducting sample and metal electrodes give inaccurate value of the electrical resistivity. These problems could be avoided by using four-point technique of measurement.

2.6.1.2 Four-Point Technique

In this techniques, four wires are connected to the rectangular bar sample as shown in figure 6b. a constant current source is connected to the end of the bar and the amount of current flowing through the bar is measured by the ammeter while the voltmeter simultaneously measure the voltage across the bar. The electrical resistivity is evaluated as

$$\rho = \frac{Vwh}{Il'} \quad \text{.....(2.8)}$$

However, for irregular shape sample, Van der Pauw technique is recommended.

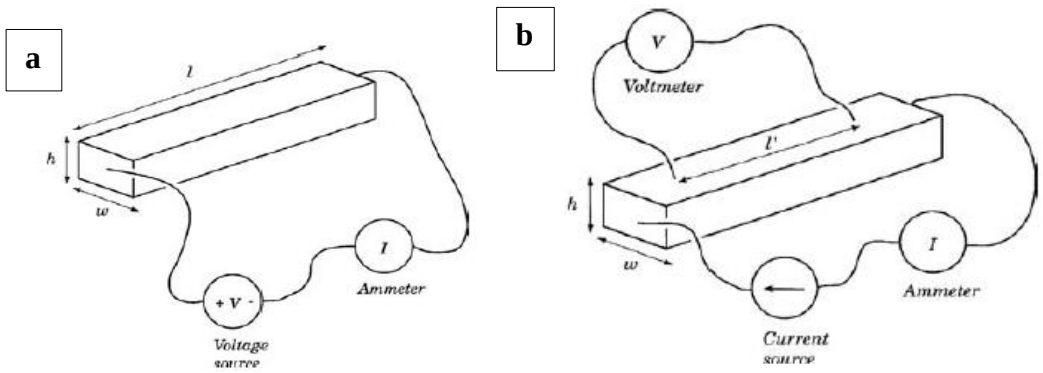

Figure 6 Electrical resistivity measurement (a) two-point technique (b) four-point technique [117].

2.6.2 Electrical conductivity of Al_2O_3-SiC Nanocomposites

The electrical conduction mechanism of Al_2O_3-SiC nanocomposites material is the result of formation of interconnected continuous network of SiC nanoparticles within the Al_2O_3 matrix. It was established that one of the most crucial factors for obtaining electro-conductive materials is the distribution of SiC nanoparticles[118]. McLachlan [119] developed mathematical model and evaluated the minimum volume fraction of SiC creating a conducting as 17vol%. However, when the volume concentration of SiC particles increase to 20vol%, electrical resistivity reduced to 10^6Ωcm. The percolation threshold of the SiC nanoparticle is affected by the level of dispersion in the matrix forming continuous network for the flow of electricity. There are two factors responsible for the formation of continuous network. The first case involves establishment of well-defined grain boundaries by the matrix that will be covered by the conductive reinforcement SiC phase and the second case is the amount of SiC that are contributing to the formation of the network.

Parchoviansky et al.[17] reported electrical conductivity of 4.05×10^{-2}S/m for 20vol% SiC-Al_2O_3 nanocomposite while 7.80×10^{-6}S/m was evaluated as the thermal conductivity of reference Al_2O_3 monolithic. It was evidence that at low SiC content (<5%SiC) there was no increase in electrical conductivity of alumina (figure 7.0). when the SiC increase beyond 5%SiC, appreciable increase in electrical conductivity was observed which indicate that there were complete interconnected network formation and the percolation threshold was achieved between 5wt% and10%wt SiC in this nanocomposite. Also the electrical conductivity was found to increase substantially with decreasing grain size of alumina matrix. This is because the pinning effect of SiC particles increase with increasing SiC content and this impairs the grain growth of alumina matrix. As such, more of the SiC particles are located at the grain boundaries of alumina which contribute to the formation of conductive network path for the flow of electricity. Borrell et al.[18] consolidated Al_2O_3-17SiC by SPS and reported electrical resistivity of 170Ωm at 1500°C while 31Ωm was the electrical resistivity at 1400°C. The enhance electrical conductivity was attributed to the formation of network of SiC in contact with each other separated by small gap of alumina matrix consequently promote tunneling effect. SPS temperature also control the electrical conductivity of Al_2O_3-SiC nanocomposites. As shown in figure 8.0, SPS temperature at 1400°C showed that the SiC particles are located mainly at the grain boundaries of alumina (figure 8a). however, when the SPS temperature increase to 1550°C, the SiC nanoparticles are located both at the grain boundaries and on the grains of alumina. The swallowed SiC particles (on the matrix grains) do not contribute to the formation of network path, so the electrical conductivity reduced. Generally, the electrical conductivity of Al_2O_3-SiCnanocomposites increase with increase SiC contents

and refinement of alumina matrix also influence the electrical conductivity of the nanocomposites.

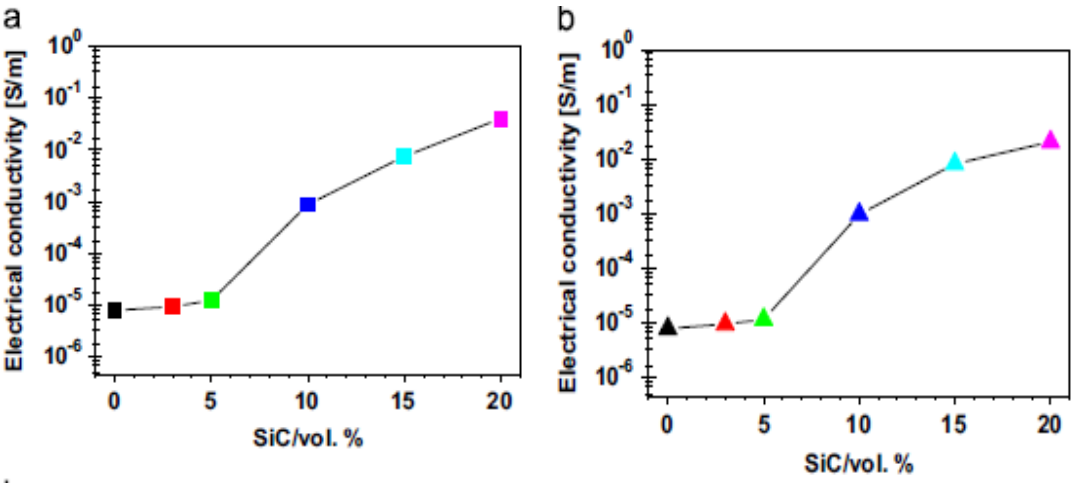

Figure 7 Electrical conductivity of Al2O3-SiC (a) fine SiC (b) coarse SiC [17].

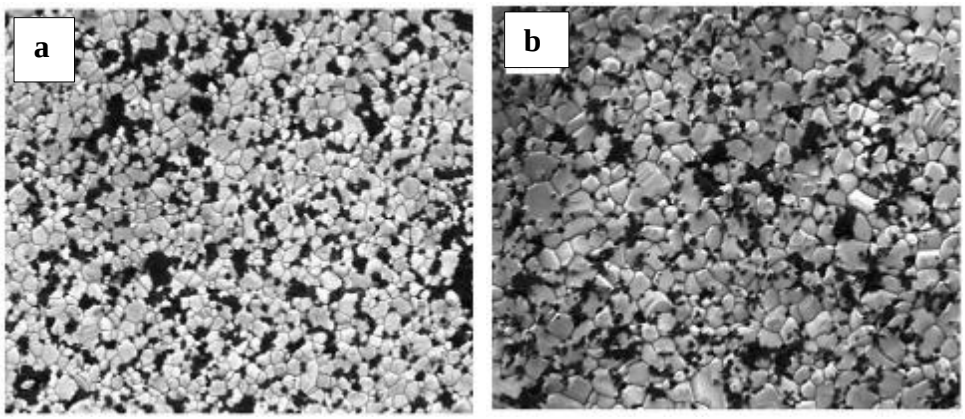

Figure 8 FE-SEM microstructure of Al2O3-SiC nanocomposites (a)1400°C and 1550°C [18].

2.6.3 Electrical conductivity of Al_2O_3-Carbon Nanotubes Nanocomposites

Researchers have made several imparts in trying to improve electrical conductivity of purely monolithic alumina by incorporating highly conductive CNT in alumina. Dramatic

increase in the electrical conductivity of Al_2O_3/CNT nanocomposite over pure Al_2O_3 was achieved when the CNT loading in the matrix attain percolation threshold. The improvement in electrical conductivity of the nanocomposite is commonly achieved by the formation of an electrically conductive network by dispersed CNT in the matrix.

Kumari et al.[85], consolidated MWCNT/Al_2O_3 nanocomposite using SPS techniques at sintering temperature of 1150 and 1450^{o}C and they discovered that electrical conductivity increase with increase in MWCNT concentration. The maximum electrical conductivity of CNT-alumina nanocomposite at room temperature was 3336S/m for 19.1.0 % MWCNT-alumina nanocomposite sintered at 1450^{o}C. Zhan and Mukherjee[71], studied the electrical conductivity of SWCNT-Al_2O_3 nanocomposite and reported 1510S/m as the room temperature electrical conductivity for 10vol%SWCNT while 3345S/m for 15vol%SWCNT. However pure alumina has electrical conductivity of 10^{-10}-10^{-12}S/m. Dramatic increase in electrical conductivity of alumina reinforced with CNT was investigated by Ahmad and Pan [120]. All the authors agreed that electrical conductivity of CNT-Al_2O_3 nanocomposites increase with CNT content. Besides, electrical conductivity also increased with the measuring temperature as the charge mobility increase with temperature. Formation of conductive network of CNT at the grain boundaries of alumina is necessary for electrical conduction. Increase dispersion of CNT in alumina will reduce the percolation threshold of CNT thus increase conductivity. The table 5 shows electrical conductivity of Al_2O_3-CNT nanocomposites reported so far in the literature. The microstructure of the Al_2O_3-CNT nanocomposites play significant role in its electrical property. The high aspect ratio of CNT enable it to form a connect bridge between the alumina grains. Increasing the grain size of alumina reduces the number of

grain boundaries and this reduce the amount of CNT require to form interconnected conductive path for the flow of electricity. As evidence in the figure 9.0, CNT enveloped the alumina matrix and as the grain size reduces, the gap between the CNT is smaller thus, enhance tunneling effect.

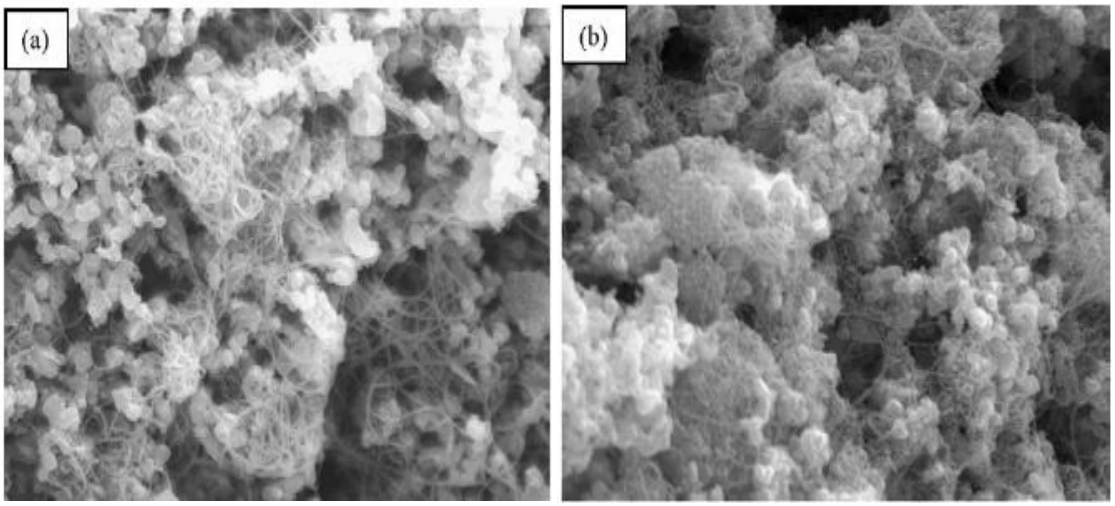

Figure 9 FE-SEM microstructure of Al2O3-CNT nanocomposites (a) 7.39MWCNT (b) 8.25MWCNT [85].

Table 5 Electrical Conductivity of Al2O3-CNT Nanocomposites.

Nanocomposites	Consolidation type	Densification (%)	Electrical conductivity (S/m)	Ref.
Alumina-3%MWCNT	SPS	----	1.245	[120]
Alumina-5%MWCNT	SPS	99	576	[70]
Alumina-19.1%MWCNT	SPS	59.7	3336	[85]
Alumina-1%MWCNT	SPS	----	2.50	[121]
Alumina-5.7%SWCNT	SPS	100	1050	[71]
Alumina-1.2MWCNT	Pressureless	92.32	10^{-4}	[87]

CHAPTER 3

MATERIALS AND METHODS

3.1 Materials

The α-alumina with average particle size of 150nm and purity of 99.85% was purchased from Chem Pur, Germany while the SiC_{β} of average particle of 45-55nm and purity of 97.5% was also procured from the same company. The multi-walled carbon nanotube (MWCNT) produced by chemical vapor deposition (CVD) with diameter 20-40nm, length 1-2μm, surface area of 40-600m^2/g was procured from Nanostructured & Amorphous material Inc., 820 Kristi lane, Los Alamos, NM 87544, USA.

3.2 Methods

3.2.1 Alumina-SiC Powder Preparation

The Alumina-SiC nanopowders was prepared according to powder to ball ratio of 10:1 for high milling process. Two set of Alumina-SiC nanopowders of 5wt% and 10%wt SiC were produced designated as alumina-5SiC and alumina-10SiC respectively. The two powders were weighed and dispersed in distilled water and magnetically stirred for 15minutes followed by ultrasonication using probe type sonicators for 2hrs. The mixture is then transferred to the zirconia vials containing zirconia balls for planetary ball milling. The milling was done at speed of 300rpm and 4hrs milling time. The slurry is dried for about 24hrs in an oven at 120^{o}C. The hard agglomerates obtained after drying was reduced to powder by planetary ball milling at 300rpm for 30minutes.

Also Alumina-SiC powder preparation was equally done at low milling conditions. In this process, 5wt%SiC-alumina and 10wt%SiC-alumina nanopowders were prepared using magnetic stirring, sonication and ball milling. Each powder was weighed and dispersed in deionized water and magnetically stirred for 15minutes and thereafter sonicated for 2hrs. The mixture was transferred into vials containing zirconia balls. The powder to ball ratio was maintained at 4:1. The mixture was milled for 2hrs to ensure homogenous distribution of SiC in alumina matrix. The slurry was dried in an oven at 120^{o}C for 24hrs. the soft agglomerates was crushed using mortar and pestle to obtain the nanopowders for consolidation.

3.2.2 Alumina-CNT Powder Preparation

As-received MWCNT was functionalized with a mixture of concentrated 300ml sulfuric acid (H_2SO_4) and 100ml nitric acid (HNO_3) using probe type sonicators. The mixture was sonicated for 3hrs and then stirred for 24hrs. After stirring, the MWCNT suspension was filtered using 0.1µm nylon filter membrane followed by washing with distilled water until the PH of the water became almost 7. The MWCNTs was dried overnight to obtain functionalized MWCNTs.

The functionalized MWCNTs was dispersed in distilled water and then magnetically stirred for 15minutes followed by sonication for 15minutes. Alumina powder was equally dispersed separately in distilled water and magnetically stirred for 15minutes. The two powders were now mixed and sonicated for 2hrs to ensure proper dispersion of MWCNT in alumina. The slurry was dried in an oven at 120^{o}C for 24hrs to obtain soft agglomerates. The soft agglomerates were crushed in a mortar using pestle to obtain fine nanopowders.

3.3 Powder Characterization

The prepared powder was characterized using scanning electron microscopy (SEM) and X-ray diffraction (XRD). The X-ray diffraction of model: 8 advanced Brucker, Germany was used to characterize the nanopowders. A step size of 0.02°/s, voltage of 30Kv, current of 30mA and copper target was employed. Cu-Kα radiation was generated from the x-ray source with Ni filter to reduce the undesirable radiations before hitting the samples. Tilting of the stage was done at angle 2θ ranging from 20° to 80°.

Prior to the SEM imaging, the powder samples were coated with gold to avoid sample charging during SEM imaging. The powder samples were inserted into the gold coat machine chamber and then flush to create vacuum at a pressure of 0.25mbar. The coating was done at a current of 40mA for 25-30secs.

Transmission electron microscopy (TEM) of the nanopowders was done using TEM machine model: JEM-2100F, JEOL company, Japan. The TEM was operated at an accelerating voltage of 200KV using copper gate.

The x-ray fluorescence was done on the nanopowders processed at low milling conditions to check the level of contaminations of the nanopowders as a result of the milling conditions. The energy dispersive x-ray fluorescence (EDXRF) machine of model spectroXEPOS was used and the analysis was done at voltage of 39.75KV, current of 1mA at pressure of 75Pa in helium atmosphere for 10minutes.

3.4 Consolidation of the Nanopowders

The powders were consolidated using spark plasma sintering (SPS) using sintering temperature of 1300°C, 1400°C, 1500°C and pressure of 50MPa. Heating was done at the

heating rate of 100°C/min and holding time of 10mins. For comparism, powder alumina was equally consolidated at different SPS temperatures (1000, 1300 and 1400°C) for 50MPa pressure, 10min holding time and 100°C/min heating rate.

3.5 Cleaning, Grinding and Polishing of the Consolidated Nanocomposites

The cleaning of the consolidated nanocomposites was done to remove the graphite on the surface of the samples. Grinding of the samples was carried out using Buehler Automet 300 using diamond abrasive of different sizes 125,74µm, 40µm, 20µ and 9µm to obtained smooth and flat surface for thermal and electrical conductivity measurement. Finally, polishing clothe was used to obtained a mirror like surface.

3.6 Densification Measurement

The bulk density of the samples was done using Archimedes method with the densification kit Mettler Toledo Model: AG 285 made in Switzerland. The relative density of the samples was determined based on the theoretical density of Alumina ($3.97 g/cm^3$), SiC ($3.21 g/cm^3$) and CNT ($2 g/cm^3$). The relative density was achieved by dividing the bulk density of the nanocomposites with the theoretical value calculated by the rule of mixture.

3.7 Thermal Properties measurement

Thermal constant analyzer of model: TPS 2500s made in Sweden was used to determine the thermal properties of the nanocomposites. The sample was inserted into the sample holder and the sensor of diameter 6mm was placed on top of the samples. Heating power

of 500W and measuring time of 2s was employed. Five measurements were taken and the average value was recorded as the thermal properties. The thermal properties evaluated include the thermal diffusivity, heat capacity and thermal conductivity. Similarly, elevated thermal properties of the nanocomposites were also measured in the temperature range of 25^{o}C to 250^{o}C to ascertain the influence of thermal properties with measuring temperatures.

3.8 Electrical Conductivity Measurement

The electrical resistivity of the nanocomposites was determine using four-point technique. Four wires were connected to the rectangular bar sample as reported in the paper[122]. In the case of Al_2O_3-MWCNT nanocomposites, a multi-meter current source model: WAVETEK 9105 was used to supply current (I) of 1.02µA through the bar and the voltage drop (V) across the bar at a given length l' was measured with the aid of voltmeter. However, in the case of Al_2O_3-SiC nanocomposites, a constant voltage of 500V was supplied to the rectangular bar sample with the aid of multi-meter current source and the current in the bar was measured using high resolution multimeter of model: HEWLET PACKARD 3458A. In each experiment, ten readings were taken and the average resistivity was determined using the mathematical expression

$$\rho = \frac{Vwh}{Il'} \quad \text{.....(3.1)}$$

Where ρ is the resistivity, h is the height of the bar and w is the bar width measured in meters.

The electrical conductivity σ, was evaluated from the electrical resistivity value calculated,

$$\sigma = {}^{1}/_{\rho} \quad \text{.....(3.2)}$$

3.9 Microstructural Characterization of the Nanocomposites

The microstructure of the fabricated nanocomposites is studied using FE-SEM and XRD to investigate the interface formed and the possibility of formation of undesirable phases during sintering process. EDS analysis was equally done to check if there was any phase form as a result of reaction or phase transformation during sintering. The samples for thermal etching was cut into rectangular sizes which was grinded using diamond abrasive of different sizes (125, 74, 40, 20, 10 and 9μm). The surface was polished with diamond paste on polishing clothe from 6μm to 0.25μm paste. The obtained mirror like surface was then sonicated for 1omins in a distilled water prior to thermal etching. The procedure for thermal etching involves heating the sample in a tube furnace for about 1hrs in an argon atmosphere.

CHAPTER 4

RESULTS AND DISCUSSION

4.1 Powder Characterization

4.1.1 SEM of As-received powders of Alumina and SiC.

The scanning electron microscopy images of the as received alumina and SiC nanoparticles were done and presented in figure 10 and figure 11 respectively. The alumina powder images (figure 10a) and the corresponding particles size (figure 10b) measured from the SEM image are shown. Figure 10b indicates that the average particle size of the alumina powder is about 150-170nm. Also, the images of SiC nanopowders is shown in figure 11a while the particle size (about 40-50nm) is indicated in figure 11b. this confirmed that the SiC is nanometer size as claimed by the supplier while the alumina powder is in micrometer size.

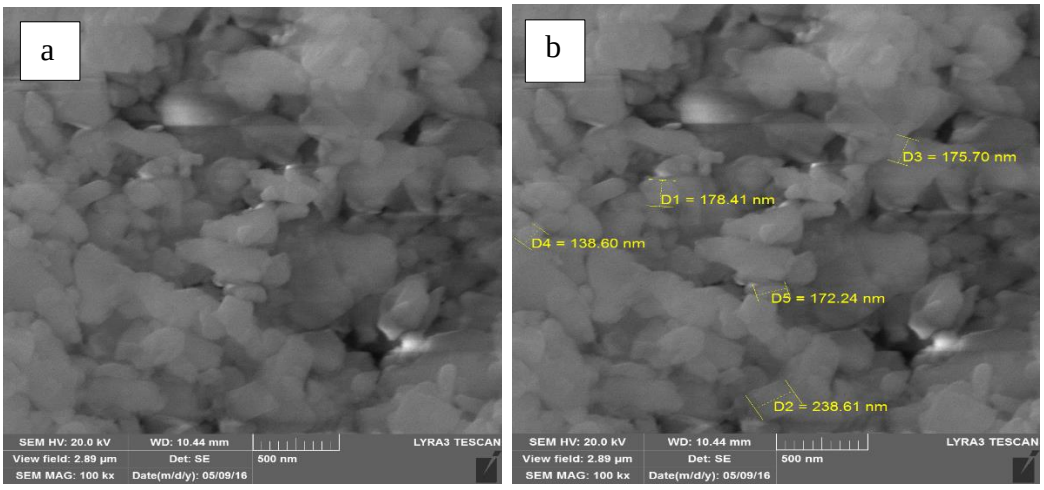

Figure 10 SEM images of as-received alumina powder (a)×500nm (b) showing average particle size.

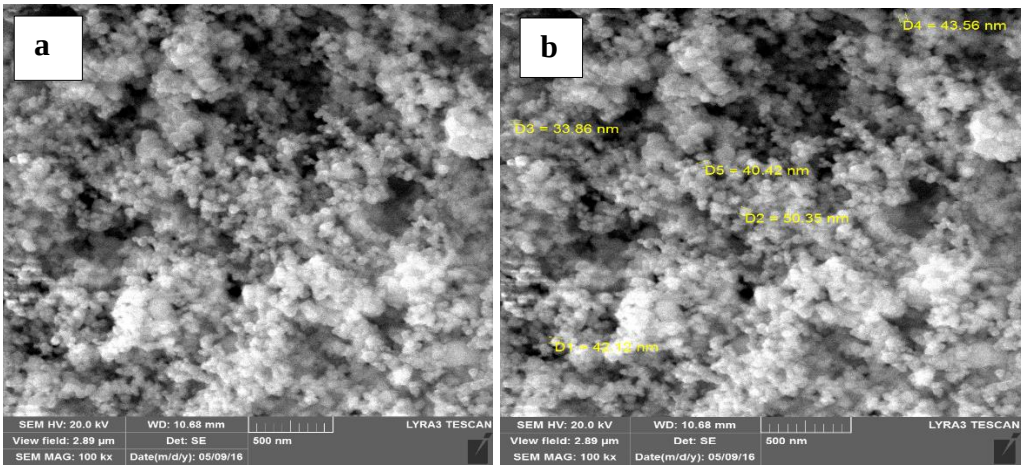

Figure 11SEM images of as-received SiC nanopowders (a)×500nm (b) showing average particle size.

4.1.2 SEM, EDX Analysis of the processed Al_2O_3-SiC Nanopowders

The SEM and EDS analysis of the processed Al_2O_3-SiC nanopowders are presented figure 12-19. The presence of SiC on alumina was observed as revealed by SEM images and EDS result in figure 12 and figure14. The EDS results showed the presence of zirconium on the nanopowders emanating from the degradation of the zirconia balls and the media during milling. This is mainly due to the high milling conditions used in the processing of the powders which result in the degradation of zirconia balls and media. Homogenous distribution of SiC nanoparticles in alumina was observed in both 5wt% and 10wt% SiC-alumina.as shown in figure 13 and figure 15 respectively. EDS mapping although do not accurately shows the distribution of the components as claimed by some authors but it gives ideas as regards the level of dispersion of one component in another. The SEM images of the powder also showed that, the SiC particles are located mainly on the grains of alumina which is clearly shown in 10wt%SiC than 5wt%SiC alumina

nanopowders. This is expected as the particle size of alumina is larger than SiC particles. For Al_2O_3-5SiC nanopowders, the average particle size of alumina was determined to be around 170nm. However, for Al_2O_3-10SiC, the average particle size of alumina was about 200nm. This disparity could be due to the agglomeration of the particles with increasing SiC contents.

The SEM images of the nanopowders prepared at low milling conditions are shown in figure16 and figure 18. There were no contaminations by zirconia as shown by EDS results presented in figure 16 and 18 both at 5wt% and 10wt%SiC nanoparticles in alumina respectively. This is because, the milling speed (100rpm) was relatively low to cause serious degradation of the zirconia balls and media or there could be little degradation that is beyond the detection limit of the EDS. The average particle size of alumina was determined by the SEM for both 5wt%SiC and 10wt%SiC in alumina as 180nm and 202nm respectively. Again, the EDS mapping presented in figure 15 and 17 showed homogenous distribution of SiC nanoparticles in alumina matrix which implies that low milling conditions chosen for the experiment was enough for the dispersion of SiC nanophase in alumina matrix.

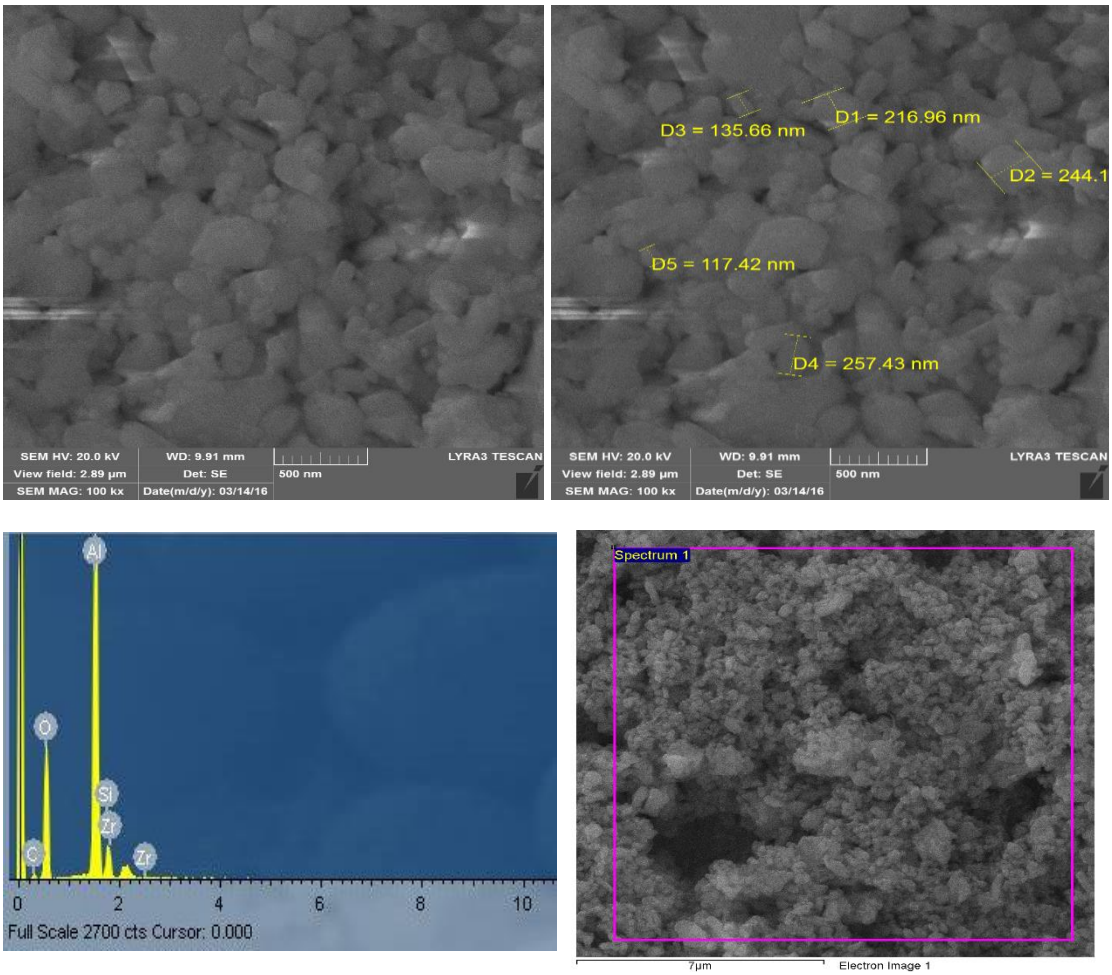

Figure 12 SEM EDS of Al2O3-5SiC nanopowders prepared at high milling conditions (300rpm, 4hrs).

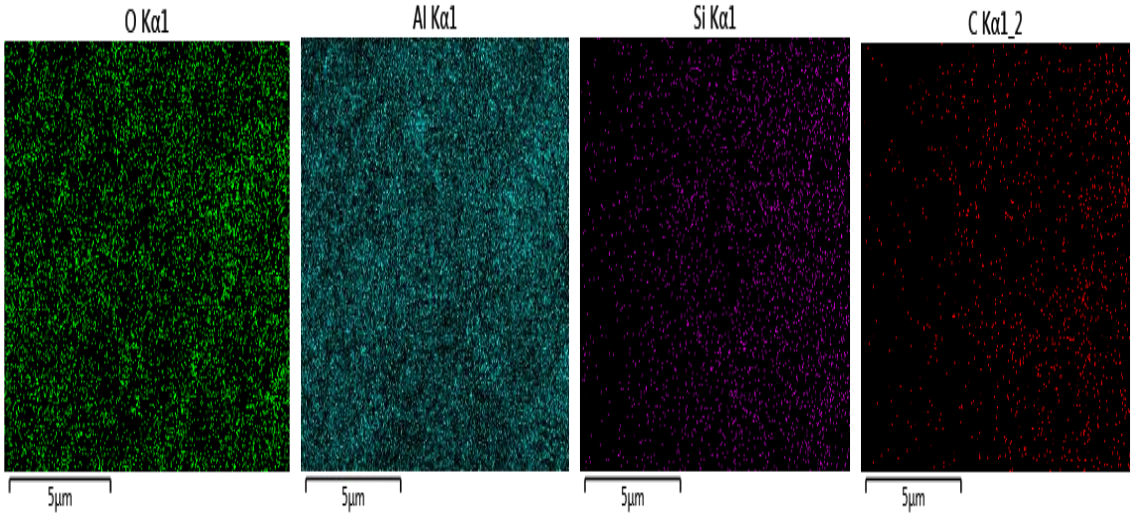

Figure 13 EDS mapping of Al2O3-SiC nanopowders at high milling conditions.

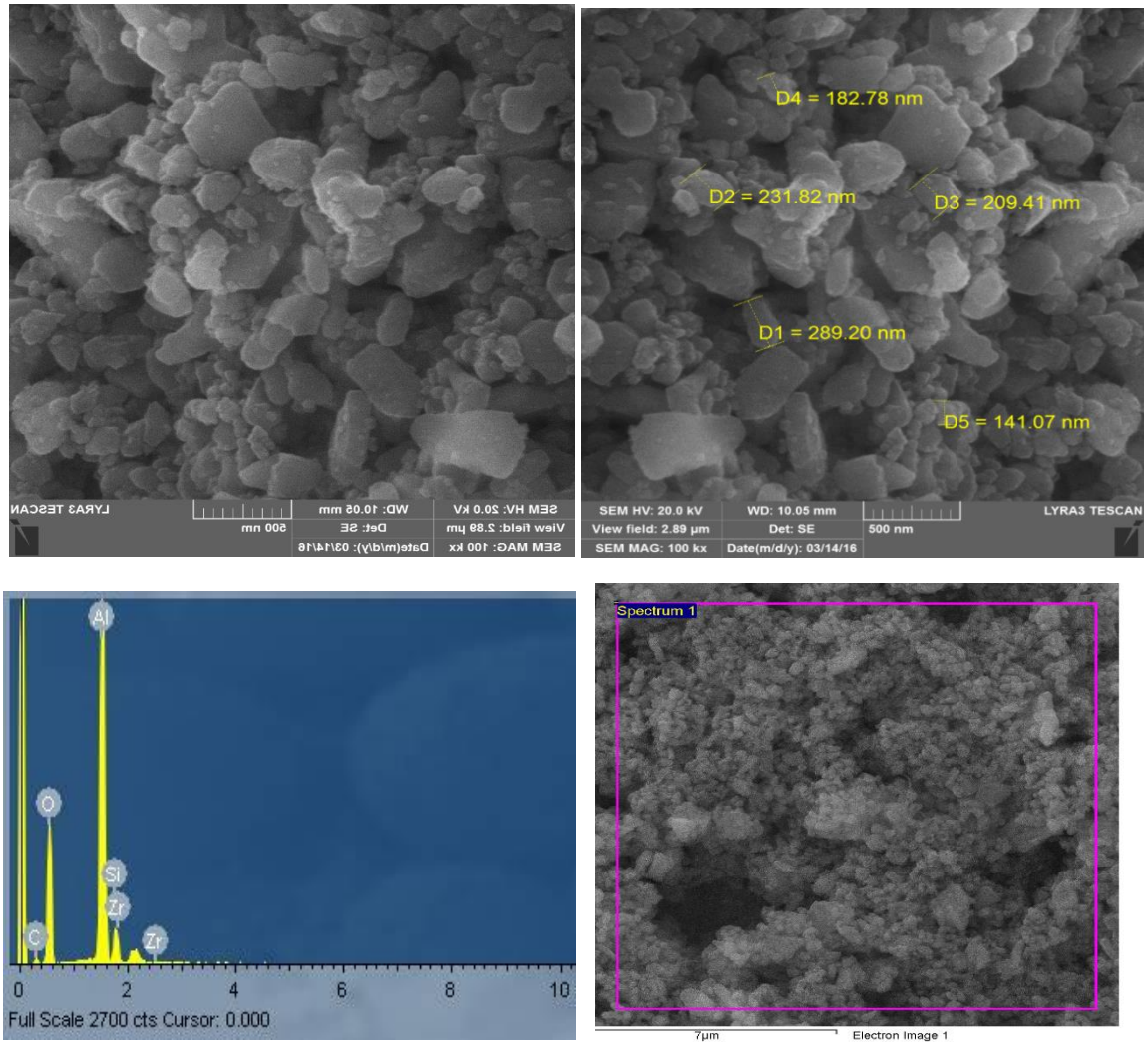

Figure 14 SEM EDS analysis of Al2O3-10%SiC nanopowders at high milling conditions (300rpm, 4hrs).

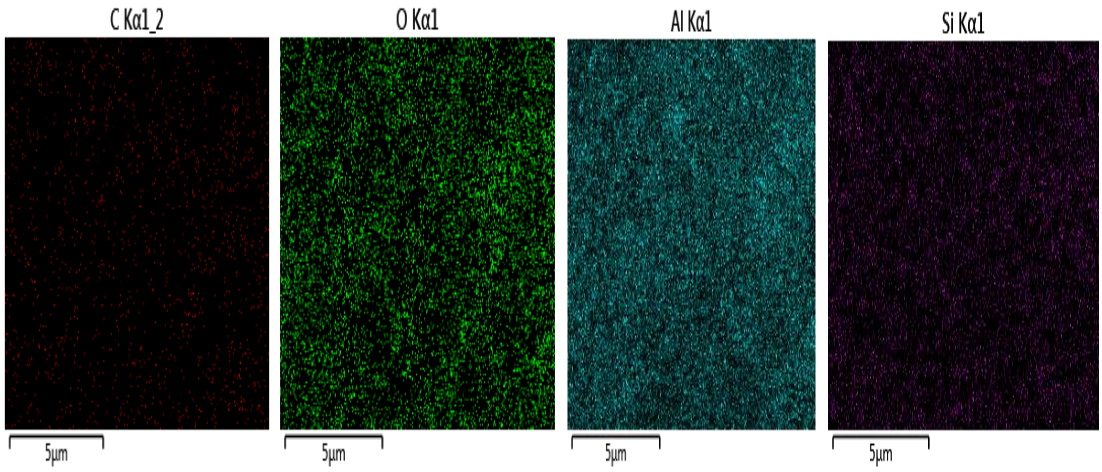

Figure 15 15 EDS mapping of Al2O3-10%SiC nanopowders at high milling conditions (300rpm, 4hrs).

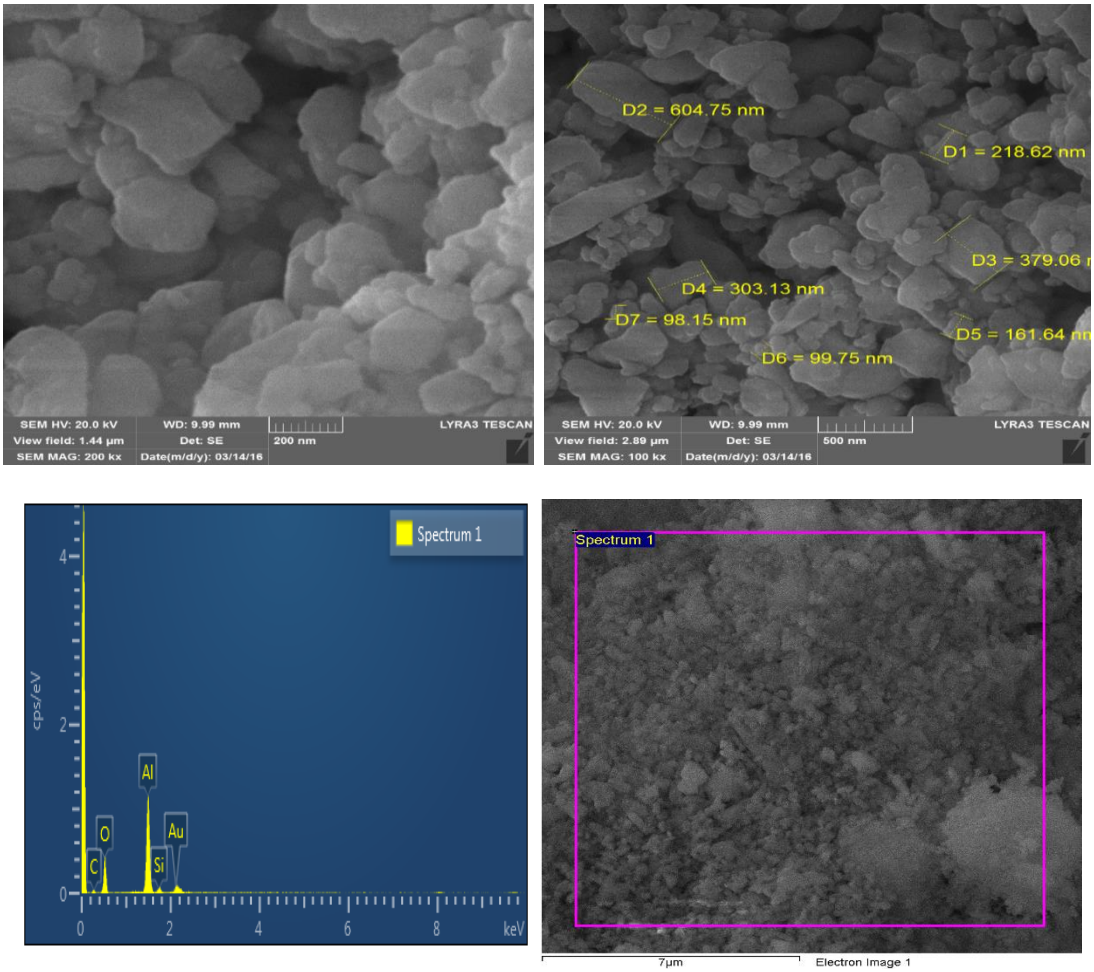

Figure 16 SEM EDX of Al2O3-5SiC nanopowders at low milling conditions (100rpm, 2hrs).

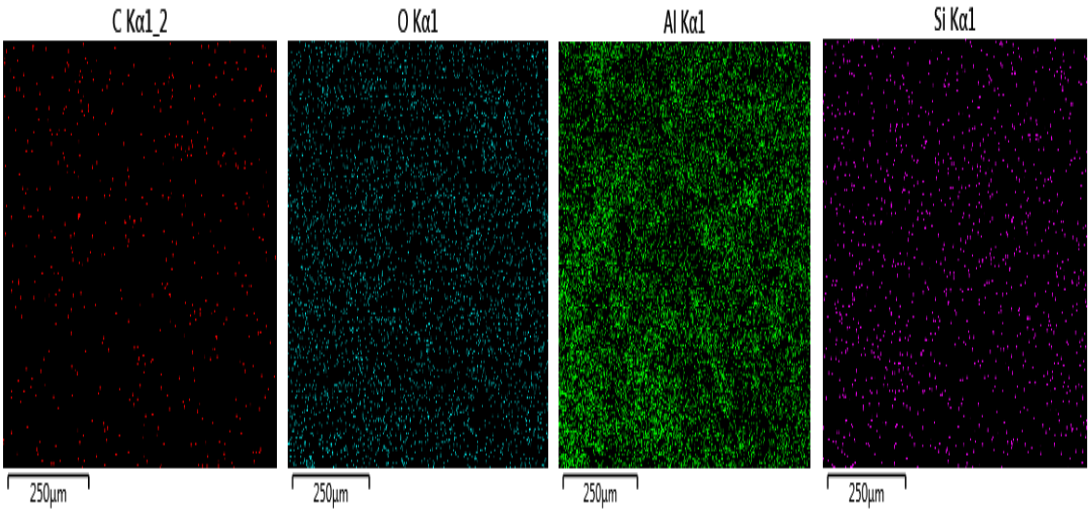

Figure 17 EDX mapping of Al2O3-5SiC nanopowders at low milling conditions.

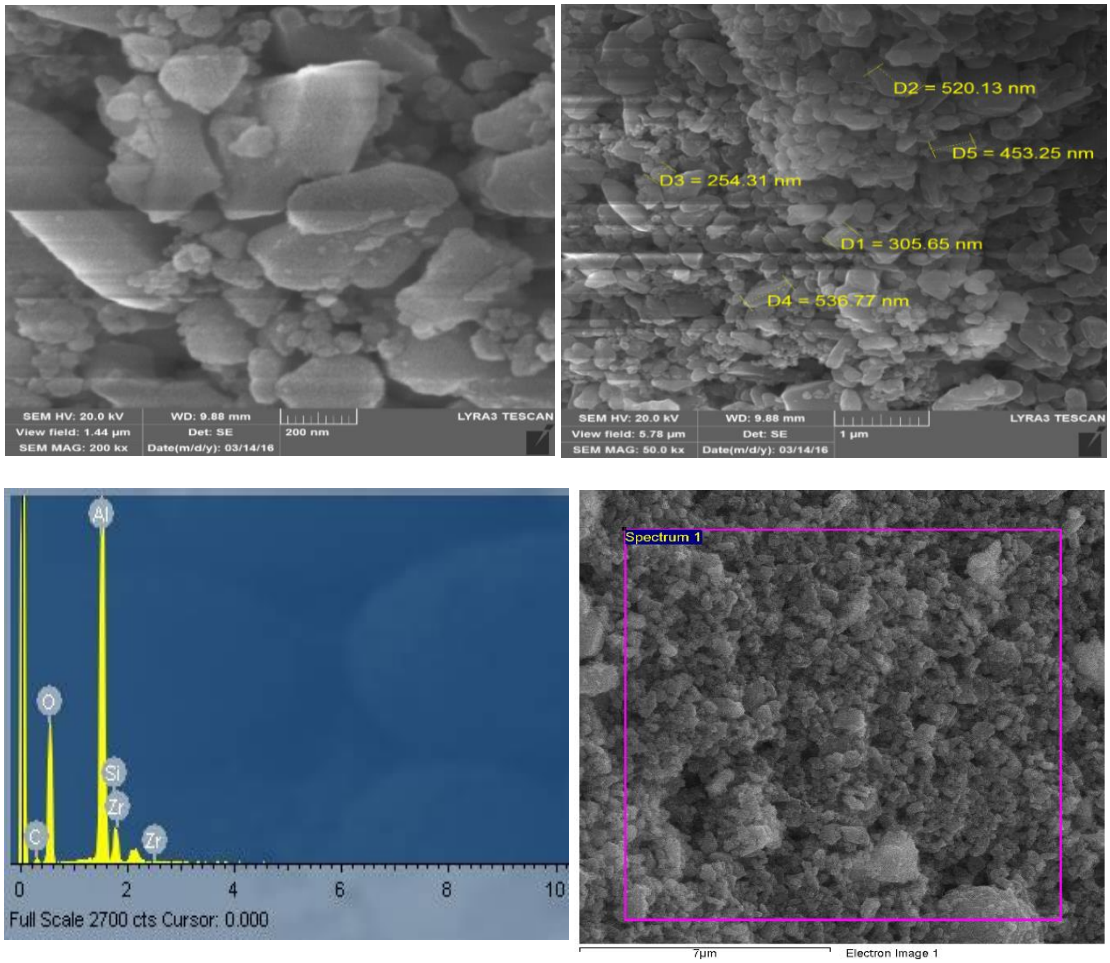

Figure 18 SEM EDX of Al2O3-10SiC nanopowders at low milling conditions.

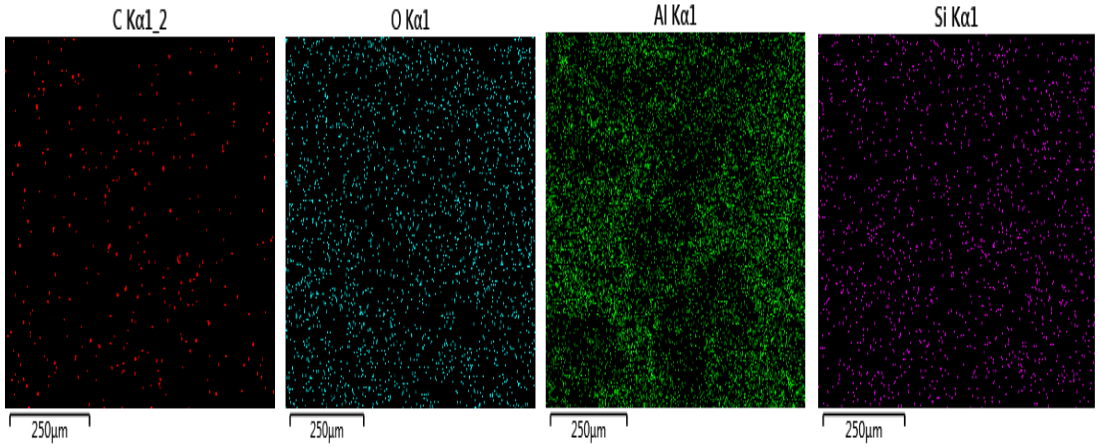

Figure 19 EDX mapping of Al2O3-10SiC nanopowders at low milling conditions.

4.1.3 XFR Analysis of Al_2O_3-SiC Nanopowders at low milling conditions.

The X-ray fluorescence of the nanopowders prepared at low milling conditions for Al2O3-5SiC and Al2O3-10SiC nanopowders are presented in table 6 and table 7 respectively. Low concentration of zirconia was observed in both compositions. The percentage concentration of zirconia is higher at 10wt%SiC than 5wt%SiC in alumina. This is expected as the wearing rate of the zirconia milling media and balls would be expected to increase with the increasing SiC content and the milling conditions. The high resolution of XRF techniques has made it possible to reveal the presence of zirconia in the milled powder at low milling conditions (100rpm, 2hrs) but with low concentrations which are beyond the detection limit of some other techniques.

Table 6 XFR of Al2O3-5SiC nanopowders at low milling conditions.

Z	Element	Concentration
13	Aluminum	25.15
14	Silicon	1.576
15	Phosphorus	0.2417
20	Calcium	0.1412
40	Zirconium	0.1014

Table 7 XFR of Al2O3-10SiC nanopowders at low milling conditions.

Z	Element	Concentration
13	Aluminum	20.38
14	Silicon	5.879
15	Phosphorus	0.1912
17	Chlorine	0.0759
20	Calcium	0.1965
40	Zirconium	0.1119

4.1.4 SEM, EDX Analysis of Al_2O_3-CNT Nanopowders.

The SEM analysis of alumina-CNT nanopowders were equally done and presented in figure 20-23. As shown in the SEM images in figure 20 and 22, the CNTs were observed on alumina matrix grains and some of the CNTs enveloped the alumina matrix grains. This is expected as the size of CNTs are far lower than the alumina matrix. The average particle size of alumina containing 1%CNTs was determine (figure 20) to be about 220nm. Again, the average particles size of alumina containing 2wt%CNT were determine to be about 180nm (figure 22). Clustering of CNTs was not observed as shown in the SEM images (figure 20 and figure 22) due to effective dispersion of CNT in alumina matrix. There was no observable contamination of the processed nanopowders as depict by the EDS result and if any, it is so minute that it is beyond EDS detection limit. Also to our expectation, we do not anticipate contamination from the powder processing

condition as milling was not involved in the process but only sonication and magnetic stirring were used in the dispersion. Homogenous distribution of CNTs in alumina was observed as indicated by EDS mapping shown in figure 21 and figure 23.

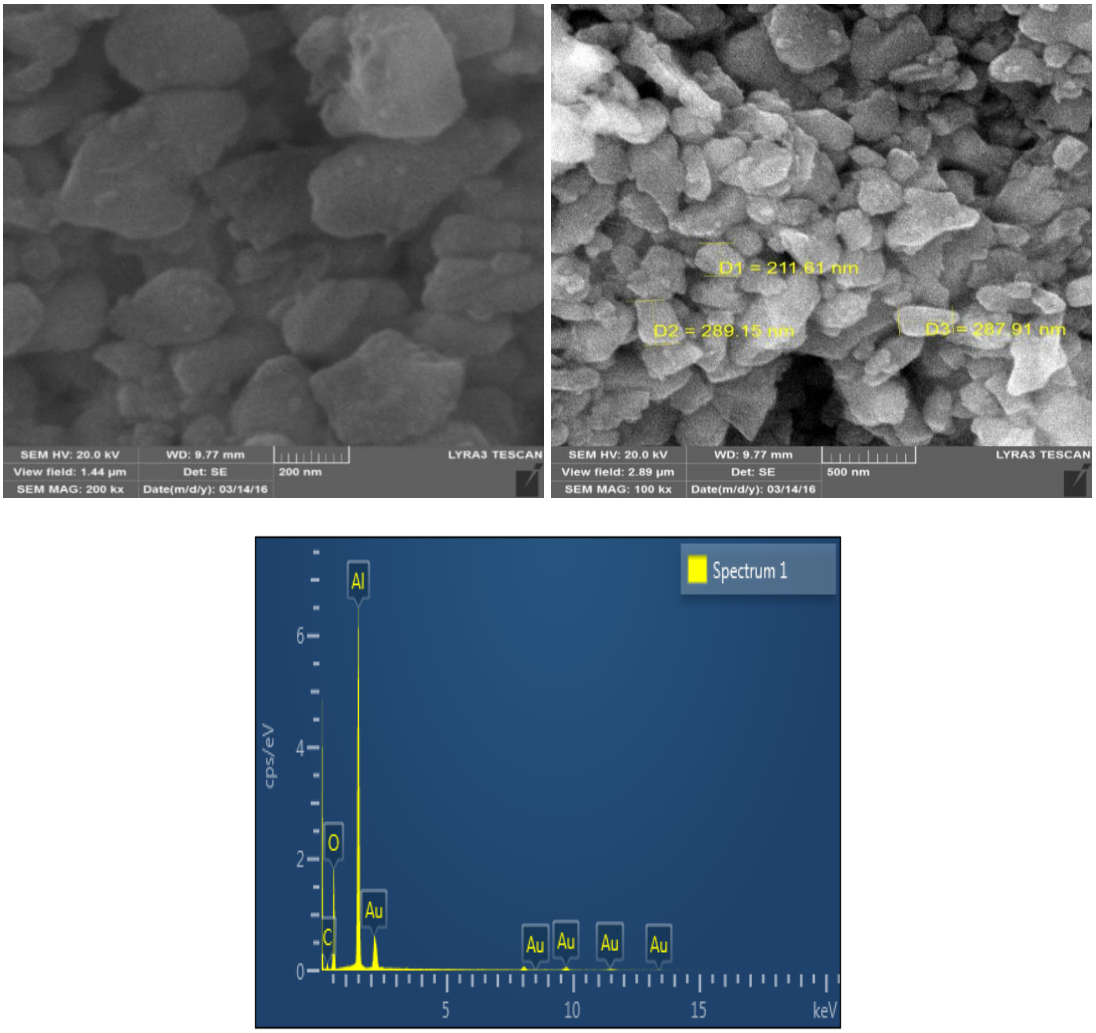

Figure 20 SEM EDX analysis of Al2O3-1%MWCNT nanopowders.

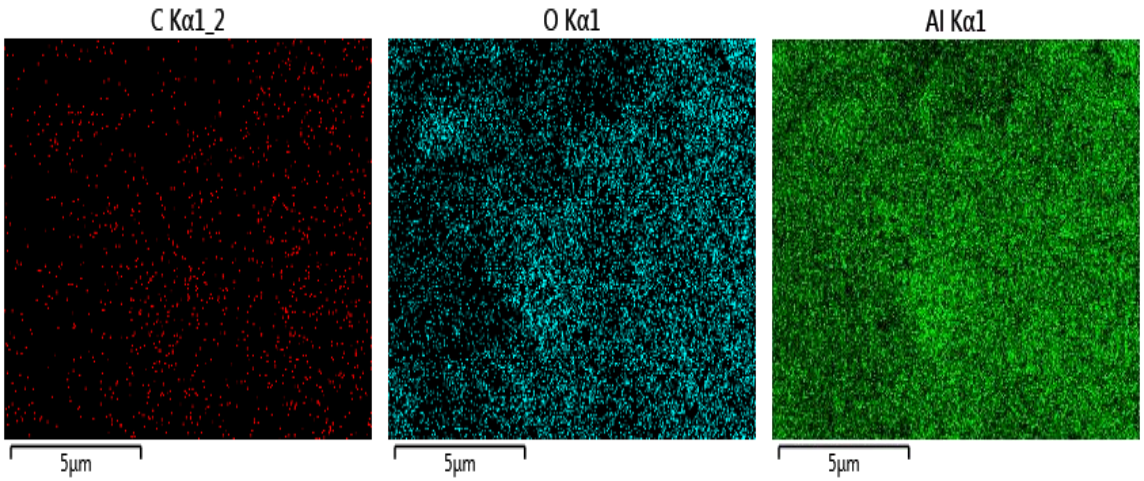

Figure 21 EDS Mapping of Al2O3-1%MWCNT nanopowders.

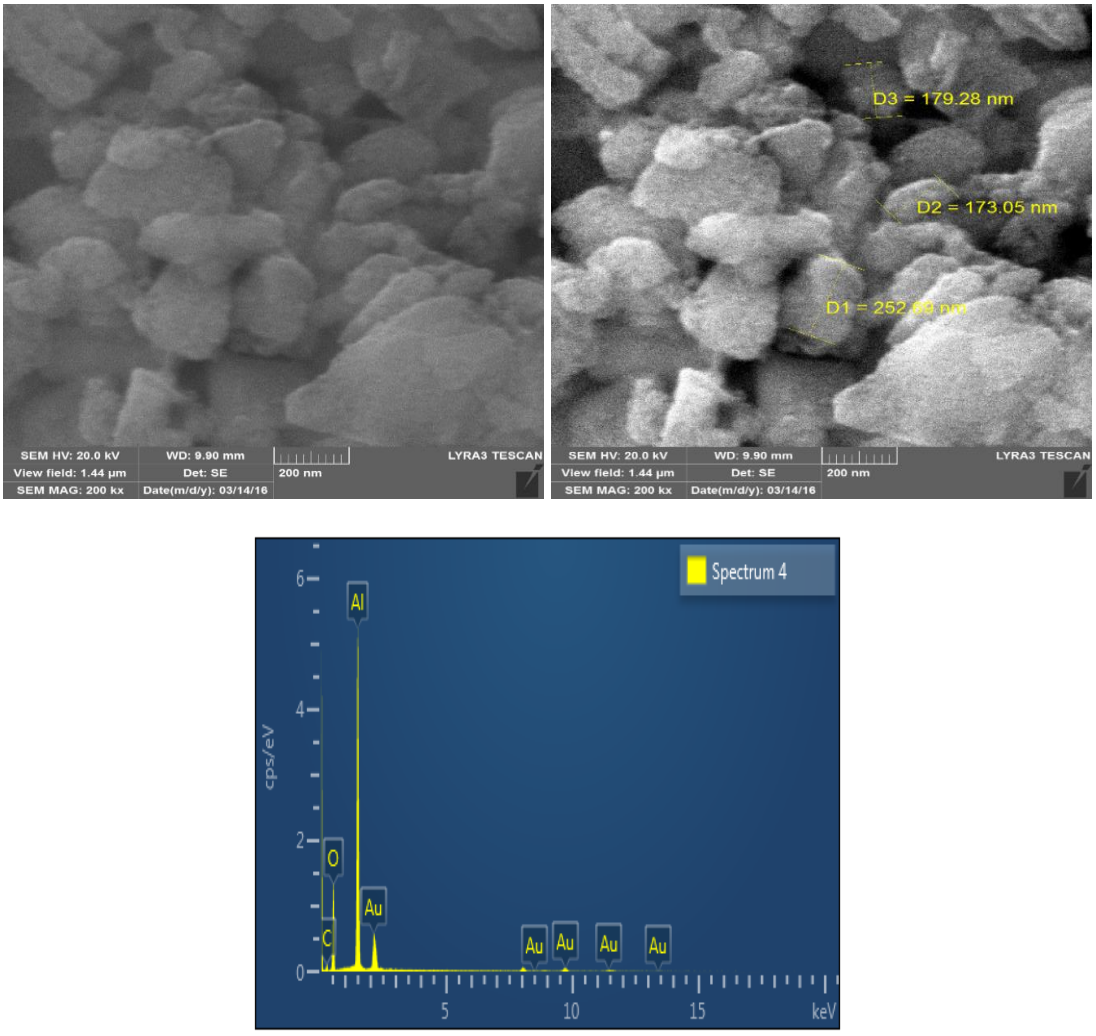

Figure 22 SEM EDS analysis of Al2O3-2%MWCNT nanopowders.

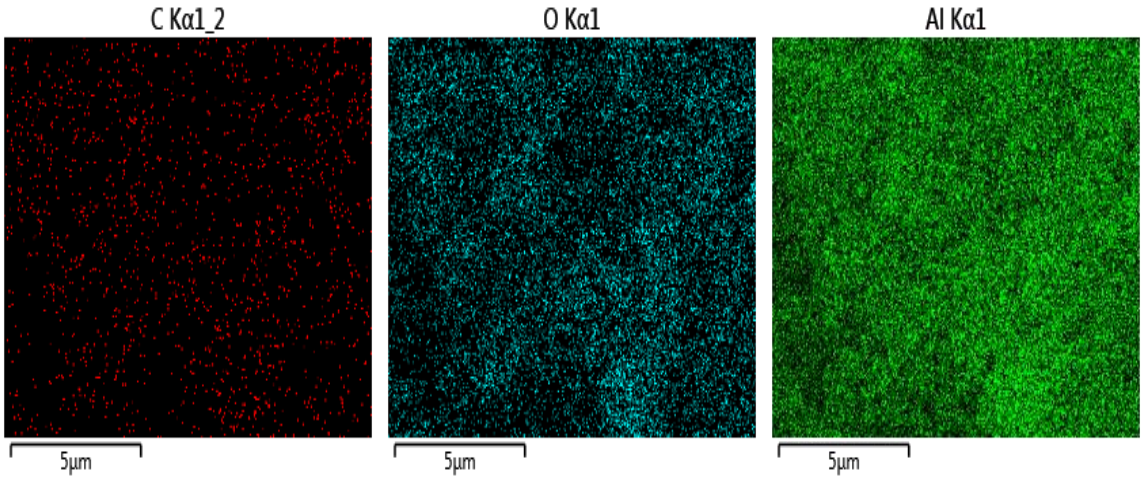

Figure 23 EDS mapping of Al2O3-2%MWCNT nanopowders.

4.1.5 TEM Powder analysis Al_2O_3-SiC and Al_2O_3-CNT Nanopowders

The transmission electron microscope (TEM) of the processed nanopowders are shown in figure 24-25 and figure 27. Figure 24 shows the TEM images of Al_2O_3-5SiC nanopowders prepared at high ball milling conditions. Presence of SiC particles on the alumina grains were observed. The average SiC particles size was determined to be about 30nm. Figure 25 indicates the TEM images of Al_2O_3-5SiC nanopowders prepared at low milling conditions. The average particle size of SiC do not change significantly (about 30nm), however, the shape of alumina matrix is different from that of high milling conditions. Flake like shape was observed here and that shows that the powders were not subjected to severe milling conditions during processing. The TEM EDX analysis of Alumina-SiC nanopowders prepared at low milling conditions is shown in the figure 26. There was no evidence of zirconia contamination and this may be due to the fact that in the TEM analysis, minute powder was used and small area was covered during the analysis. So the little contaminations of zirconia might have escaped the TEM EDS during the analysis.

Similarly, the TEM images of alumina-CNT nanopowders is shown in the figure 27. The CNTs were found linking alumina matrix grains and some enveloped the alumina grains. The average particle size of alumina was determined to be about 160nm which is actually close to the true value of the starting alumina powder (150nm).

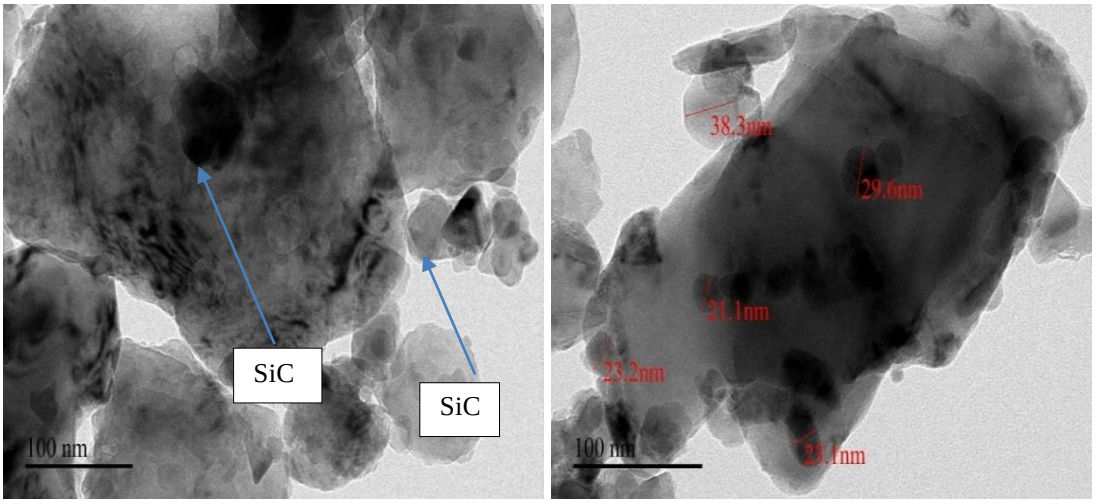

Figure 24 TEM images of Al2O3-5SiC nanopowders at high milling conditions.

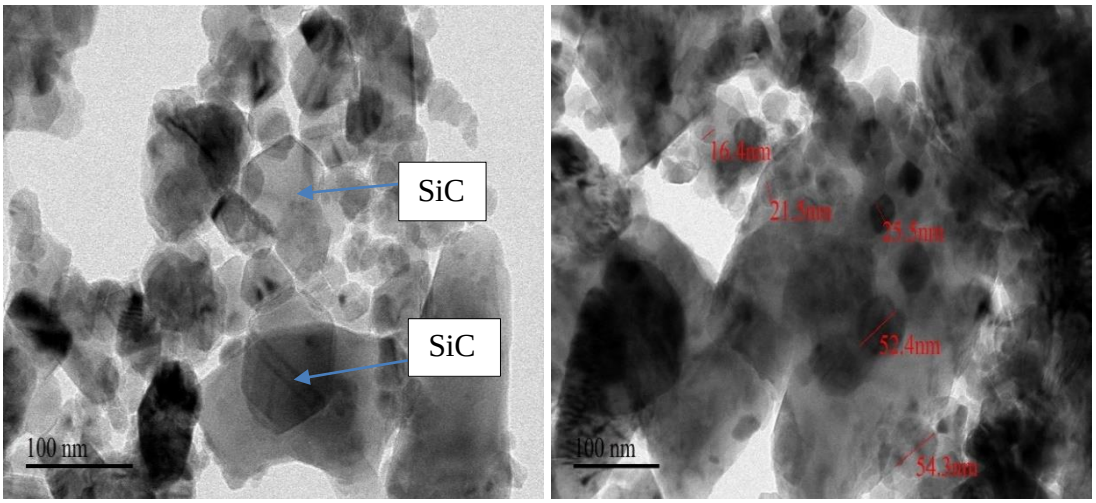

Figure 25 TEM images of Al2O3-5SiC at low milling conditions.

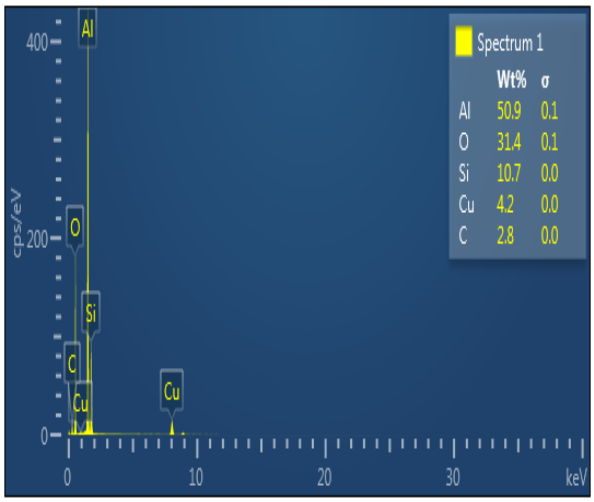

Figure 26 TEM EDS analysis of Al2O3-SiC Nanopowders Prepared at low milling conditions.

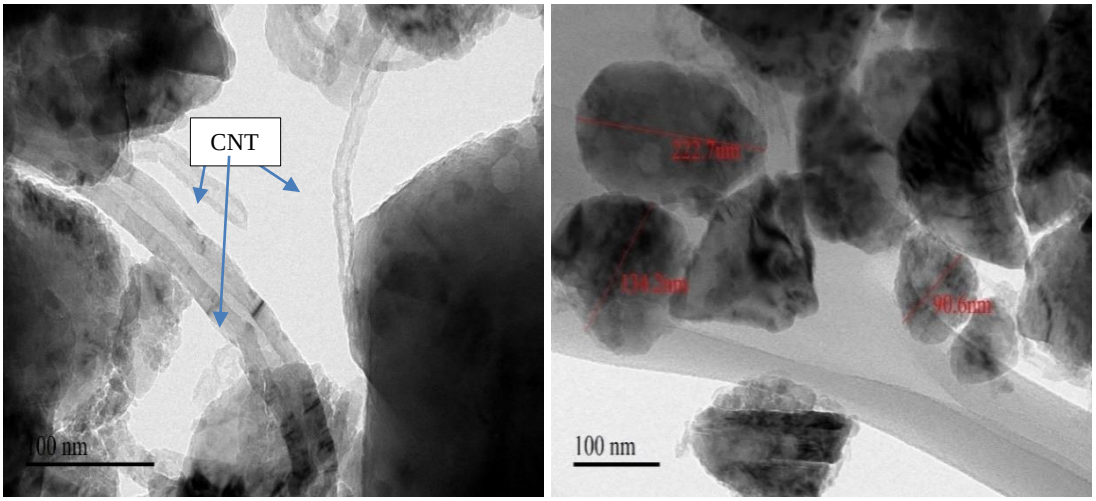

Figure 27 TEM images of Al2O3-CNT Nanopowders.

4.1.6 XRD Analysis of the Nanopowders

X-ray diffraction of the as-received alumina and SiC nanopowders is presented in figure 28. The peaks of α-alumina were identified while that of the β-SiC peaks were also

discovered. This confirmed that the as-received powder alumina is α-alumina (corundum) and while the as-received SiC nanopowders is β-SiC nanopowders.

Figure 29 shows the XRD peaks of alumina containing 5wt% and 10wt% SiC nanopowders prepared at high milling process (300rpm, 4hrs). The peak of β-SiC was identified as indicated in the figure while α-alumina peaks were also revealed which dominate that of the β-SiC peaks as the concentration of alumina is much higher than the SiC nanoparticles. Aside these two materials, there was no extra peaks corresponding to other materials and that implies that the concentration of zirconia as reveal by EDX is beyond the detection limit of XRD.

The processed Alumina-SiC nanopowders at low milling speed of 100rpm and 2hrs milling time is shown in the figure 30. The XRD peaks corresponding to β-SiC and α-alumina were identified as presented in the figure 30. There was slight increase in peak width in alumina containing 5wt%SiC than the alumina containing 10wt%SiC. This implies that there was particle size reduction with the addition of more SiC to alumina. Although other things such as the peak position and the intensity of the peaks are almost the same but the intensity of the β-SiC is higher in alumina containing 10wt%SiC nanopowders than the intensity at 5wt%SiC in alumina. Besides, there was no extra peaks identified in the spectrum and this could mean that contamination if any was below the detection limit of the XRD instrument. Comparing figure 29 and figure 30, we have observed that there was peak broadening in figure 29 than figure 30 and this is expected as high milling of powder (figure 29) involves particle size reduction as well as

homogenous distributions of the nanoparticles while in figure 30 (low milling process) is simply dispersion of the SiC nanoparticle in alumina matrix.

Figure 31 shows the XRD spectrum of as received alumina and MWCNT functionalized. Figure 32 indicates the XRD peaks of alumina-MWCNT nanopowders prepared using a combination of sonication and magnetic stirring. Only α-alumina peaks were identified which means that there was no extra peak observed and that indicates that there was little or no contaminations during the preparation of the powders or if contamination occurred, it is so minute that the XRD cannot detect it. The peaks are all α-alumina as the concentration of MWCNT (1 and 2%) are too low to be detected by the XRD instrument.

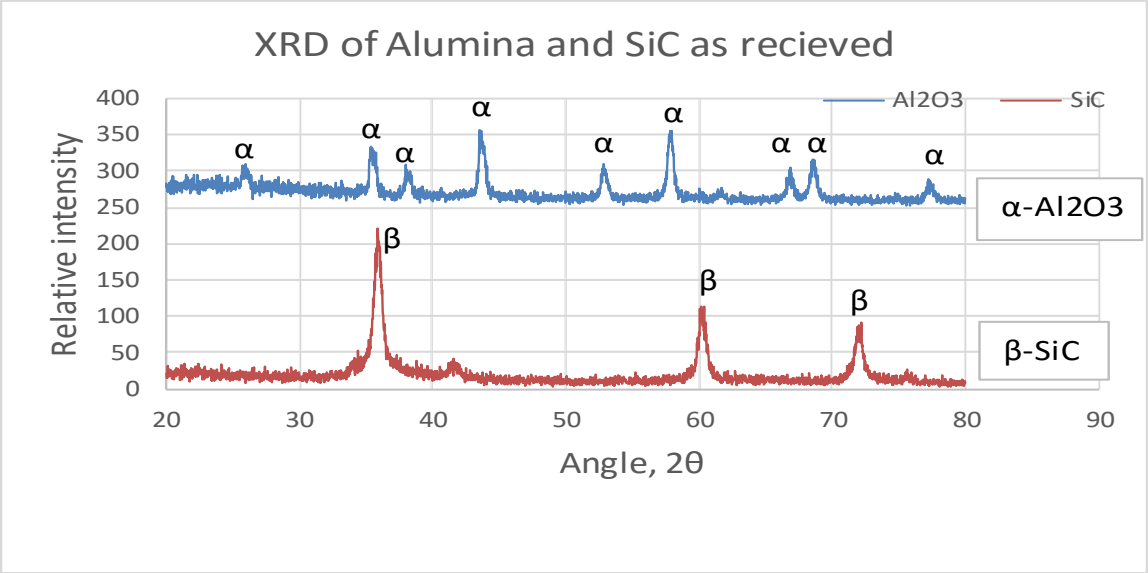

Figure 28 X-ray diffraction of alumina and SiC powders as -received.

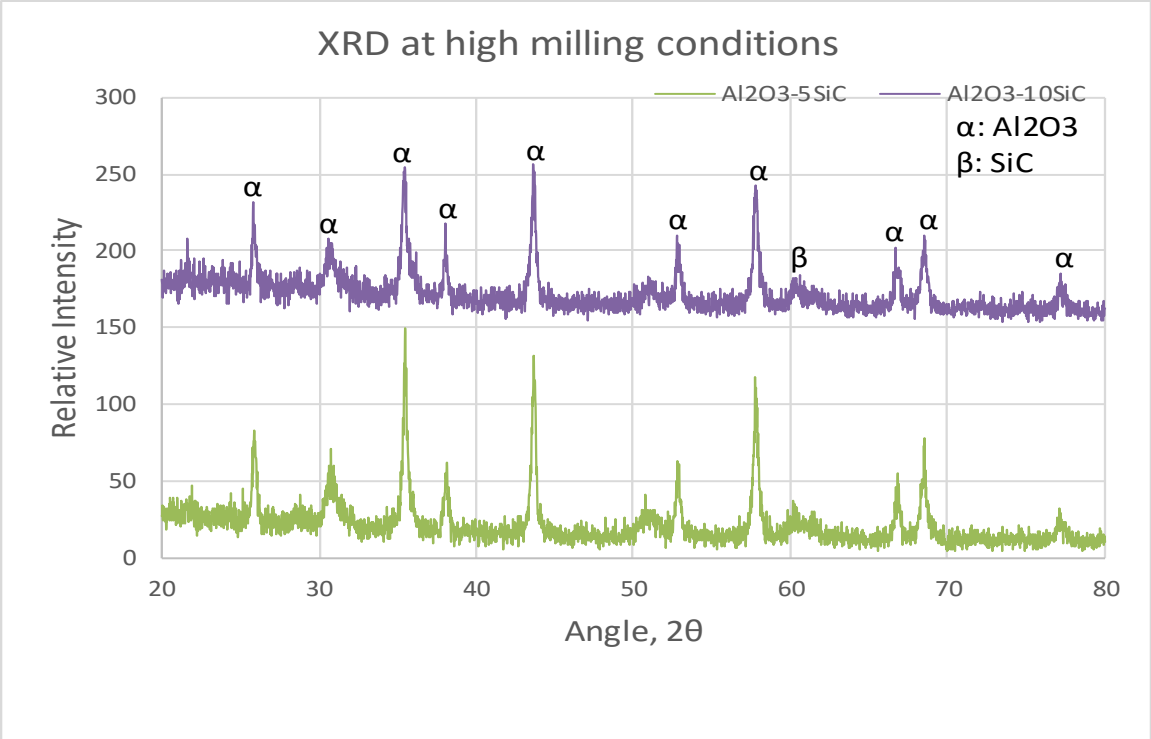

Figure 29 XRD of Alumina-SiC nanopowders prepared at high milling conditions.

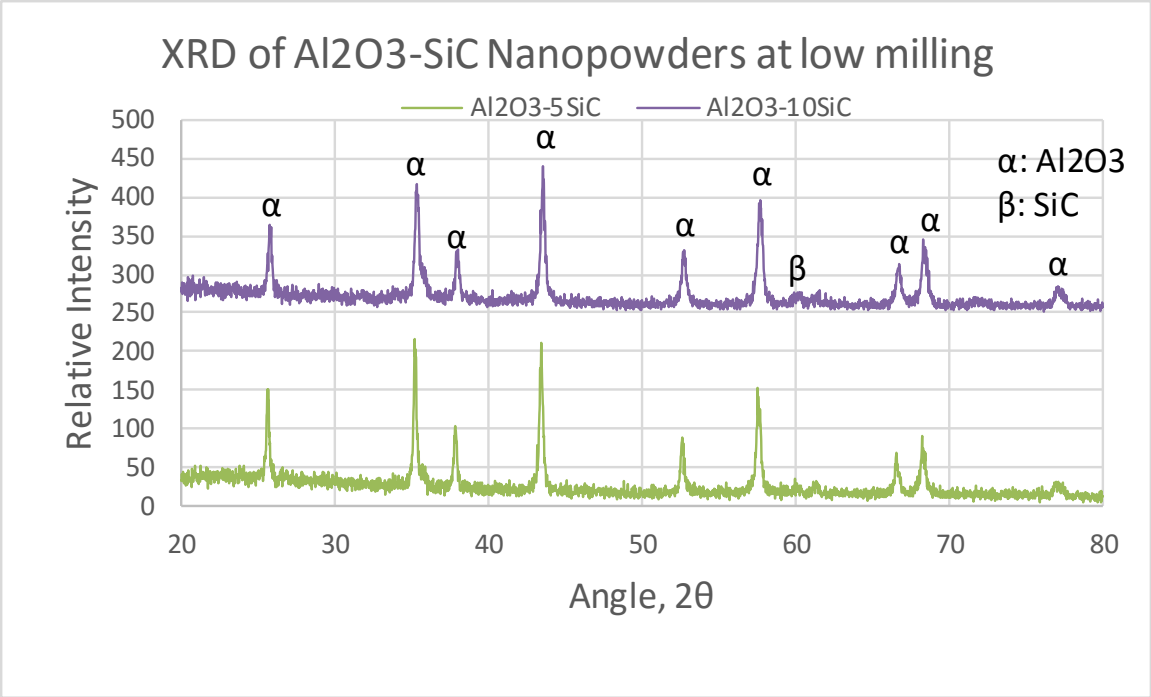

Figure 30 XRD of Alumina-SiC nanopowders prepared at low milling conditions.

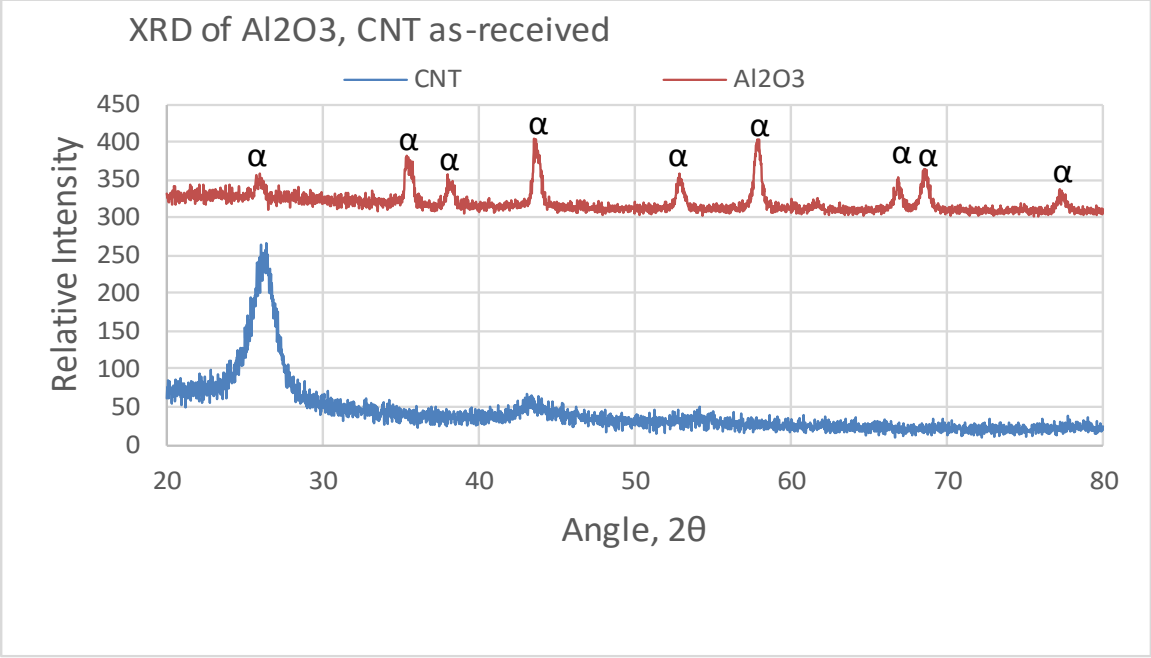

Figure 31 XRD of as received alumina and MWCNT Powders.

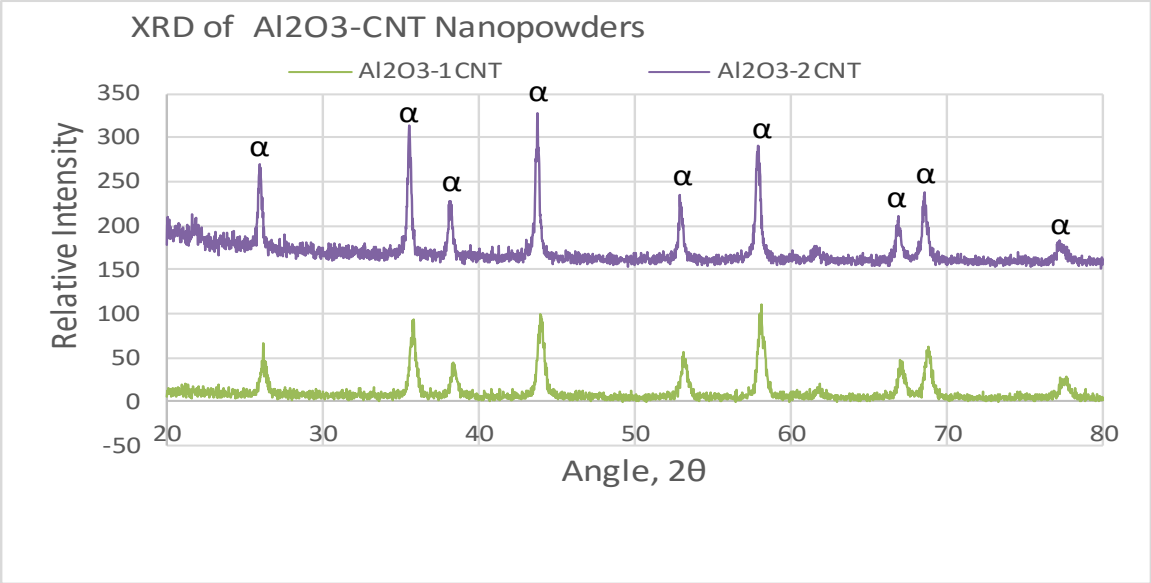

Figure 32 XRD of Alumina-MWCNT nanopowders.

4.2 Nanocomposites Consolidated by Spark Plasma Sintering

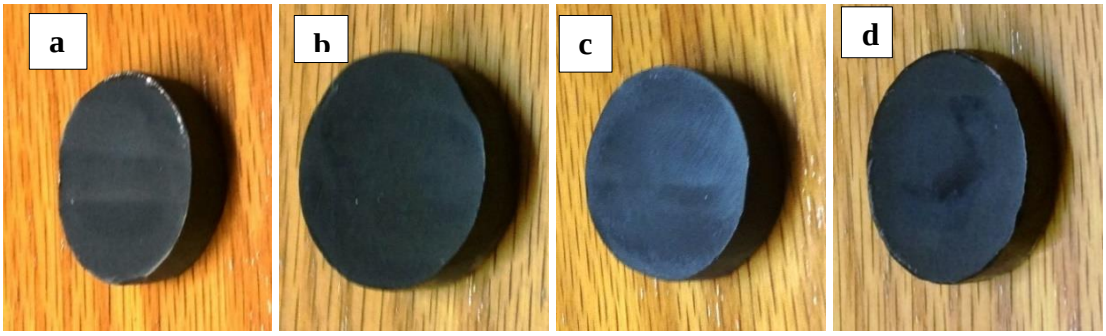

Figure 33 (a) Al2O3-10SiC (b) Al2O3-5SiC, (c) Al2O3-2MWCNT and (d) Al2O3-1MWCNT nanocomposites sintered at 1500°C.

4.3 Densification of the Nanocomposites

The bulk density of the nanocomposites was measured using Archimedes' method. The densification which is the measure of the level of porosity in the samples was determined by dividing the bulk density of the nanocomposites by the theoretical density calculated using the rule of mixture The term densification refer to the reduction in the porosity of the sintered body which occurred through solid state diffusion. Solid state diffusion is broadly categorized into surface diffusion, grain boundary diffusion and volume diffusion. Surface diffusion occur at relatively low temperature and this does not contribute significantly to densification. Volume diffusion takes place at moderate temperature and the contribution to the porosity reduction is not that significant as well. However, grain boundary diffusion occurs at a relatively high temperature and this contribute immensely to the densification of the sintered body. Figure 34 shows the relative density of monolithic (pure) alumina consolidated at 1000, 1300 and 1400°C. low relative density (66.5%) was achieved in the monolithic alumina at 1000°C. The relative

density increase as the SPS temperature is increase to 1300°C and maximum relative density was achieved at 1400°C. Interestingly, there is no significant difference in the densification value between 1300° (99.1%) and 1400° (99.6%) SPS temperature. Thus, increasing the sintering temperature of alumina from 1300°C to 1400°C do not result into significant pore reduction rather, the grain growth of alumina occur which could degrade the interesting properties of alumina. Figure 35 shows the relative density of the nanocomposites prepared at high milling conditions (300rpm, 2hrs). The relative was found to increase slightly with SPS temperature while it decreases with increasing SiC contents. Also figure 36 shows the relative density result of Alumina-SiC nanocomposites prepared at low milling conditions (100rpm, 2hrs). Higher densification (low porosity) was achieved at higher sintering temperature. As shown in figure 35 and 36, maximum densifications (98.57% and 99.01%) was achieved for Al_2O_3-5SiC nanocomposites sintered at 1500°C prepared at high milling conditions and low milling conditions respectively. For Nanocomposites prepared at high milling conditions (300rpm and 4hrs milling), the relative density reduced slightly as the sintering temperature decrease from 1500°C to 1400°C. Increasing densification with temperature is due to increase in grain boundary diffusion as the sintering temperature is raised. This close the pore spaces in the powders which clearly formed define grain boundaries. Also, as the SiC content increase from 5wt% to 10wt%, the density of the nanocomposites decrease slightly with the increasing SiC particles in alumina. This is because, at 5wt% SiC in alumina, there was less efficient pinning of the alumina grain and as such the grain boundary can migrate more efficiently leading to the closure of the pores. When the content of the SiC nanoparticles increase to 10wt%, the pinning effect was enhanced and

the grain boundary sliding is inhibited. Therefore, grain boundary diffusion is reduced with increasing content of the SiC nanoparticles. Moreover, the nature of the nanocomposite powders preparation involves microstructural arrangement in which the SiC nanoparticles are located at the interfaces of alumina grains that act as an obstacle to grain boundary migration by pinning mechanism. The use of pressure assisted techniques such as SPS can enhance grain boundary diffusion and accelerate grain boundary motion as compared to pressureless sintering techniques. Besides, pressureless sintering cannot achieve higher densification when the volume fraction of the SiC nanoparticles exceed 10vol%. The combination of magnetic stirring, sonication and mechanical ball milling during powder preparation as used in this work result in the distribution the SiC particles and position it at the interfaces between the alumina grains acting as obstacles to densification; retarding grain boundary migration through pinning mechanism. The pinning efficiency of the SiC particles on the alumina grains increase with increasing content of the SiC particles. Spark plasma sintering is highly efficient in the densification of ceramic-based nanocomposites with excellent mechanical properties due it high heating rate and short holding time which reduce the problem of grain growth in nanostructured materials. Although Parchiovansky et al.[17], reported maximum relative density of 98.7% on alumina containing 5vol% SiC and this decrease slightly to 98.2% when the SiC content increased to 10vol% after hot pressing at a temperature of 1740°C. The high relative density (99.01%) achieved in this work have shown that SPS is an efficient consolidation technique for Alumina-SiC nanocomposites. The slight disparity in the densification result achieved in this work and the previous work of Parchoviansky et al. may be due to the differences in the consolidation techniques employed even

though high sintering temperature (1740°C) was employed in the case of Parchiovansky et al. it does not give better densification result than SPS as evident in this work. Moreover, Alumina-SiC nanocomposites lose their thermal stability beyond 1500°C through grain growth; that impairs the mechanical and some functional interesting properties of the nanocomposites. Thus, to preserve the nanofeatures of the Alumina-SiC nanocomposites, SPS is a better technique of consolidation.

Figure 37 shows the densification result of alumina-CNT nanocomposites prepared by spark plasma sintering (SPS). Above 99% relative density was achieved on alumina containing 1wt%MWCNT consolidated by SPS at 1500°C. The densification reduced to 98.42% when the MWCNT content increase to 2wt%. Also, slight increase in relative density with SPS temperature was equally observed in the nanocomposites of the same compositions. For example, alumina containing 1wt%MWCNT nanocomposites has a measured relative density of 99% at 1500°C SPS temperature and this decreases to 98.77% as the sintering temperature fall to 1400°C. It appears as shown in figure 37, that the effect of MWCNT content on densification is more prominent than the SPS temperature. The high aspect ratio, high specific surface area and chemical incompatibility with the alumina matrix contributed to the reduction in densification with the increasing CNT contents. CNTs reduces densification through efficient pinning of the alumina grains that results in the reduction of grain boundary mobility which impairs densification. Imperfect de-agglomeration of CNTs can equally reduce densification as agglomerates acts as solid obstacles at the grain boundary interfaces which hamper densification. The effect of densification with increasing content has been studied by Kumari et al.[19], after hot pressing alumina containing 7.39MWCNT.82.4% was

reported densification and this decreases to 59.2 as the MWCNT content increase to 19.1wt% at SPS temperature of 1550°C. Also, Inam et al.[70], reported 88% densification on alumina-CNT nanocomposites containing 2wt% CNT at SPS temperature of 1400°C and this increase to 98% densification when the SPS temperature increase to 1600°C.

The densification process in CNT-alumina composites involves elimination of pores and mass transportation by bulk diffusion or surface diffusion and this are the two most important factors that determine the resultant density of the material. It was conceived that existence of CNTs in the grain boundaries act as barriers to avoid the closing up of the grains. As reported by Kumari et al.[19], the grain growth of the alumina matrix is inhibited greatly by CNTs and that makes it unfavorable to the densification when the content of CNT is relatively high. Also the presence of clusters of CNTs at the grain boundaries due to improper de-agglomeration can equally lead to low density of the CNT-alumina nanocomposite. Agglomerated CNTs are more efficient than the individual nanotubes as the later act as solid obstacles at grain boundaries interfaces which reduces grain boundary mobility and impair densification. This buttress the notion that, the densification of alumina containing CNTs nanocomposites becomes difficult, when the content of CNTs increased. The relative density of 10vol%SWCNT-alumina nanocomposites was studied by Zhan and Mukherjee[71], after SPS consolidation. The relative density was found to decrease from 95.2% to 86%when the sintering temperature is reduced from 1150°C to 1100°C which clearly demonstrated that spark plasma sintering is an effective technique to obtained near full densification of nanocomposites with minimum damage to CNTs.

Based on the results achieved in this work, we can therefore conclude that the density of Alumina-SiC and alumina-CNT nanocomposites decrease with the increasing contents of the nanophase (SiC and MWCNT) but the density of the nanocomposites increases with the SPS temperature. The high densification of the nanocomposites achieved in this work relative to the reported result in the literature shows that spark plasma sintering is an effective tool in the densification of alumina-based nanocomposites.

The use of pressureless sintering of alumina-MWCNT nanocomposites have been reported in literature[87,95], which is usually carried out in the temperature range of 1200 and 1800°C in an inert atmosphere to avoid oxidation damage to CNTs. for example Sarkar and Das[87], consolidated alumina containing 1.2wt%MWCNT by pressureless sintering at 1800°C and reported 92% relative density. Compare the relative density achieved in this work with the one reported by Sarkar and Das, it is clear that at all SPS temperature (1300, 1400 and 1500°C) and compositions (1 and 2wt%MWCNT) the relative density is higher and that shows that pressureless sintering even though it is done at relatively high temperature cannot achieve high densification relative to SPS. Yamamoto et al.[99], also observed decrease in densification of alumina-MWCNT nanocomposite sintered by SPS from 99% to 94% when the MWCNT content increase from 0.5vol% to 3vol%. The high heating rate, use of relatively low sintering temperature and shorter sintering time offer by SPS has made it a better technique to achieve high densification and produce nanocomposites of fine grain microstructure with better mechanical properties. In conclusion, the slight increase density of alumina-MWCNT nanocomposites with SPS temperature as reported in this work is due to enhance grain boundary diffusion with temperature and consequently closure of the pores

between the nanoparticles. Again, the slight decrease in the relative density of nanocomposites with increasing content of MWCNT was due to the formation of agglomerations and the position of the CNTs at the grain boundaries which tend to reduce the grain boundary migration. The high the content of the CNTs at the boundaries, the more effective in retarding the grain boundary sliding and this deceases the relative density of the nanocomposites.

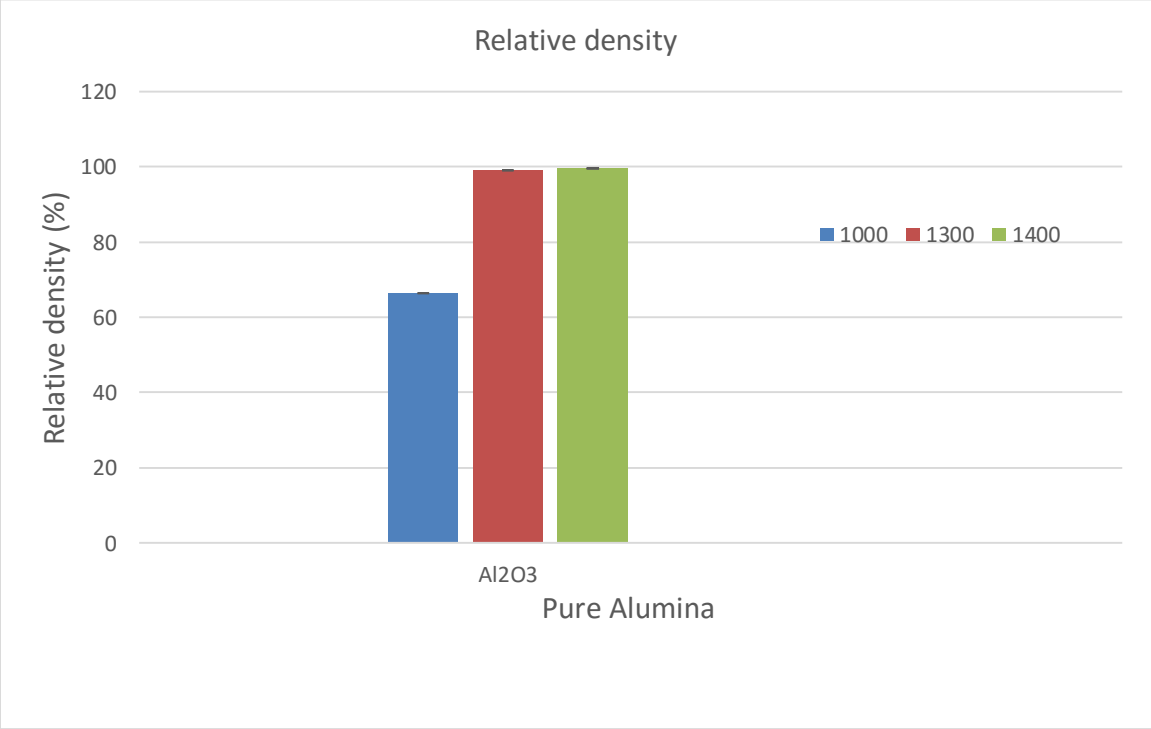

Figure 34 Relative density of pure alumina at different SPS temperature.

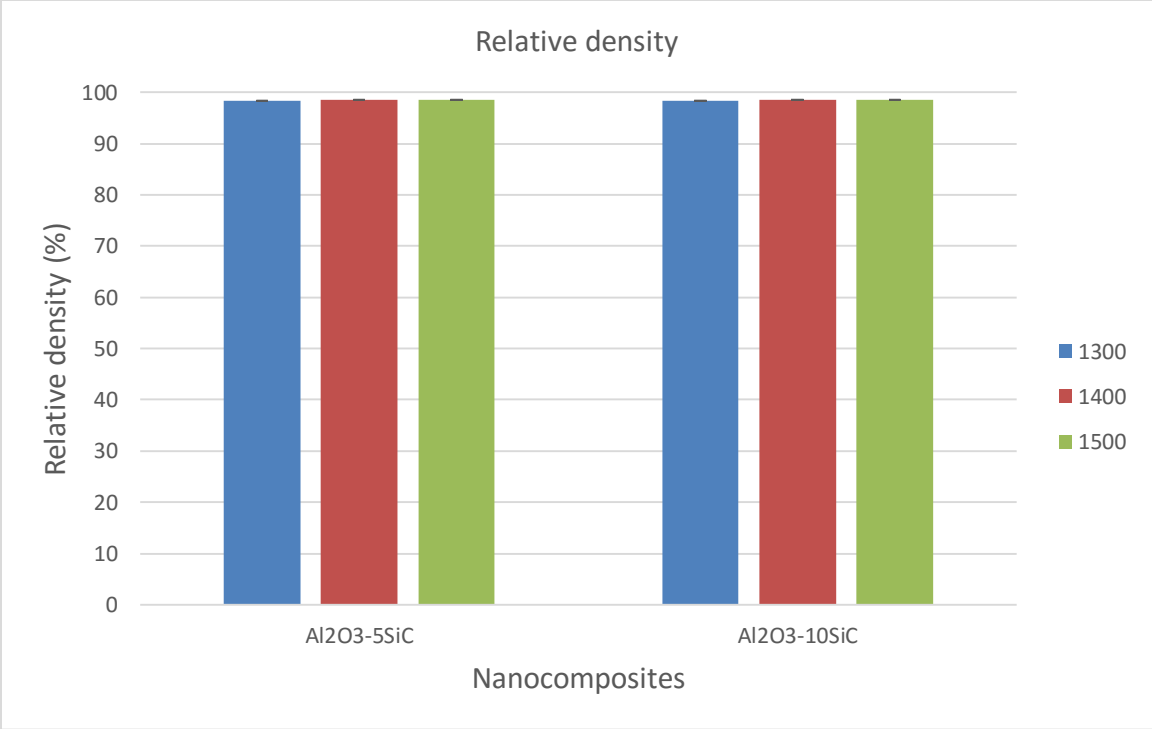

Figure 35 Relative density of Al2O3-SiC Vs SPS Temperature prepared at high milling conditions.

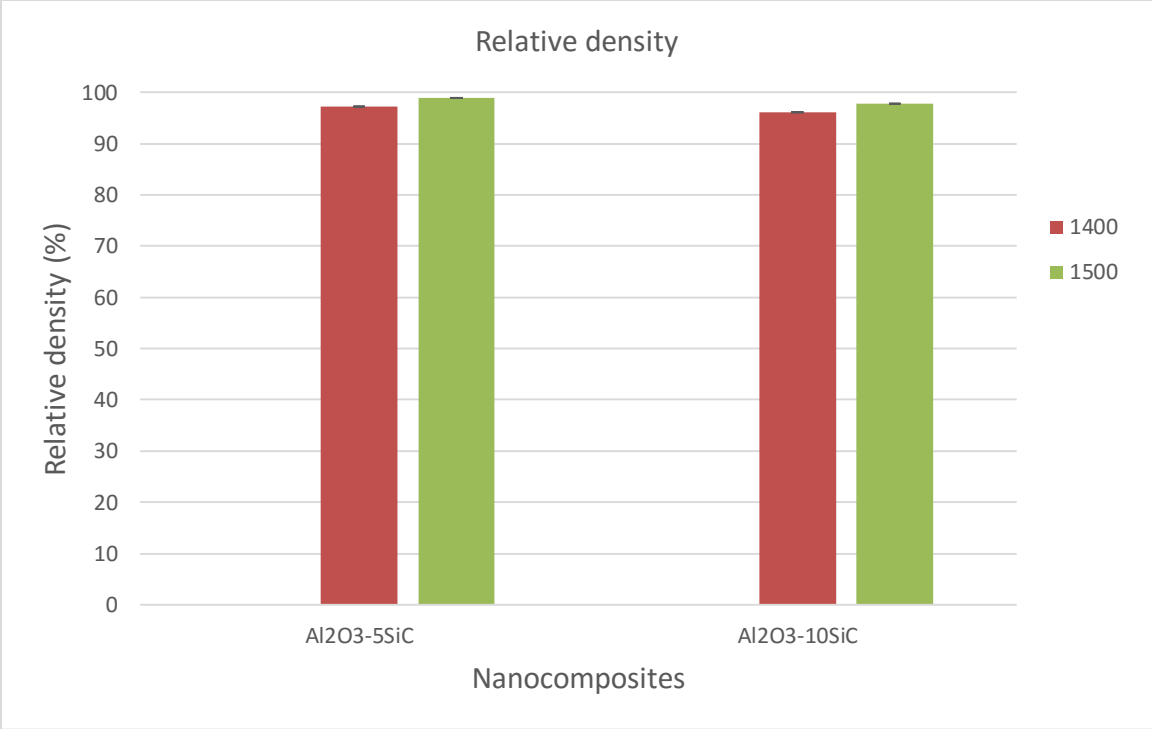

Figure 36 Relative density of Al2O3-SiC nanocomposites prepared at low milling conditions.

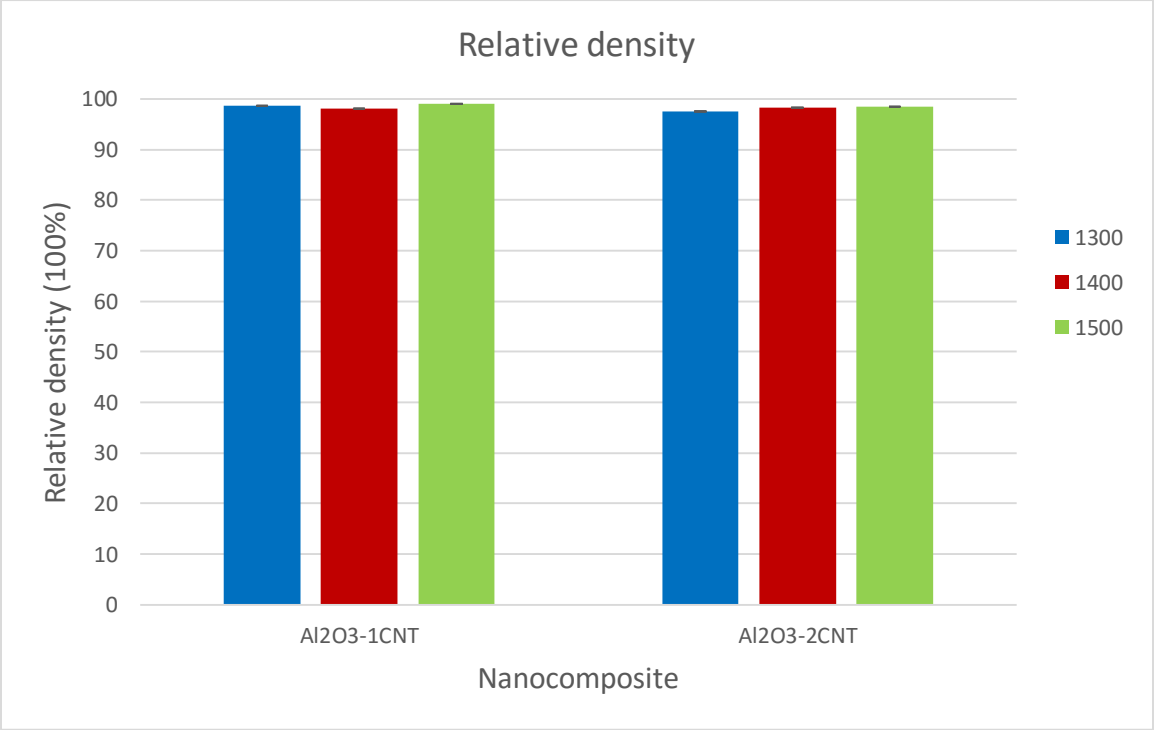

Figure 37 Relative density of Al2O3-CNT Nanocomposites.

4.4 Thermal Properties of Alumina-based Nanocomposites

It is important to remark here that the thermal properties of the Alumina-SiC nanocomposites prepared at high milling conditions (300rpm, 4hrs and p: b 1:10) will not discussed as the powder analysis have shown that there was zirconia contamination which will definite affect the thermal properties of the nanocomposites.

4.4.1 Thermal Diffusivity

Thermal diffusivity is the measured of the speed with which thermal energy is propagated through a material by conduction. Nanocomposite materials have high surface area which promotes scattering of phonons with the ultimate reduction in the thermal diffusivity. Figure 38 shows the thermal diffusivity of monolithic alumina densified by SPS. The thermal diffusivity increase with the SPS temperature and this could be due to reduction in the porosity. At 1000°C SPS temperature, the thermal diffusivity was 3.15mm^2/s which increased to 7.52mm^2/s as the sintering temperature is raised to 1300°C. This thermal diffusivity result is in support of the densification result which clearly shows that densification is the major factors controlling the thermal diffusivity of monolithic alumina. Figure 40 indicates the room temperature thermal diffusivity of Al_2O_3-5SiC and Al_2O_3-10SiC nanocomposites consolidated by SPS at 1400^o and 1500^{o}C. Thermal diffusivity was found to increase with increasing sintering temperature and the content of the SiC nanoparticles. The thermal diffusivity increase with sintering temperature was previously reported. This increase in thermal diffusivity with SPS temperature was due to the slight reduction in the level of porosity which act as scattering site for phonons.

Porosity, impurities and numerous grain boundaries which exist in nanocomposite materials reduce the phonon mean free path and this reduces the thermal diffusivity of the material. Again, increasing SiC content (from 5wt% to 10wt%) enhance thermal diffusivity of the nanocomposite by a factor of 0.011 as shown in figure 40. This is actually in the trend of the results of Parchiovansky et al.[17], who reported increase in room temperature thermal diffusivity of alumina from $0.093cm^2/$ to $0.135cm^2/s$ on addition of 20vol%SiC particles to alumina. The room temperature thermal diffusivity of Al_2O_3-SiC composites reported in the literature is in the range of 0.13 to $0.16cm^2/s$ [105,110,111]. Although, the thermal diffusivity of nanocomposites densified by SPS as shown in this work is expected to be lower than the reported values in the literature due to high grain boundaries and fine microstructures offered by SPS. Fine microstructures result in large grain boundaries which increase the chances of phonon scattering. As reported in this work, the thermal diffusivity of alumina containing 5wt% SiC nanocomposites increase from $6.037mm^2/s$ to $6.19mm^2/s$ as the sintering temperature increase from 1400°C to 1500°C. Obviously this is a slight increase in thermal diffusivity with temperature as there was no significant change in the densification when the SPS temperature was raised from 1400°C to 1500°C. Also, there was increase in thermal diffusivity from $6.19mm^2/s$ to $6.26mm^2/s$ as the content of SiC nanoparticles in alumina is increased from 5wt% to 10wt%. Comparing the thermal diffusivity of pure alumina (figure 38) and that of Al2O3-SiC nanocomposites (figure 40) it is obvious that the thermal diffusivity of alumina ($7.62mm^2/s$) is higher than the Al_2O_3-10wt%SiC nanocomposites ($6.26mm^2/s$) consolidated at 1500°C. Indeed, the thermal diffusivity of alumina decrease with SiC addition and this reduction depends on the amount of SiC

added and the SPS temperature. Thus, trend of thermal diffusivity increment with sintering temperature and SiC content have stated in the previous work [17,45,105], however, the thermal diffusivity achieved in the current work is lower than the value reported by some authors for both alumina-SiC nanocomposite and monolithic alumina. This disparity could be due to the high aspect ratio of whiskers and platelets which can conduct heat better than the particles. Moreover, SPS consolidation do not promote grain growth leading to fine microstructures with large interfacial boundaries as in the case of this work. This contributes immensely to the scattering of the phonons that lowers the thermal diffusivity of the nanocomposites.

The mechanism of room temperature thermal diffusivity in alumina-CNT nanocomposites is different from that of Alumina-SiC nanocomposites. As shown in figure 41, the room temperature thermal diffusivity of alumina-CNT nanocomposites decrease with increasing CNT content from 1wt% to 2wt%. The high aspect ratio of CNTs increases the chance of forming agglomeration as the content increase. Agglomerated CNTs can form scattering sites which reduce the thermal diffusivity. This is also in agreement with Kumari et al.[19], after SPS consolidation of alumina containing 7.39wt%MWCNT at 1550^{o}C and reported 13.98mm^2/s which decrease to 5.24mm^2/s as CNT content increase to 19.10wt%. However, thermal diffusivity generally increases with sintering temperature due to reduction in porosity. The high efficiency in the pinning mechanism of CNT on alumina matrix also contributed to the reduction in the thermal diffusivity of alumina-CNT nanocomposites with increasing CNTs content. according to Kumari et al, thermal diffusivity of pure alumina was measured to be 8.7mm^2/s which is almost the same value (8.77mm^2/s) achieved in this work for alumina

containing 1wt%MWCNT nanocomposites sintered at 1500°C. Based on the densification results presented in this work, the effect of porosity is not significant as there was no significant difference in the densification results between 1500°C and 1300°C SPS temperature. The effect of interfacial resistance resulting from refine microstructure and poor quality in the interface play dominant role in the reduction of thermal diffusivity achieved in this work.

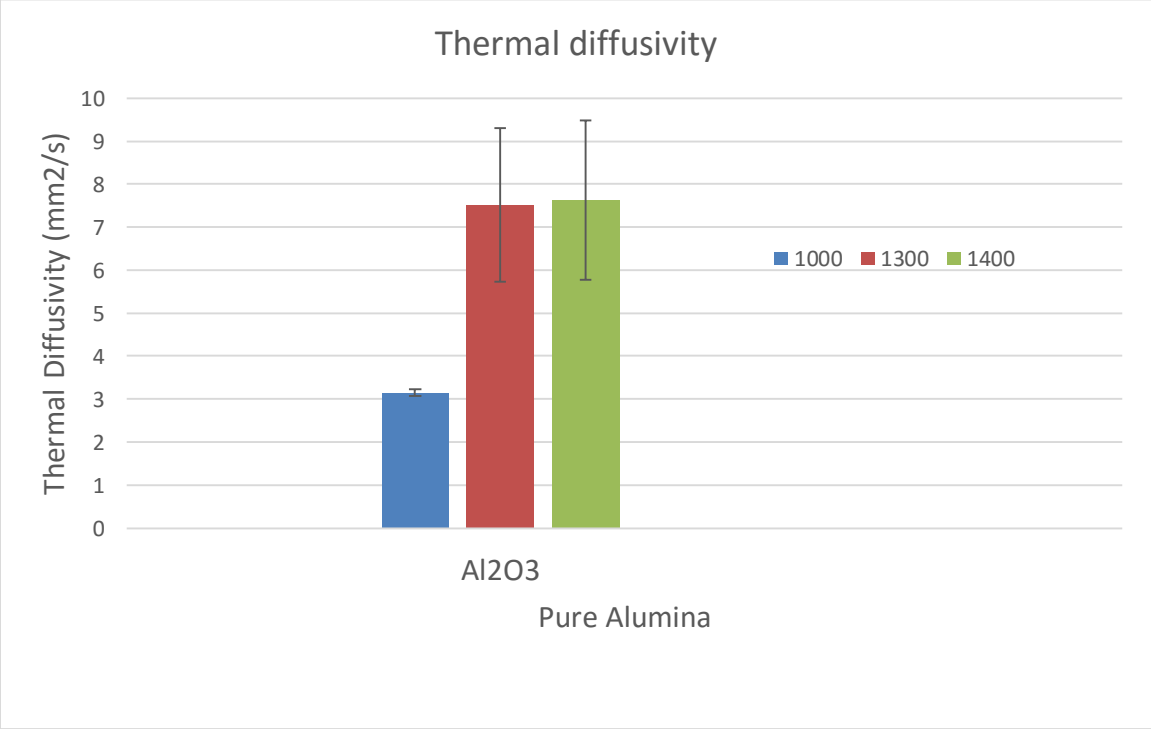

Figure 38 Thermal diffusivity of pure Alumina at different SPS temperature.

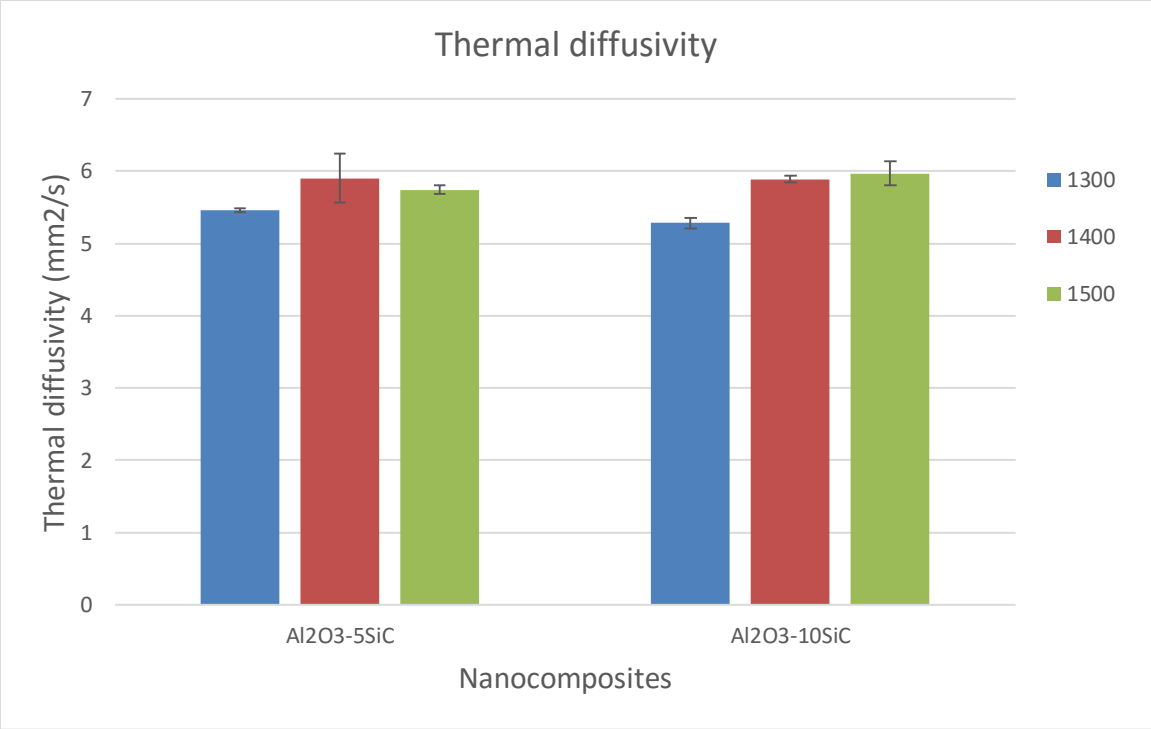

Figure 39 Thermal diffusivity of Al2O3-SiC nanocomposites prepared at high milling conditions.

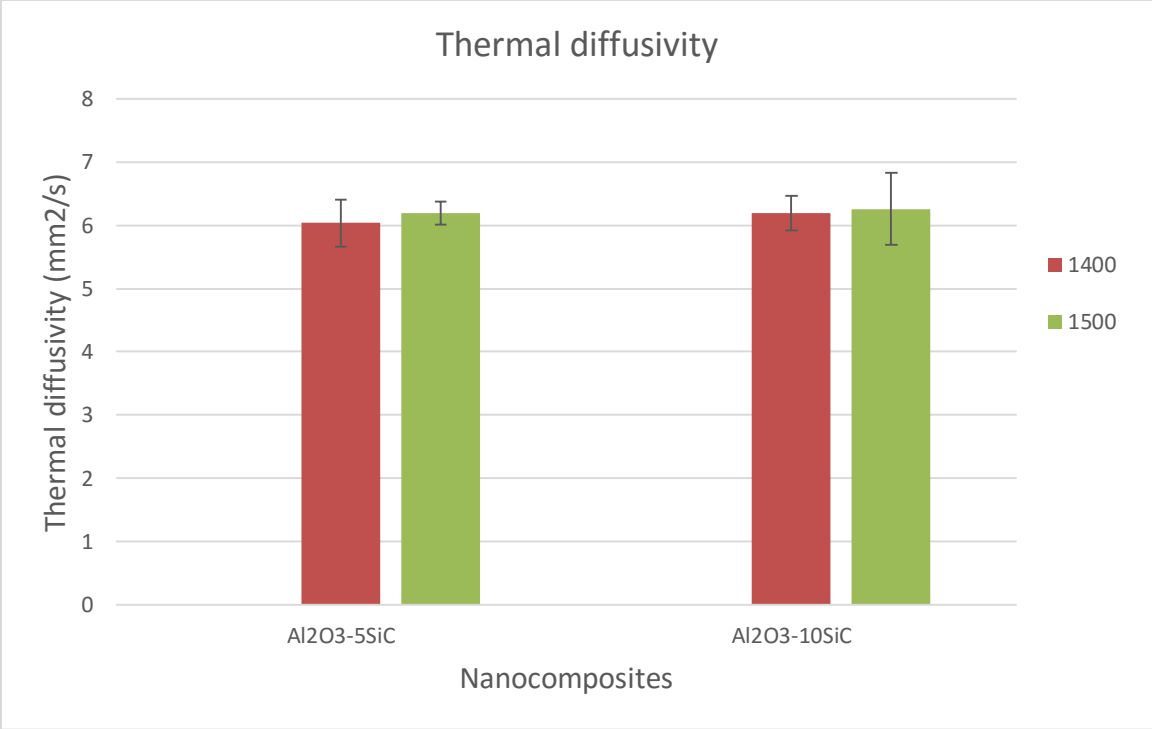

Figure 40 Thermal diffusivity of Al2O3-SiC Nanocomposites prepared at low milling conditions.

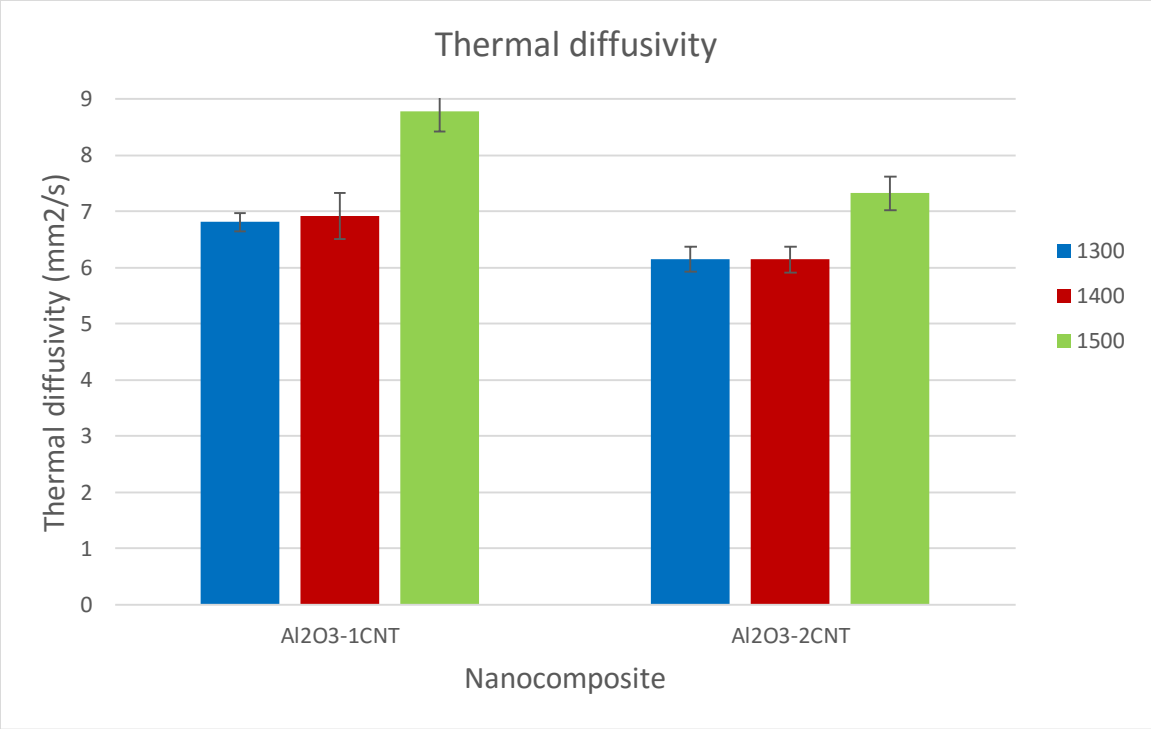

Figure 41 Thermal diffusivity of Al2O3-CNT Nanocomposites.

4.4.2 Specific heat Capacity of the Alumina-based Nanocomposites

Specific heat capacity is one of the thermal properties of materials which measured the ability of the material to absorb heat energy. Specific heat capacity of pure alumina after SPS consolidation at 1000, 1300 and 1400°C is reported in figure 42. Just like thermal diffusivity, the specific heat capacity increase with the increasing SPS temperature and maximum specific heat capacity (1.22J/gK) of monolithic alumina was obtained at 1500°C sintering temperature. Figure 44 shows the room temperature specific heat capacity of Alumina-SiC nanocomposites consolidated by SPS at 1400°C and 1500°C. The specific heat capacity does not increase significantly with SPS temperature however it decreases with the SiC particle content. for example, the specific heat capacity of

alumina containing 5wt%SiC nanoparticles sintered by SPS at 1500°C is 1.01J/gK while that at sintered at 1400°C is 0.996J/gK. When the SiC concentration increase to 10wt%, but at the same SPS temperature (1500°C) the specific heat capacity decrease to 0.896J/gK. The mechanism of specific heat capacity with SPS temperature is not yet clear, although specific heat capacity has direct relation with temperature. The motion of molecules in a matter is a direct measure of it temperature and the greater the motion the higher the temperature. Again, motion of molecules required energy and the more energy the matter acquired, the higher the temperature. The specific heat capacity of 1.01J/gK achieved on alumina containing 5wt% SiC nanoparticles as reported in this work means that 1.01 joules of heat is required to heat 1g of the nanocomposites at 25°C, but when the SiC content increased to 10wt%, the specific heat capacity of 0.896J/gK was achieved and that implies that 0.896 joules of heat is required to heat 1g of the nanocomposites at 25°C. It therefore logical to say that less energy is required for the motion of molecules of alumina containing 5wt%SiC than alumina containing 10wt%SiC nanoparticles. Addition of SiC nanoparticles led to reduction in the energy required to set the molecules in motion as the SiC is a relatively high conducting material. Most high conductivity metals have lower specific heat capacity, for example the specific heat capacity of gold, copper and aluminum are 0.129, 0.385 and 0.902J/gK respectively. Thus, addition of SiC to alumina is expected to increase the thermal conductivity of alumina and lower its specific heat capacity. However, for nanocomposites system with high surface area and large grain boundaries, the energy transportation could encounter obstacles that causes scattering and this result to low thermal conductivity.

Figure 45 shows the specific heat capacity of alumina-CNT nanocomposites prepared by SPS. The maximum specific heat capacity was attained at 1400°C. Almost the same trend exhibited in Alumina-SiC nanocomposite was displayed by alumina-CNT nanocomposites except that highest specific heat capacity was achieved at 1400°C instead of 1500°C SPS temperature in both 1wt%MWCNT and 2wt%MWCNT. For instance, increasing the SPS temperature from 1400°C to 1500°C for alumina containing 1wt%MWCNT decrease the specific heat capacity from 1.093J/gk to 0.865J/gK. Again, decreasing the SPS temperature from 1400°C to 1300°C reduced the specific heat capacity of alumina containing 1wt%MWCNT nanocomposites to 1.093J/gK. This behavior might be attributed to the high aspect ratio of the CNT. At lower SPS temperature, there was little porosities that scattered the energy of the molecules leading to low specific heat capacity. At high SPS temperature of 1500°C, kinks and twists might have formed in the nanotubes and this restrict their transportation efficiency.

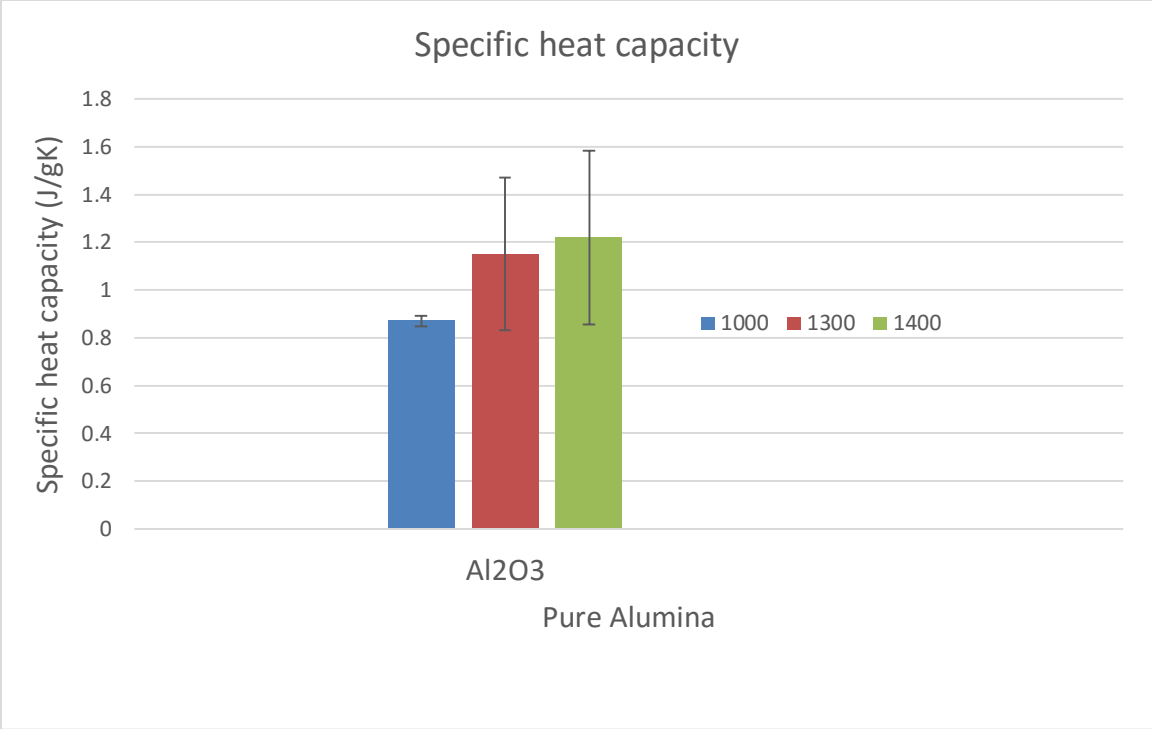

Figure 42 Specific heat capacity at different SPS temperature.

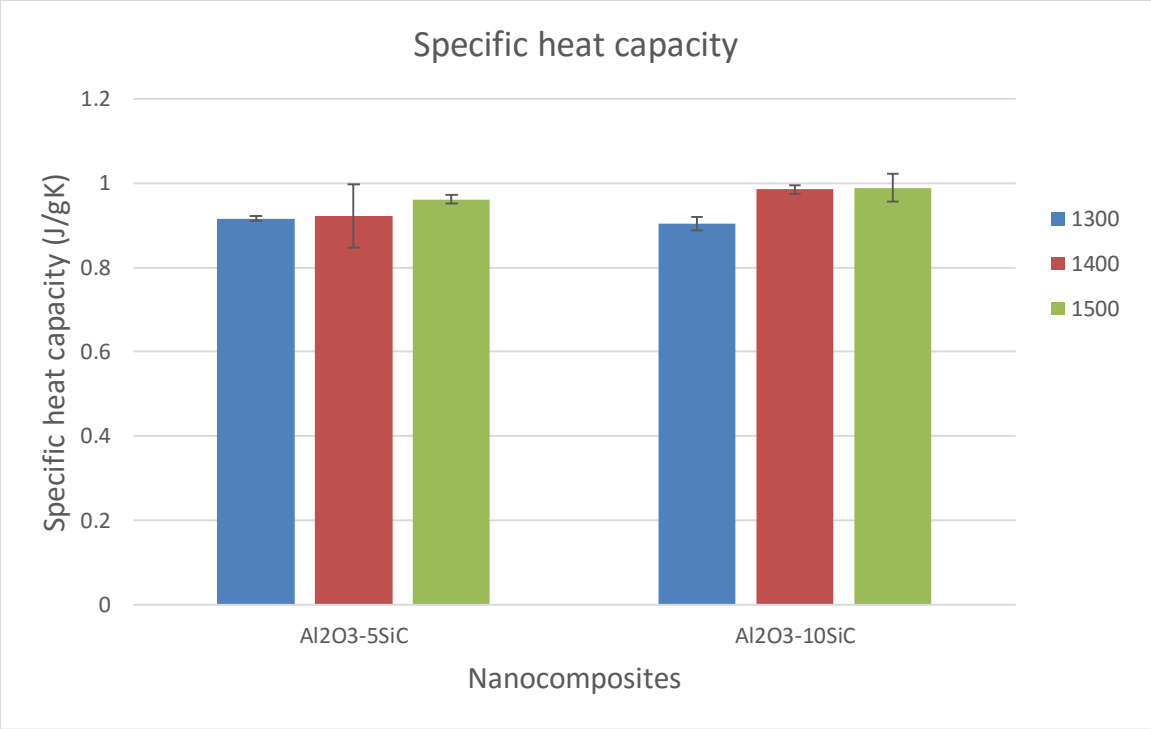

Figure 43 Specific heat capacity of Al2O3-SiC Nanocomposites prepared at high milling conditions.

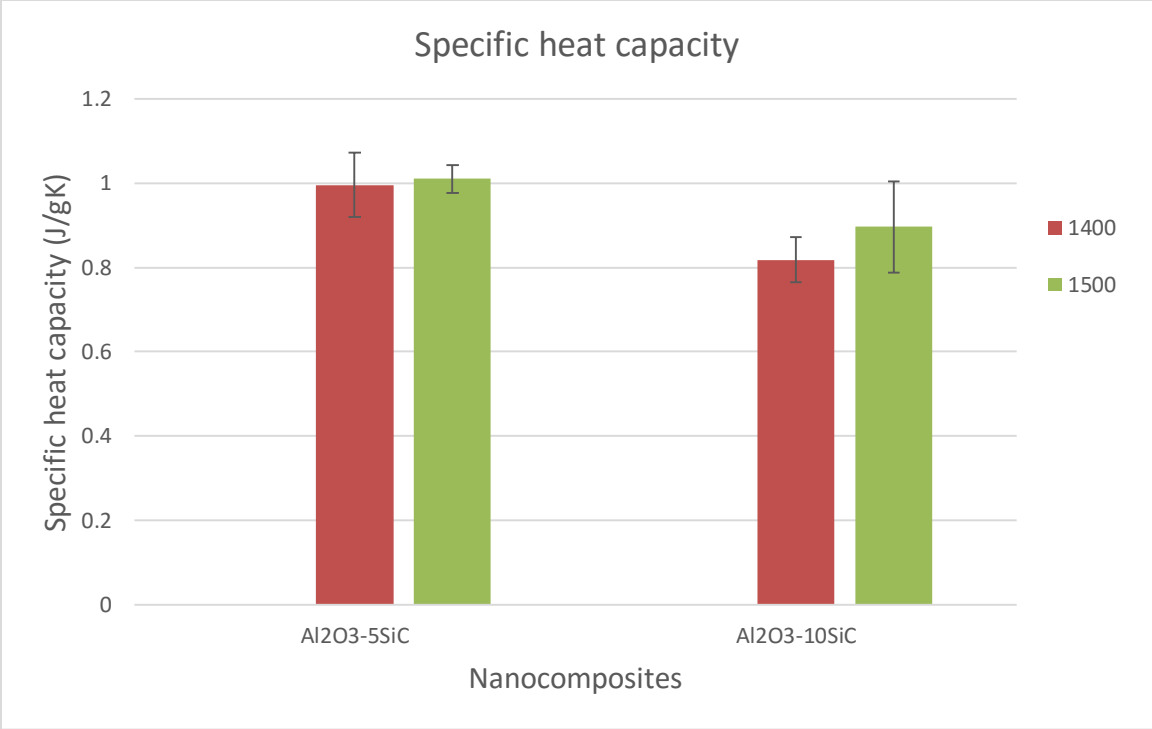

Figure 44 Specific heat capacity of Al2O3-SiC Nanocomposites prepared at low milling conditions.

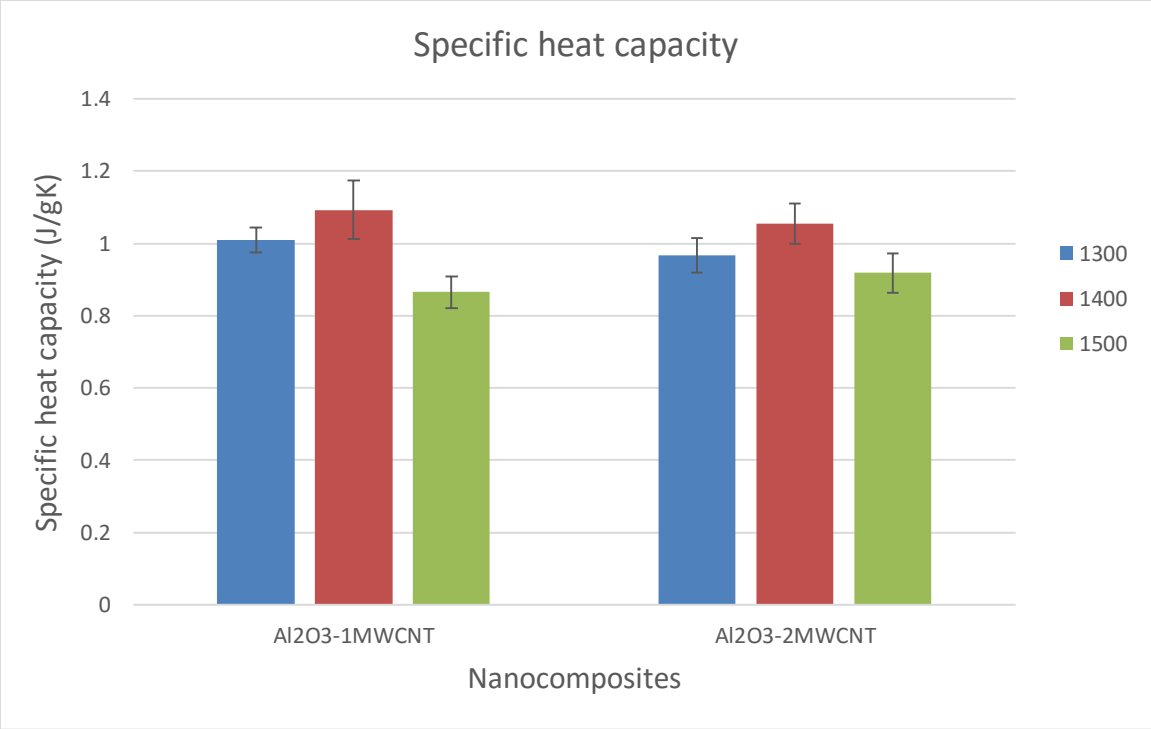

Figure 45 Specific heat capacity of Al2O3-CNT Nanocomposites.

4.4.3 Thermal Conductivity of Alumina-based Nanocomposites

The mechanism of heat conduction in alumina-based ceramics nanocomposites is by the vibrations of the alumina crystal lattice called phonons. The lattice vibrations are energy demanding which is distributed in all directions that reduces the ability of the material to conduct heat in a regular manner. For monolithic alumina, porosity play a significant role in the thermal conductivity as evident in figure 46. Low thermal conductivity (7.24W/mK) was reported for monolithic alumina after SPS densification at 1000°C. This implies that there was high level of porosities present in the samples as the thermal conductivity improved to 31.72W/mK when the SPS temperature increased to 1300°C. Further increase in SPS temperature result in increasing thermal conductivity to

34.44W/Mk at 1400°C. The thermal conductivity of Alumina-SiC nanocomposites densified by SPS at 1400 and 1500°C is shown in figure 48. Maximum thermal conductivity (24.15W/mK) was achieved on alumina containing 5wt%SiC sintered at 1500°C and this decrease to 22.87W/mK as the SPS temperature decrease to 1400°C. Increasing SiC nanoparticles from 5wt% to 10wt% do not increase the thermal conductivity of alumina rather decrease the thermal conductivity as evident in this work (Figure 48). Considering the thermal conductivity of pure alumina (28-38W/mK)[59] and 34.44W/mK reported in this work and also SiC (110-150W/mK)[123]; taken the thermal conductivity of alumina to be 34.44W/mK and SiC average thermal conductivity as 110W/mK, the thermal conductivity of alumina containing 5wt%SiC nanocomposites can be evaluated by rule of mixture as 38.21W/mK while that of 10wt%SiC is 42W/mK which is against our experimental value of 24.15W/mK and 21.14W/mK for alumina containing 5wt%SiC and 10wt%SiC respectively sintered at 1500°C SPS temperature. Thus our experimental results is in contrary to the theoretical calculations and the claims of other researchers[17,45,105], who reported increase in thermal conductivity with increasing SiC content. Moreover, SiC in various forms have been used in the reinforcement of alumina for the improvement in the its thermal conductivity by researchers. The use of SiC whiskers for the improvement of thermal conductivity of alumina was reported by Mccluskey et al.[111] and Fabbri et al.[105]. Maximum thermal conductivity of 34-42W/mK were reported while the use of SiC platelet in the improvement of alumina have been successful with maximum thermal conductivity of 49W/mK achieved on alumina containing 30wt%SiC platelets after hot pressing. Recently, parchiovansky et al.[17] reported maximum thermal conductivity (38W/mK) of

alumina containing 20vol%SiC particles after hot pressing. Thus implies that the thermal conductivity depends on the shape of the SiC used in the reinforcement of alumina and minimum thermal conductivity is expected when the SiC is used in the form of particles. The high thermal conductivity of platelet and whiskers containing nanocomposites is as a result of their high aspect ratio (>1) which enable them to conduct better than the particles with aspect ratio of 1. The directional dependent on thermal conductivity was studied by Barea et al.[45], as the thermal conductivity measured in perpendicular direction (49W/mK) was higher than the one measured in parallel direction (42W/mK). Barea et al. concluded that the thermal property measured on alumina containing SiC platelet depends on the direction of measurement.

Based on the intrinsic high thermal conductivity of SiC (700W/mK for theoretical value calculated, 490W/mK for single crystals and 270W/mK for pure polycrystalline) higher thermal conductivity of alumina containing SiC is expected. This disparity is due to the existence of interfacial thermal resistance between SiC and alumina which act as barrier to heat conduction leading to lower thermal conductivity. Other factors such as impurities, composition of the powder mixture (volume fraction of the SiC), porosity and microstructure (grain size and grain boundaries) critically affect the thermal conductivity of nanocomposite materials. The relationship between the SiC addition and the thermal conductivity of alumina-based nanocomposites is somehow difficult to comprehend. Hasselman and John[124], developed a mathematical model for estimating thermal conductivity of composites taking into consideration the grain boundary interfacial resistance effect. For spherical dispersion, the mathematical expression for estimating thermal conductivity after first approximation is given

$$\frac{K_{eff}}{K_c} = \frac{\left[2\left(\vartheta - \frac{K_{SiC}}{ah} - 1\right)\emptyset + \vartheta + \frac{2K_{SiC}}{ah} + 2\right]}{\left[\left(1 - \vartheta + \frac{K_{SiC}}{ah}\right)\emptyset + \vartheta + \frac{2K_{SiC}}{ah} + 2\right]} \quad \text{.....(4.1)}$$

Where Kc is the thermal conductivity of alumina, ϑ is Ksic/Kc, $\emptyset$ is the volume fraction of SiC, a is the radius of inclusion and Keff is the effective thermal conductivity of the composite. Thus, the contribution of thermal barrier resistance depends on the value of a in the above equation. If the value of a is higher, the thermal barrier resistance is lower and this explain the relatively higher thermal conductivity composites containing micrometer size SiC particles. According to Hasselman's model[125], the estimated interfacial resistance for composites containing second phase particles is $1.8\times10^{8}Wm^{2}K$ at room temperature. Also Rayleigh-Maxwell[59] developed a mathematical equation for estimating thermal conductivity of particulate composites;

$$K_c = \frac{K_m[2k_m + K_p - 2f_p(K_m - K_p)}{2K_m + K_p + f_p(K_m - K_p)} \quad \text{.....(4.2)}$$

Where Km is the matrix thermal conductivity, Kp is the second phase particle thermal conductivity fp is the volume fraction of the particle and Kc is the composite thermal conductivity. The theoretical estimation of thermal conductivity of composites containing micro particles take it into consideration the shape and volume fraction of the incorporated particles. However, this approach cannot be used for estimating nanocomposite system containing nanoparticles. Indeed, various factors need to be taken into account for nanocomposite system but for microscale particles, these factors can be disregarded. This is because, the interface resistance and phonon scattering become so high in the case of nanoscale particles such that the mathematical equations for

estimating thermal conductivity cannot longer accurately predict the true value the system thermal conductivity[126].

The heat conduction in dielectric material is responsible by the phonons which are scattered at the interface of two dissimilar materials. The dissipation of heat on the surface of nanoscale particles is higher than that of microscale particles. Besides, the small size of the SiC particles lead to high interfacial surface area and large interfacial thermal resistance, which increase the levels of the phonon scattering. It is also important to know that particles with high aspect ratio>1 as in the case of whiskers and platelet display better heat conduction in one direction as compared to sphere particles (aspect ratio=1) of the same volume fraction. Thus the lower thermal conductivity of Alumina-SiC nanocomposites achieved in this work is attributed to several factors which includes

- The small size of the SiC particles (40-50nm) with a non-modified surface lead to poor contact between the SiC and alumina matrix which hindering the thermal transport across the interface.
- Large interfacial area which play a significant role in the scattering of the phonons that led to lower thermal conductivity of the nanocomposites.
- Spark plasma sintering (SPS) do not allow grain growth of the alumina matrix even at high sintering temperature of 1500°C leading to small microstructure with numerous grain boundaries which increase the scattering of the phonons.
- Microstructural refining due to addition of SiC nanoparticles to alumina through pinning mechanisms another factor leading to poor thermal performance of the nanocomposites.

Thus our experimental results have shown that the thermal conductivity of alumina containing nanoparticles SiC densified by SPS do not increase with the addition of SiC due to the factors mentioned above. The powder characterizations and the densification results have shown that porosity and impurities have paltry effect on the thermal conductivity reductions of the nanocomposites but the effect of the microstructure, grain boundaries and the acoustic mismatch between the SiC and alumina matrix determine the degree of the phonon scattering. Composite system with largest nanoparticles size which means lowest particle surface area would have the highest thermal conductivity as the interfacial barrier is relatively low in contrast to nanocomposites. In conclusion, the thermal conductivity of alumina decrease by 42.6% on addition of 5wt%SiC and 62.9% when 10wt%SiC nanoparticles were added to alumina matrix consolidated by SPS at 1500°C and this shows that the extent reduction depends on the volume fraction of the SiC nanoparticles added. The higher the volume fraction of the SiC nanoparticles added to alumina, the greater the degree of thermal conductivity reduction.

The room temperature thermal conductivity of alumina-CNT nanocomposites is shown in figure 49. Highest thermal conductivity (29.62W/mK) was achieved on the alumina containing 1wt%MWCNT sintered at 1500°C while that of 2wt%MWCNT nanocomposites is 25.94W/mK. Again, when the sintering temperature is reduced to 1400°C, the thermal conductivity of alumina containing 1wt%MWCNT and 2wt%MWCNT are 29.11 W/mK and 24.94W/mK respectively. Increasing the content of MWCNT from 1wt% to 2wt% results in decreasing the thermal conductivity as shown in the figure 49. There was no significant difference in the thermal conductivity of nanocomposites of the same composition but different SPS temperature and this is

actually in conformation with the densification results. Based on the thermal conductivity of monolithic alumina (34.44W/mK) and MWCNT thermal conductivity (200-3000W/mK)[127,128], the addition of MWCNT to alumina is expected to tremendously enhance the thermal conductivity of alumina-CNT nanocomposites. The theoretical estimation of thermal conductivity by the rule of mixture based on the average thermal conductivity of alumina (34.44W/mK) and MWCNT (500W/mK); the thermal conductivity of 1wt%MWCNT-Alumina nanocomposites and 2wt%MWCNT-Alumina nanocomposites are 39.09W/mK and 43.75W/mK respectively. Thus, the experimental thermal conductivity of 1wt%MWCNT-Alumina nanocomposite and 2wt%MWCNT-Alumina nanocomposite consolidated at 1500°C as reported in this work is 31.9% and 68.6% lower than the theoretical values calculated by the rule of mixture. Zhan and Mukherjee[71] after SPS consolidation of alumina containing SWCNT, explained that the thermal conductivity of CNT-Alumina nanocomposites is affected by several scattering process which include grain boundary, interfacial boundary, point defects, impurities and phonon etc. Zhan and Mukherjee reported thermal conductivity of 11.4W/mK for 10vol%SWCNT-alumina nanocomposites and this decrease to 7.3W/mK as the volume fraction of the SWCNT increase to 15vol%. Recently, Sakar and Das[87], consolidated multi-walled carbon nanotubes-alumina using pressureless sintering and reported thermal conductivity of 44.13W/Mk for 0.3wt%MWCNT-Alumina nanocomposites and this decrease to 13.37WmK when the MWCNT content increased to 1.2wt%. also, Kumari et al.[19], reported significant thermal conductivity of 90.44W/MK for 7.39vol%MWCNT -Alumina nanocomposites after SPS consolidation and this decrease to 22.62W/mK when the MWCNT content increase to 19.1vol%. It is therefore

reasonable to say that the thermal conductivity alumina-CNT nanocomposites initially increase with addition of CNTs reaching maximum and then decrease when further increase in the content of the nanotubes in alumina matrix. Although there has not been general trend as regards the increasing or decreasing in thermal conductivity of CNT-Alumina nanocomposites. Various researchers express their opinions on the decreasing thermal conductivity of alumina-CNT nanocomposites with increasing content. For example, Sakar and Das[87], explained that the poor thermal conductivity of alumina containing ≥1.2vol%CNT compared to pure alumina are the scattering of phonons by residual pores in the incomplete densified samples, low thermal conductivity of clustered CNTs due to tube-tube interactions and the presence of kinks or twists in the agglomerated CNTs which decrease the aspect ratio of CNTs and reduce their effective transport properties. Zhan and Mukherjee[71], attributed the reduction in thermal conductivity of SWCNT-Alumina nanocomposites to the difference in thermal properties of an individual tube and rope of SWCNTs. Tube-tube interactions according to Zhan and Mukherjee are the dominant barrier to phonon transport in the rope of the nanotubes. Kumari et al.[19], also acknowledged that the agglomeration of CNTs with increasing contents contributed immensely towards the scattering of the phonons and this gives lower thermal conductivity in the MWCNT-Alumina nanocomposites. Kumari et al. further explained that the single-walled carbon nanotubes (SWCNT)-Alumina nanocomposites cannot give high thermal conductivity of multi-walled carbon nanotubes (MWCNT)-Alumina nanocomposites as the mean free path of SWCNT (0.5-1.5μm) is larger than the MWCNT mean free path (20-500nm) as such, the tube-tube interaction do not significantly reduce the mean free path of MWCNT in alumina matrix.

It is important to know that the distribution of CNTs in ceramic matrix is a crucial factor in realizing the intrinsic thermal properties of CNT-ceramic composites. Homogenous dispersion of CNTs in ceramic reduce the percolation threshold (formation of interconnected network of CNTs) in the ceramic matrix and once the percolation is established, further increment in the nanotube content result in agglomeration[4]. Agglomerated CNTs in ceramic matrix reduce densification as agglomerated pores are difficult to remove without grain growth. Besides, agglomerated CNTs promote scattering of the phonons thereby reducing their mean free path. Thus, combination of porosities and the agglomerated CNTs in the ceramics matrix perhaps is the reason for the reduction of thermal conductivity of CNT-alumina nanocomposites with increasing content of CNTs. However, in our own case, the effect of porosity on the thermal conductivity reduction was minimal as the MWCNT-Alumina nanocomposites at different level of SPS temperature are highly densified (figure 37). Also, interfacial resistance which exist as a result of acoustic mismatch between CNTs and alumina matrix was also reduce due to functionalization of MWCNT prior to dispersion in alumina matrix. This contributed to the quality of the interface between the ceramic matrix and the MWCNT thereby minimizing the interfacial resistance. Thus, the major factor contributing to the reduction in the thermal conductivity alumina with increasing content of the functionalized MWCNT in the current work is the increasing possibility of agglomeration of CNTs after the percolation threshold is reached. Maximum thermal conductivity of 29.62W/mK achieved in this work for 1wt%MWCNT-Alumina nanocomposite showed that percolation threshold is lower than 1wt%MWCNT. Increasing the content of MWCNT to 2wt% reduced the thermal conductivity to

25.94W/mK due to agglomeration. Our result is actually in the trend of the result of Sakar and Das[87], however, the thermal conductivity reported in this work at 1wt% and 2wt%MWCNT-alumina matrix at different SPS temperature (1300, 1400 and 1500°C) is higher than the result reported by Sakar and Das (13.37W/mK for 1.2wt%MWCNT and 5.05W/mK for 2.4wt%MWCNT) in alumina matrix even though the consolidation was done at high temperature (1700°C). The disparity in thermal conductivity of the current result and that reported in the literature is based on the clean effect of SPS consolidation which maintain the integrity of the nanotubes with significant reduction in porosity of the nanocomposites. Moreover, the functionalization of MWCNTs used in this work have contributed to the reduction in the interfacial resistance between the CNT and alumina matrix which promote effective thermal transport in the CNT-alumina interface that led to low phonon scattering and give better thermal properties. In conclusion, simple wet mixing of alumina-CNT preparation do not require much weight fraction of CNTs (>1wt%) to attain percolation threshold and give higher thermal conductivity as evident in the current work and that of Sakar and Das[87], but CNT-alumina prepared by chemical vapor deposition (CVD) in the case of Kumari et al.[19], high weight fraction of MWCNT is required to establish percolation threshold as the techniques give better distribution of CNTs in alumina matrix with little agglomerations. In nutshell, homogenous distribution of CNTs in ceramic matrix is the prerequisite for achieving high thermal conductivity in the ceramic-CNT nanocomposites.

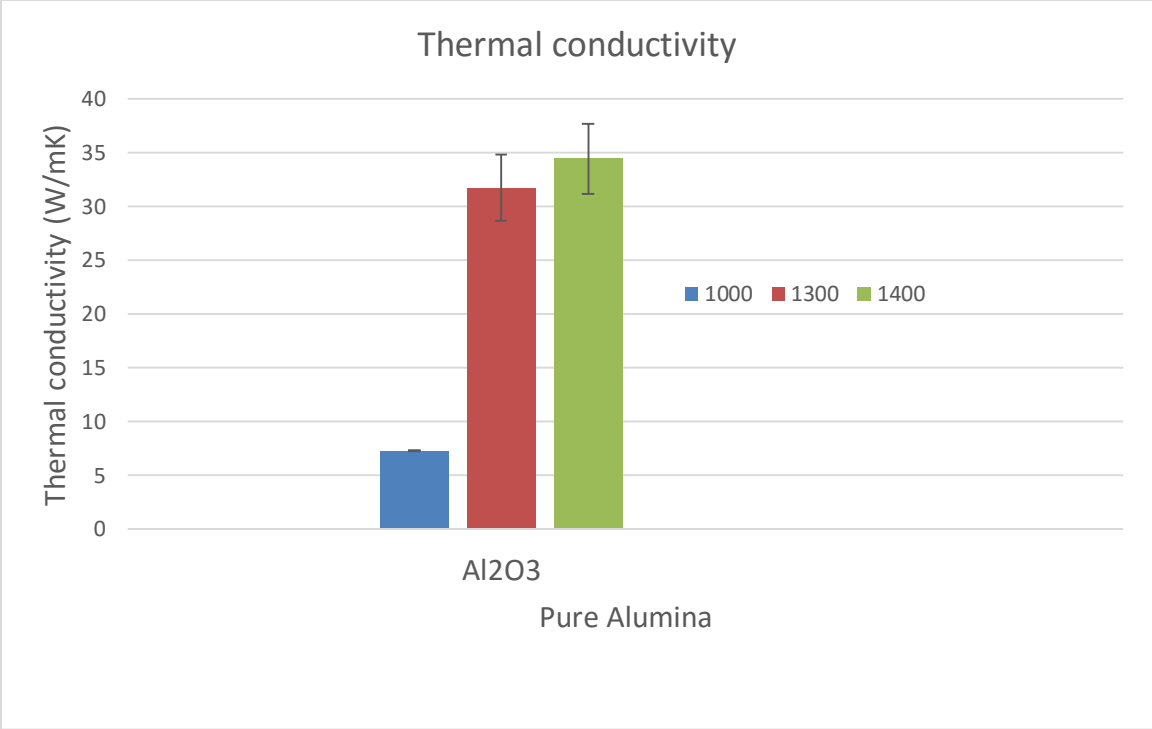

Figure 46 Thermal Conductivity of Pure Alumina at different SPS temperature.

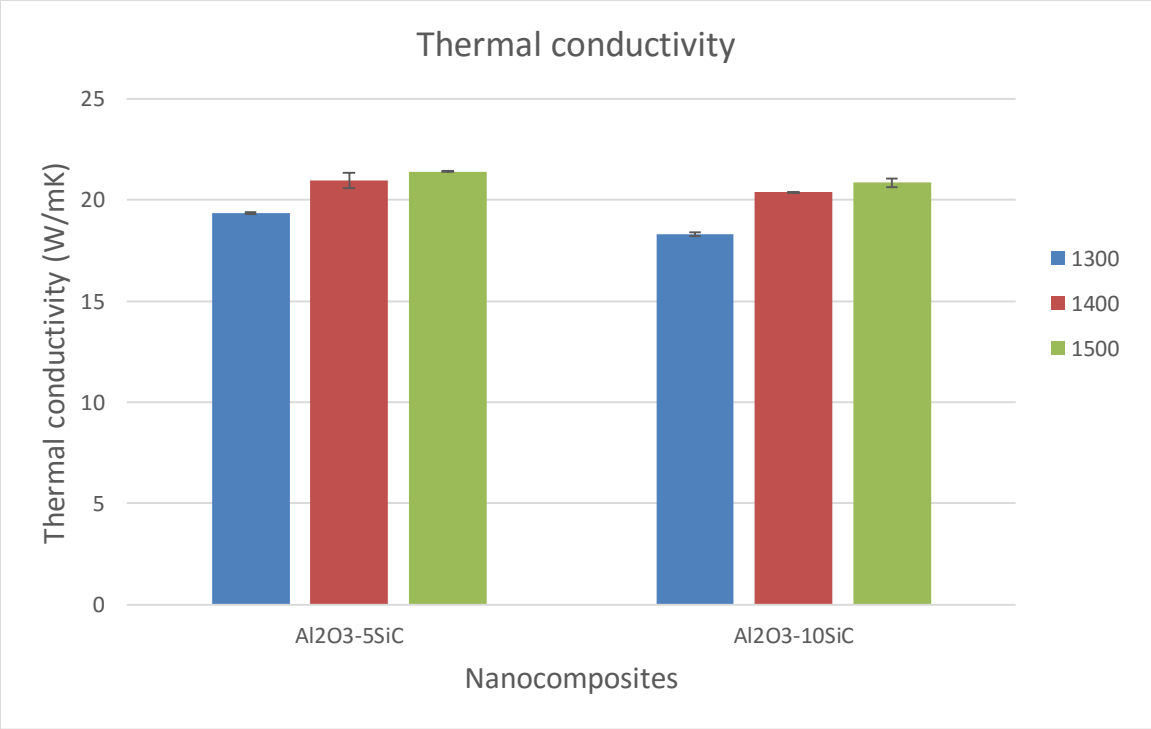

Figure 47 Thermal conductivity Alumina-SiC nanocomposites prepared at high milling conditions.

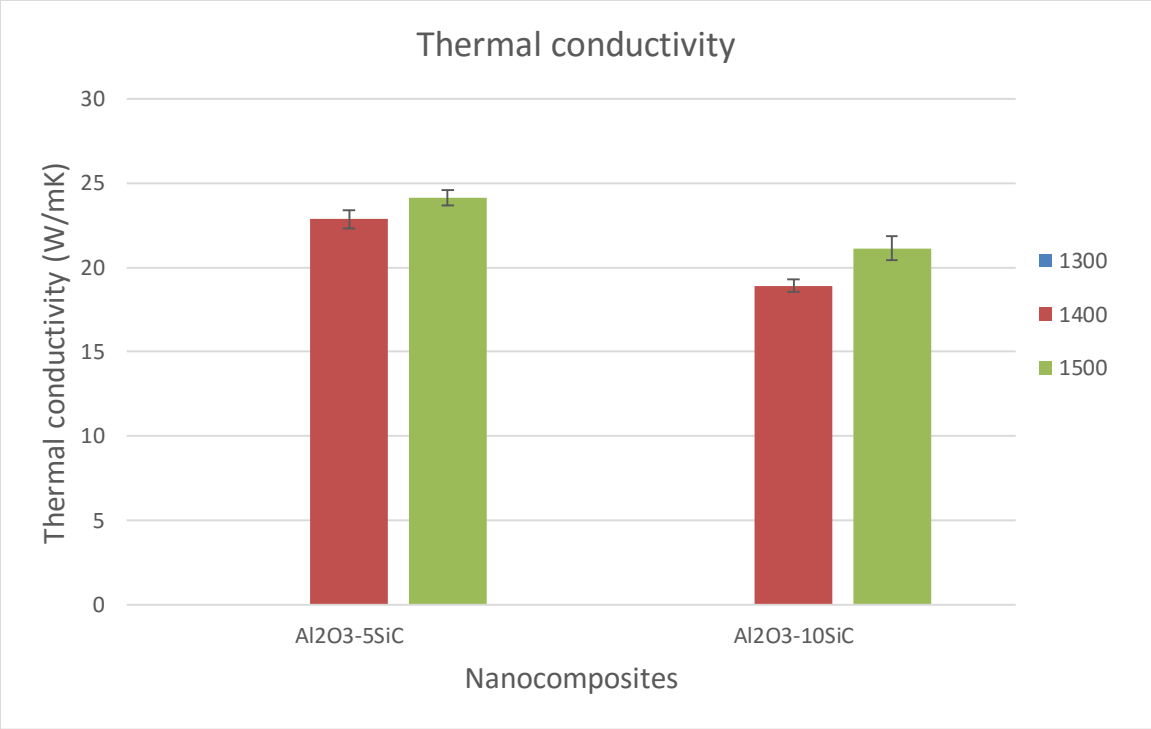

Figure 48 Thermal conductivity of Alumina-SiC nanocomposites prepared at low milling conditions.

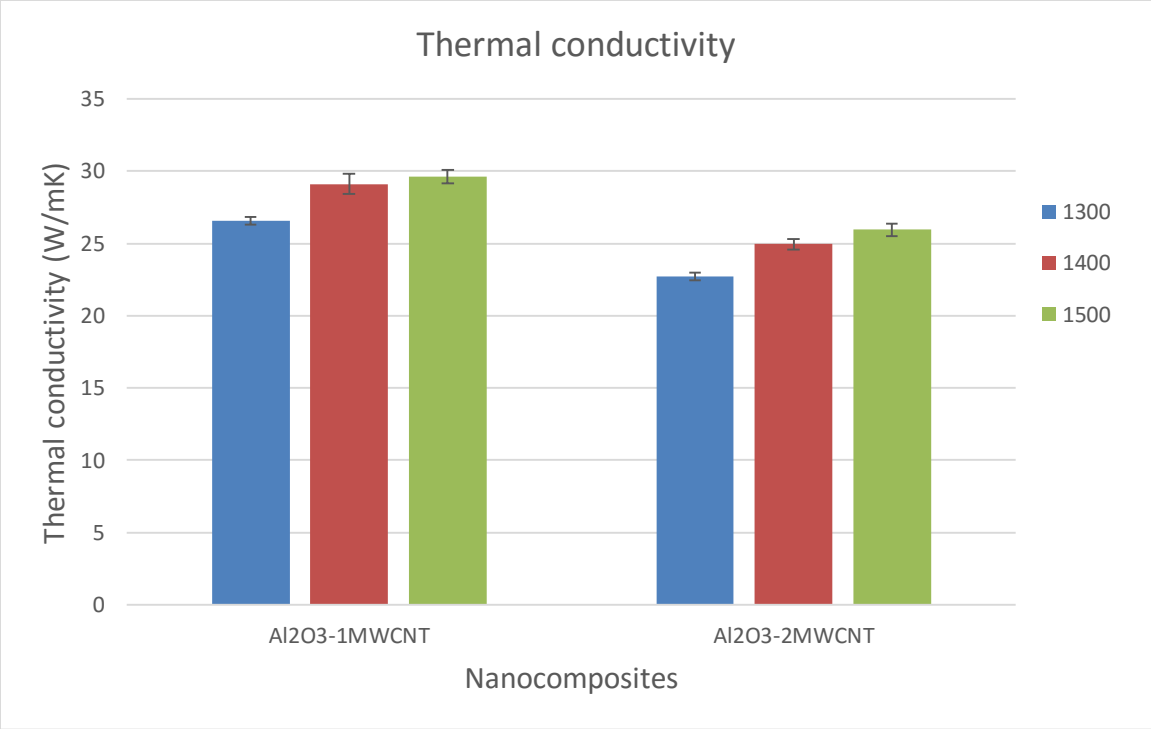

Figure 49 Thermal conductivity of alumina-CNT Nanocomposites.

4.4.4 Thermal Properties of Al_2O_3-SiC nanocomposites at elevated temperatures

Thermal properties of materials are usually affected by the measuring temperature. Figure 50 indicates the thermal diffusivity of pure alumina measured in the temperature range of 50-250°C and it was discovered that the thermal diffusivity decrease with the measuring temperature. Maximum thermal diffusivity was achieved at room temperature for the alumina at all SPS temperatures (1000°C, 1300°C and 1400°C). The trend of specific heat capacity (figure 51) of monolithic alumina with temperature is contrary to thermal diffusivity. Specific heat capacity increase progressively with the measuring temperature and at high temperatures, it appears constant with the measuring temperatures. For example, alumina sintered at 1400°C, the specific heat capacity measured at 25°C was 1.22J/gK which increase to 1.55J/gK as the measuring temperature is increased to 250°C. The variation of thermal conductivity of monolithic alumina with temperature is presented in figure 52. It is obvious that the thermal conductivity of pure alumina decrease with the measuring temperature. At room temperature the thermal conductivity of monolithic alumina is 34.44W/mK which steadily reduced to 18.3W/mK at 250°C.

The influence of temperature on the thermal properties (thermal diffusivity, specific heat capacity and thermal conductivity) of Alumina-SiC nanocomposites are shown in the figure 53, figure 54 and figure 55 respectively. The thermal diffusivity decrease with the measuring temperature (figure 53). At room temperature of 25°C, the thermal diffusivity of all the nanocomposites are in the range of 6-7mm^2/s. The thermal diffusivity decrease with temperature and at 250°C, the thermal diffusivity of all the nanocomposites are in

the range of 3-4mm^2/s. The reduction in the thermal diffusivity can be linked to the increasing crystal lattice vibration of alumina matrix as the temperature increase. The more the crystal lattice vibrations, the more the phonons are scattered and the less the thermal diffusivity. Parchiovansky et al.[17] stated that the thermal diffusivity decrease gradually with the measuring temperature such that at 1000°C, the thermal diffusivity is one magnitude lower than the thermal diffusivity at room temperature for Alumina-SiC nanocomposites. Other researchers[105,111] equally agreed that the thermal diffusivity and thermal conductivity decrease with the measuring temperature. The trend of specific heat capacity variation with the measuring temperature is actually in the opposite sense to that of thermal diffusivity and thermal conductivity. The specific heat capacity (figure 54) increase gradually with the measuring temperature. The specific heat capacity of all the nanocomposites at 25°C are in the range of 0.7-0.9J/gK and this increase to 0.92-1.2J/gK at 250°C. However, it is clear from the figure 54 that the specific heat capacity at high temperature (200°C and above) do not change significantly with the measuring temperature.

The mechanism of specific heat capacity increment with the measuring temperature is still not clear. The increasing specific heat capacity with temperature can be link to increase in the amplitude of atomic vibrations with rise in temperature and the larger this vibration, the higher the thermal energy. The thermal energy is the measure of all the phonons (vibrational waves) existing in the crystals of material at a given temperature. The trend of thermal conductivity variation with the measuring temperature is the same as that displayed by thermal diffusivity. The thermal conductivity decrease progressively with measuring temperature and this is due to the increasing higher amplitude of thermal

vibrations of alumina crystal lattice at high temperatures which scattered the propagation of phonon waves. As shown in figure 48, the thermal conductivity of alumina-5wt%SiC nanocomposite measured at room temperature is about 24W/mK but this decreases to 16W/mK at 250°C. Thus, thermal diffusivity and thermal conductivity decrease with the measuring temperature while that of specific heat capacity increase as the measuring temperature increased.

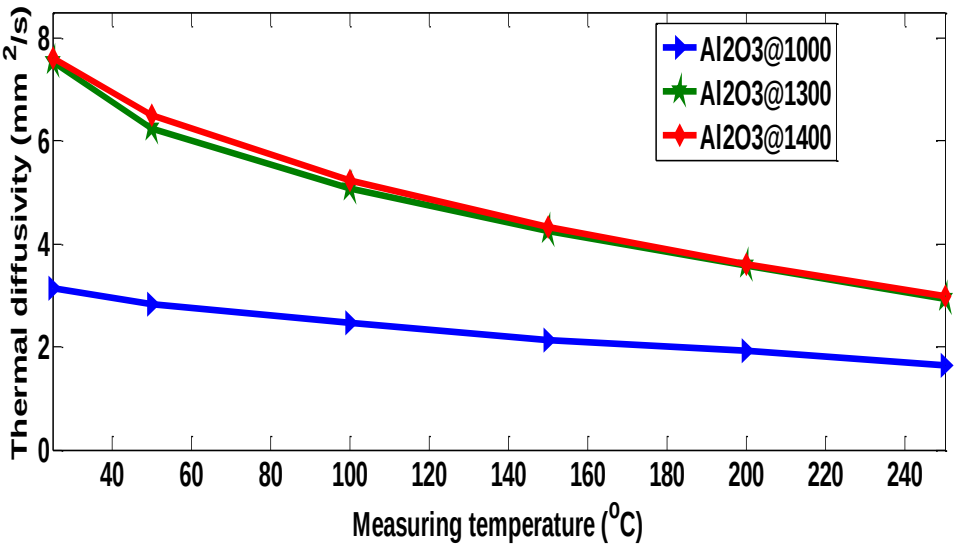

Figure 50 Variation in thermal diffusivity of Alumina with temperature.

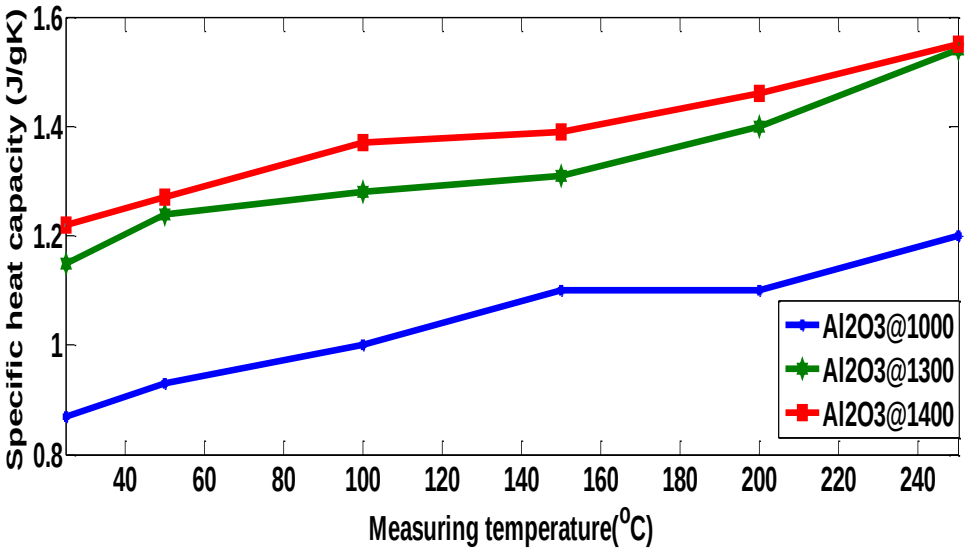

Figure 51 Variation in Specific heat capacity of Alumina with temperature.

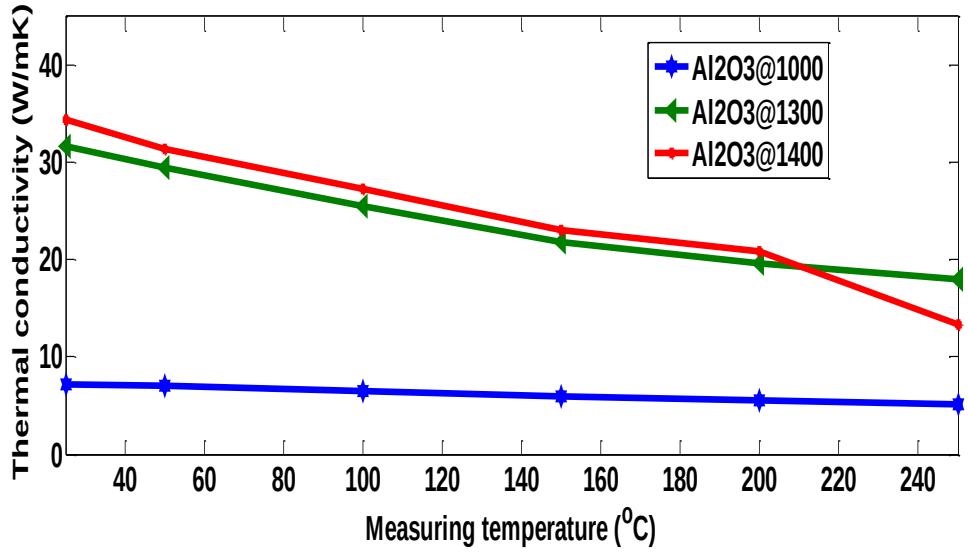

Figure 52 Variation in thermal conductivity of Alumina with temperature.

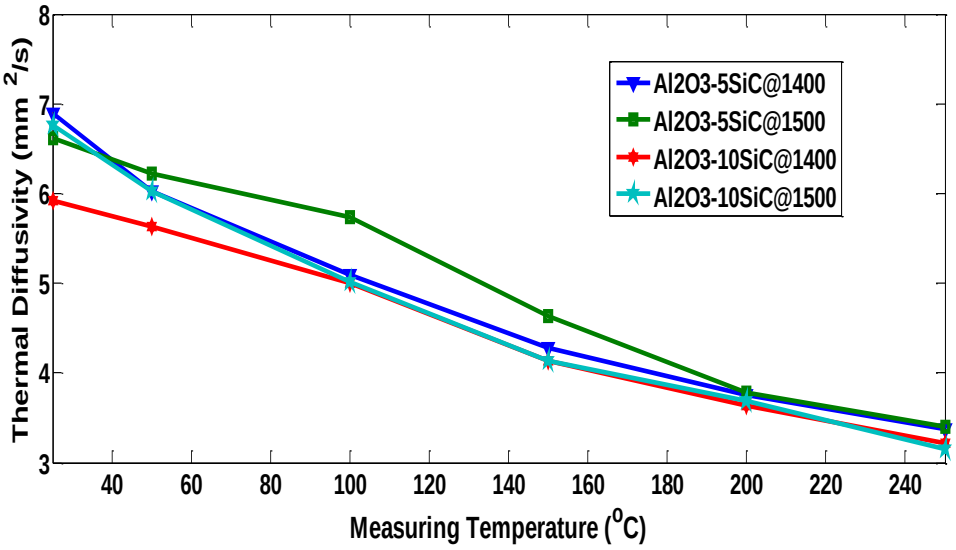

Figure 53 Variation of thermal diffusivity with Measuring temperature.

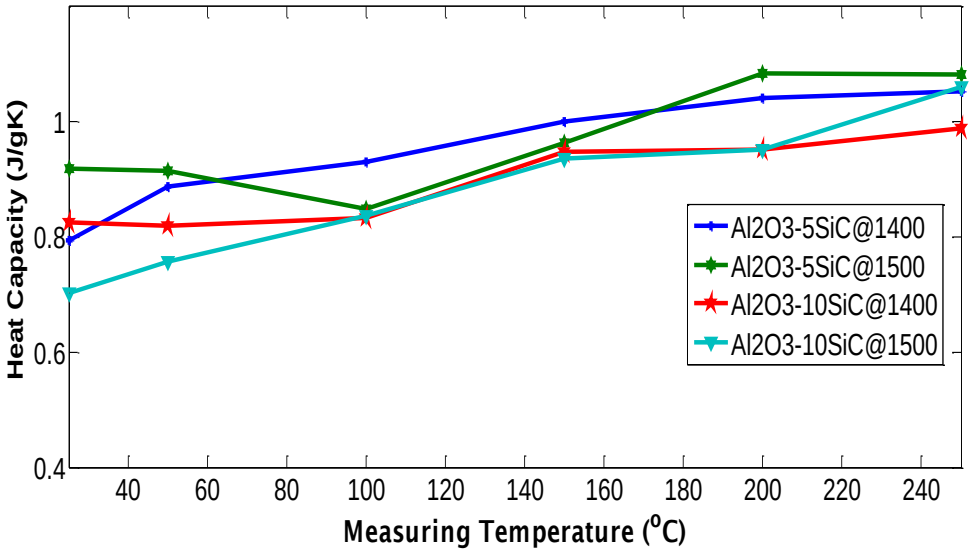

Figure 54 Variation of Heat capacity with Measuring temperature.

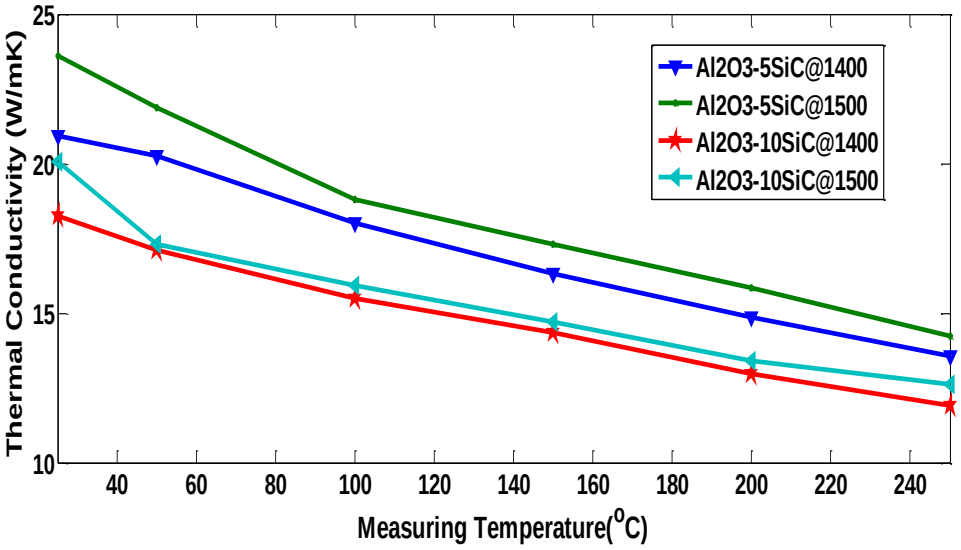

Figure 55 Variation of Thermal Conductivity with measuring temperature.

4.5 Electrical Conductivity of alumina-based Nanocomposites

4.5.1 Electrical Conductivity of Alumina-SiC Nanocomposites

The electrical conductivity of Al_2O_3-SiC nanocomposites prepared at high milling conditions presented in table 8 shall not be discussed due to contamination problem that result to change in the milling condition from high to low milling process.

The electrical conductivity mechanism of Alumina-SiC nanocomposite material is as a result of establishment of conductive interconnected network of SiC nanoparticles in the alumina matrix. The magnitude of electrical conductivity achieved on the Al2O3-SiC nanocomposite depends on the extent of distribution of the conductive SiC nanophase in the dielectric alumina matrix. Again, the position of SiC nanoparticles will be affected by the alumina matrix evolution. Table 9 shows the DC electrical conductivity of Alumina-SiC nanocomposites measured at room temperature. The electrical conductivity was found to increase with SPS temperature and the SiC nanoparticle volume fraction. For instance, alumina containing 10wt%SiC densified at 1500°C by SPS has the maximum DC electrical conductivity (2.65E-05) among the Alumina-SiC nanocomposites and this reduced to 4.04E-06S/m when the sintering temperature decreased to 1400°C. The results achieved in the present work is in agreement with the room temperature DC electrical conductivity results reported by Borrel et al. [17] after hot pressing alumina containing 17vol%SiC at a sintering temperature of 1740°C. Maximum DC electrical conductivity of 4.05×10^{-2}S/m was measured at room temperature. The trend of the result achieved in this current work indicates that electrical conductivity increase with SiC contents. This is because, as more SiC particles are added

to alumina, more connected network of SiC conductive paths are formed and this facilitates the flow of electricity in the nanocomposite material. The influence of electrical conductivity of dielectric system with addition of conductive second phase can be explained by the concept of percolation theory[119,129], that describes the correlation between electrical conductivity and the volume fraction of the dispersed second phase particles. Percolation theory explain the probability of formation of conductive network with the addition of a given volume fraction or concentration of the conductive second phase material. Homogenous distribution of the conductive nanophase can significantly reduce the percolation threshold (the amount of conductive second phase required to form a conductive network path). Stauffer and McLaclan[119], estimated 17Vol% as the minimum volume fraction of second phase to create a conductive network path. Sawaguchi et al.[88], reported 10^{13}Ωcm as the electrical resistivity of Al2O3/SiC composites containing 10vol%SiC. However, when the volume fraction of SiC increased to 20vol%, the electrical resistivity decreased to 10^{6}Ωcm. H o et al. [130], stated that when the volume concentration of the conductive secondary phase is in the proximity of percolation threshold, the electrical conductivity of the composite was affected by the microstructure. The effect of volume fraction and the grain size (coarse or fine-grained) of SiC particles as well as the mean size of the Al_2O_3 matrix was investigated by Parchiovansky et al. [17]. They concluded that the electrical conductivity of Al_2O_3 was improved significantly with the increasing volume faction of the SiC content. The maximum electrical conductivity of 4.05×10^{-2}S/m was evaluated for alumina containing 20vol% coarse SiC. Lux[118], affirmed that for Al_2O_3-SiC nanocomposites, electrical conduction is entirely through the connected network of SiC located in the alumina or at

the grain boundaries. Thus, the observations of all the authors are in agreement with the results achieved in this current work. The enhancement in DC electrical conductivity of Alumina-SiC nanocomposites with SPS temperature as presented in this work can be explain in two ways. Firstly, Increasing SPS temperature encourages the growth of alumina grain at constant SiC particle contents. Large grains imply low density grain boundaries and this means that there are small paths available for the SiC particles to form interconnected paths. Thus increase the electrical conductivity. Secondly, the mechanism of SPS consolidation involves simultaneous heating and pressing of the nanopowders to form bulk nanocomposites. This act decreases the gap between the individual nanoparticles and nanocrystalline thereby promoting tunneling effect. Effective distribution of SiC particles in alumina using sonication and planetary ball milling as used in this work could be the factor responsible for low percolation threshold. Zhan and Mukherjee [71], reported that the DC electrical conductivity of pure alumina is the range of 10^{-10}-10^{-12}S/m. Therefore, the result achieved in this work showed that the electrical conductivity of the alumina has been improved with the addition of as low as 5wt%SiC nanoparticles. It is important to know that the grain refinement which impairs thermal properties of Al_2O_3-SiC nanocomposites as reported in this work promote the electrical conductivity of the nanocomposites. This is because the mechanism of electrical conduction is different from that of thermal transport. Electrical conduction in semi-conductors is entirely by holes and electrons while that of thermal transport is by phonons. Decreasing the grain size of alumina reduce the amount of SiC particles submerged by the alumina grains and this increase the number of SiC particles at the interpositions (grain boundaries). SiC nanoparticles located at the grain boundaries

contribute to the formation of the interconnected network paths for electrical conduction[18]. Thus refined microstructure in this case favor the electrical conductivity of the nanocomposites.

DC electrical conductivity of alumina-CNT nanocomposites are presented in table 10. The electrical conductivity of Al_2O_3-MWCNT nanocomposites increase with the MWCNT contents and the SPS temperature. Maximum electrical conductivity of alumina-CNT nanocomposite achieved in this current work is 101S/m on alumina containing 2wt%MWCNT at 1500°C SPS temperature while the minimum electrical conductivity was 0.43S/m on alumina containing 1wt%MWCNT consolidated at 1300°C. CNTs has significant effect on the electrical behavior of alumina dielectric. Addition of small amount of CNT as low as 0.5wt% can change the electrical behavior of alumina from insulator to a semi-conductor[120]. The high aspect ratio of CNT has profound influence on its electrical behavior. Electrons can easily flow through the CNTs than spherical particles which has short mean free path than CNTs. The electrical conductivity of ceramics-CNT nanocomposite obey the powder law equation.

$\sigma_{dc} = \sigma_c(P_{MWNT} - P_C)^t$, for $P_{MWNT} > P_c$ .....(4.3)

Where σ_{dc} and $\sigma_c$are the DC conductivities of the composite and conducting component respectively. P_{MWNT} and P_C are the weight fraction of the MWNT and the percolation threshold. The exponent t is a dimensional constant usually in the range of 1.33-2.0. For alumina-CNT nanocomposites, the tunneling resistance due to inter-nanotube connections or the alumina insulating barrier between the nanotubes play significant role in the effective electrical conductivity of the nanocomposites and that implies that the

electrical conductivity in this nanocomposites is controlled by the fluctuation induced tunneling mechanism. The hoping transport of electron through CNT separated by insulating barrier dictates the conductivity behavior of CNT-ceramics nanocomposites. Thus, the CNT contents (1 and 2wt%) used in this work is greater than the percolation threshold value, hence the change in electrical behavior of alumina from insulator to semi-conducting material. comparing the current result with Ahmad and Pan[120] who reported maximum DC electrical conductivity of alumina containing 3wt%CNT as 1.35S/m, we can say that the electrical conductivity of alumina has been improved significantly. Also, Inam et al.[70], reported 80S/m as the DC electrical conductivity of alumina containing 2wt%MWCNT sintered by SPS at 1600^{o}C. The higher result achieved in this current work is as a result combination of effective distribution of CNT in the alumina matrix and the use of SPS consolidation techniques which prevent damage to the nanotubes and maintained their functional integrity.

Table 8 DC Electrical conductivity of Al2O3-SiC Nanocomposites prepared at high milling conditions.

Nanocomposites	SPS temperature (°C)	Electrical Conductivity (S/m)
Al_2O_3-10SiC	1500	1.00E-05±4.00078E-07
Al_2O_3-10SiC	1400	9.50E-07±1.06978E-08
Al_2O_3-10SiC	1300	3.20E-07±4.05194E-09
Al_2O_3-5SiC	1500	5.27E-08±2.13312E-09
Al_2O_3-5SiC	1400	2.91E-09±2.55624E-10
Al_2O_3-5SiC	1300	1.28E-09±4.34809E-11

Table 9 DC electrical conductivity of Alumina-SiC nanocomposites prepared at low milling conditions.

Nanocomposites	SPS temperature (°C)	Electrical Conductivity (S/m)
Al_2O_3-10SiC	1500	2.65E-05±1.52475E-08
Al_2O_3-10SiC	1400	4.04E-06±2.58079E-08
Al_2O_3-5SiC	1500	1.29E-07±4.05531E-09
Al_2O_3-5SiC	1400	9.57E-08±1.05451E-08

Table 10 DC electrical conductivity of alumina-CNT nanocomposites.

Nanocomposites	SPS temperature (^{o}C)	Electrical Conductivity (S/m)
Al_2O_3-2MWCNT	1500	101.1181±2.195
Al_2O_3-2MWCNT	1400	96.54306±1.696
Al_2O_3-2MWCNT	1300	65.49757±0.5039
Al_2O_3-1MWCNT	1500	7.770615±0.0839
Al_2O_3-1MWCNT	1400	1.386913±0.01026
Al_2O_3-1MWCNT	1300	0.431754±0.00599

4.6 Microstructural Analysis of Nanocomposite

4.6.1 FE-SEM microstructure of the Nanocomposites.

The microstructure Alumina-SiC nanocomposite can be control through the careful addition of SiC particles. SiC particle can refine the alumina matrix through the pinning of the alumina matrix grains. Also the nature of the interface formed between the SiC and the alumina determine the magnitude of the interfacial thermal resistance. High thermal resistance can degrade the thermal diffusivity and thermal conductivity of the composites. Figure 56 shows the FE-SEM images of thermal etched Alumina-SiC nanocomposites at 1500^{o}C SPS temperature. The grain sizes are very small as found in the images which implies large grain boundaries. From the FE-SEM image (figure 56a) the average grain size of alumina is around 120nm and this explain the reduction in the thermal conductivity of alumina with addition of SiC nanoparticles. Reduction in the size of the alumina grains due to increase in SiC nanoparticles content to 10wt% result in decreasing the alumina grain size (figure 56b) such that the grain boundaries are now difficult to see. Thus corroborates the lower thermal conductivities of alumina-10wt%SiC nanocomposites as reported in figure 48.

Figure 57 shows FE-SEM fractured surface images of monolithic alumina and Al_2O_3-5wt%SiC nanocomposite. Monolithic alumina (pure alumina) has large grain size (figure 57a) relative to the nanocomposite (figure 57b) and this clearly shows that addition of 5wt%SiC nanoparticles to alumina reduce the grain size and strengthened the grain boundaries. Refinement of the alumina grain by the SiC nanoparticle addition is well established in the literature. This form the basis of superior mechanical properties of

Al2O3-SiC nanocomposites; although thermal properties reduce as evident in this work due to existence of large grain boundaries that promotes phonon scattering. Also, figure 58 represent the FE-SEM of pure alumina and alumina containing 10wt%SiC nanocomposites. The same phenomenon exhibited in figure 57 is equally displayed here. It is obvious that the alumina grain size reduced drastically with the addition of 10wt%SiC nanoparticles. Thus, it is clear that SiC nanoparticle inclusion in alumina matrix refine the microstructure of alumina and this explain the reduction in the thermal properties of alumina. Microstructural refinement does not have immense effects on the electrical conductivity of Alumina-SiC nanocomposites as the SiC nanoparticles inclusion promote the electrical conductivity of alumina as shown in table 10.

Figure 59 shows the FE-SEM of fractured surface of Al2O3-1wt%MWCNT and Al2O3-2wt%MWCNT nanocomposites. The presence of CNTs at the grain boundaries of alumina were observed. The inhibition of the growth of alumina grains with the addition of MWCNT is more glaring in alumina containing 2wt%MWCNT (figure 59b) than 1wt% MWCNT (figure 59a). figure 60 shows the agglomeration of MWCNTs in alumina matrix and this occurs in both alumina 1wt%MWCNT (figure 60c) and 2wt%MWCNT (figure 60d). the agglomerated CNTs impairs the thermal properties of the nanocomposites through phonon scattering although formation of connected network of CNTs in the alumina matrix as shown in figure 60 enhances the electrical conductivity of the nanocomposites.

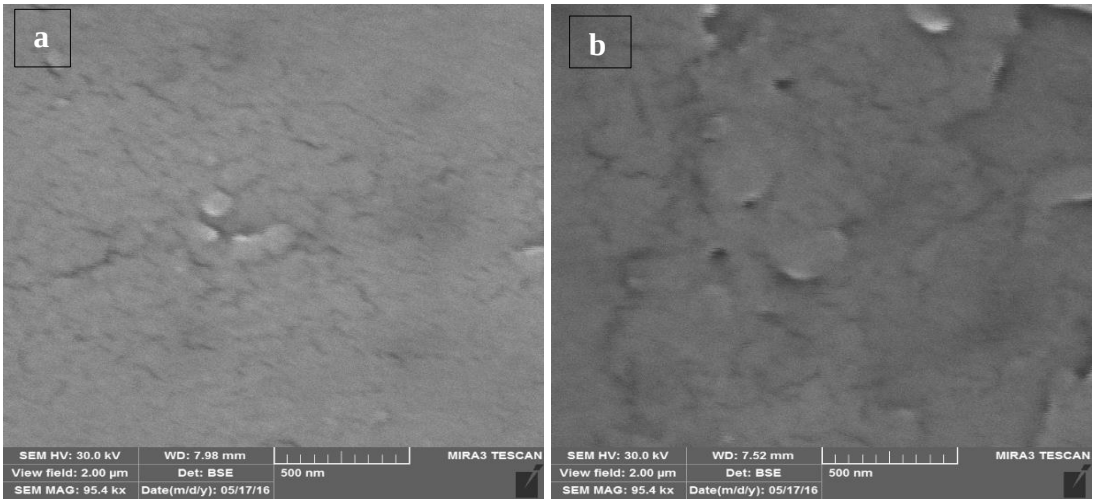

Figure 56 FE-SEM images (a) alumina-5wt%SiC (b) alumina-10wt%SiC Nanocomposites after thermal etching.

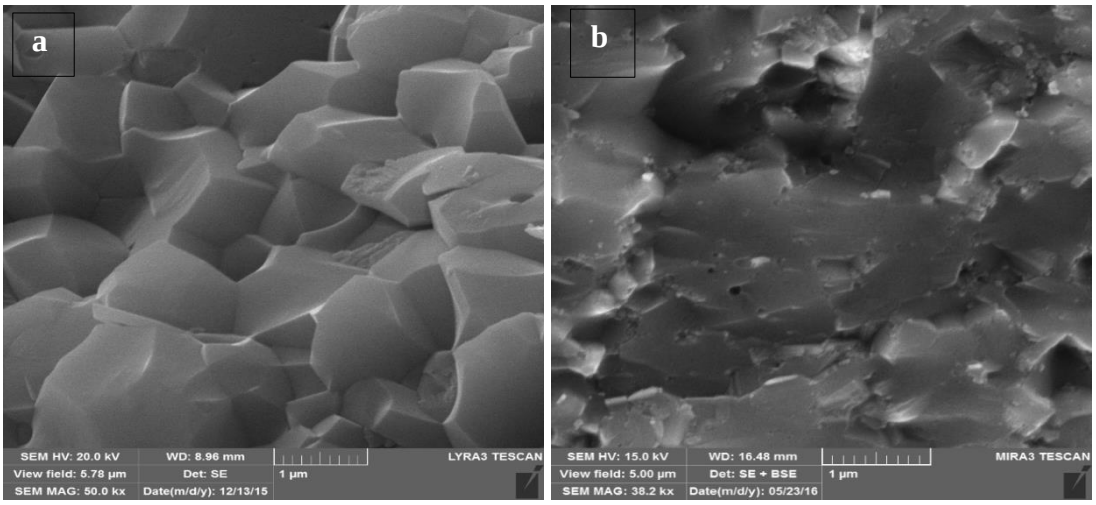

Figure 57 FE-SEM images of fractured surface (a) pure alumina (b) Al2O3-5SiC nanocomposite at SPS 1500^{o}C.

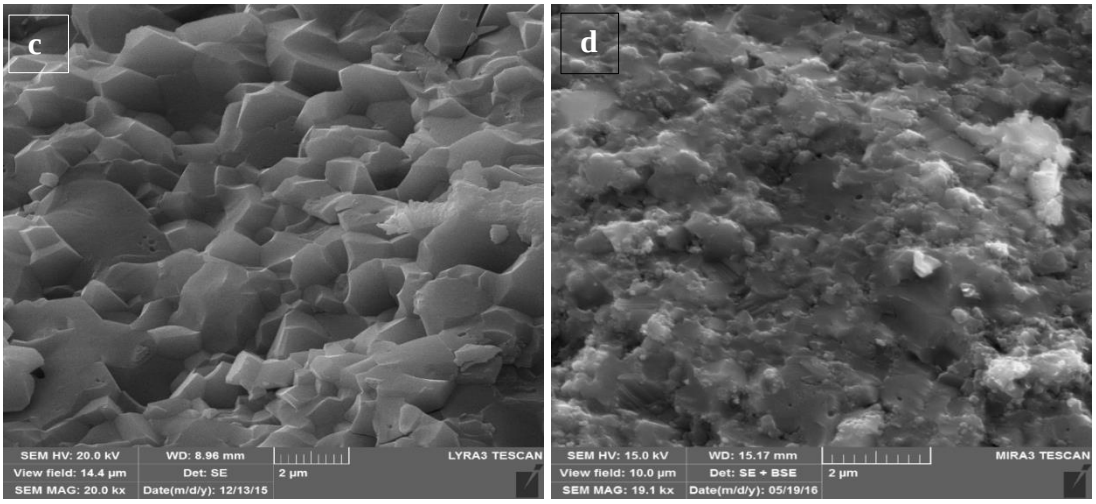

Figure 58 FE-SEM images of fractured surface (c) pure alumina (b) Al2O3-10SiC nanocomposites at SPS 1500°C.

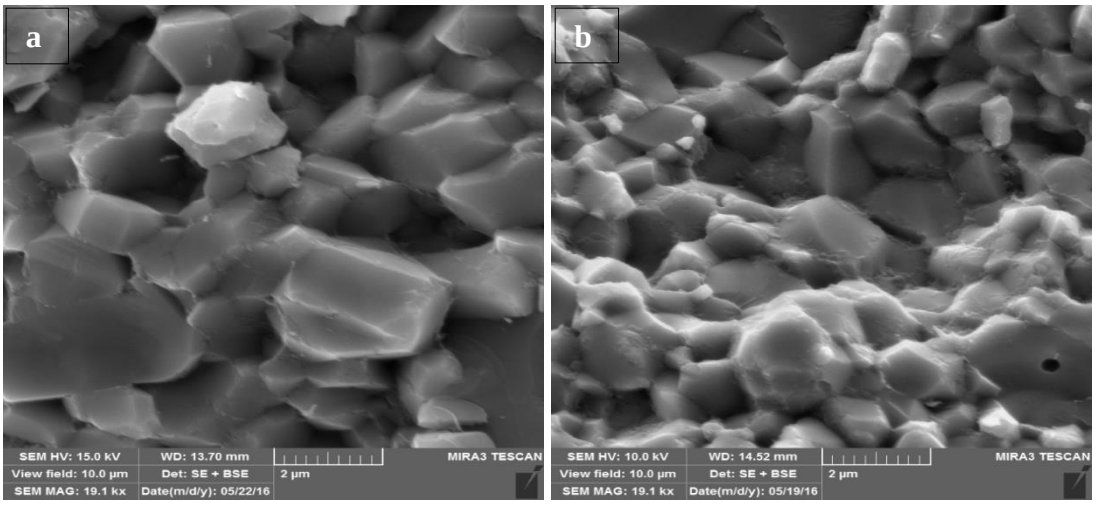

Figure 59 FE-SEM images of Al2O3-MWCNT Nanocomposites (a) 1wt%MWCNT (b)2wt%MWCNT at SPS 1500°C.

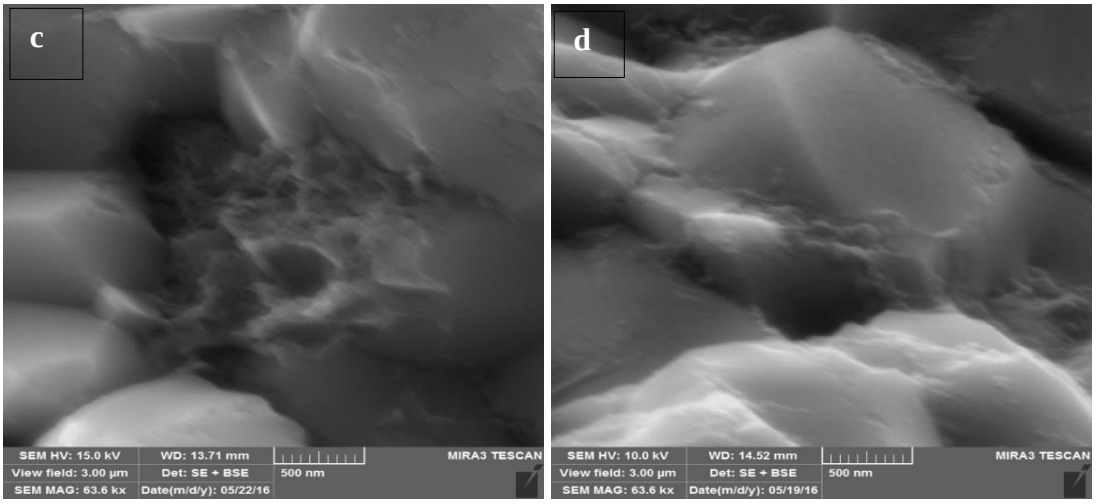

Figure 60 FE-SEM of Al2O3-MWCNT nanocomposites showing agglomeration (a) 1wt%MWCNT (b) 2wt%MWCNT at SPS 1500°C.

4.6.2 XRD Analysis of Nanocomposites

X-ray diffraction analysis was done on the nanocomposites to determine if there is any phase formed during sintering of the nanopowders. Figure 61 is the XRD of Alumina-5wt%SiC nanocomposites at SPS 1400°C and 1500°C. The peaks of α-alumina and β-SiC were identified and they are equally matching with the standard peaks as evaluated with the EVA software (not shown). There were no other peaks identified and that probably means that there were no other phases exist or not to measurable extent of the XRD instrument. Slight shift in the peaks position between the Al2O3-5wt%SiC at 1400 and 1500°C SPS temperature was observed which might due to the strain developed as a result of the elastic and coefficient thermal expansion mismatch between the SiC and alumina matrix. Figure 62 shows the XRD of Al2O3-10wt%SiC nanocomposites at 1400 and 1500°C respectively. The peaks of α-alumina and β-SiC were equally identified. There was no other peak observed which implies that the nanocomposites were thermally

stable even at 1500°C SPS temperature. Besides, there was no observable difference in the peak width between 1400 and 1500°C SPS temperature meaning that there was no significant grain growth of the nanocomposites as the SPS temperature increase from 1400°C to 1500°C.

The X-ray diffraction of alumina-CNT nanocomposites were equally studied. Figure 63 shows the XRD of alumina-1wt%MWCNT nanocomposites densified by SPS at 1300 and 1500°C. The peaks at 1300°C match with the peaks at 1500°C and there was no new phase formed to measurable extent of the XRD instrument. This clearly showed that there was no reaction between alumina and CNT as equally evident in the FE-SEM images. Also, CNT integrity was maintained even at high temperature of 1500°C. Thus, the electrical performance of the nanocomposites is attributed to the stability of the electro-conductive nanophase added to alumina sintered at high SPS temperature of 1300°C, 1400°C and 1500°C respectively.

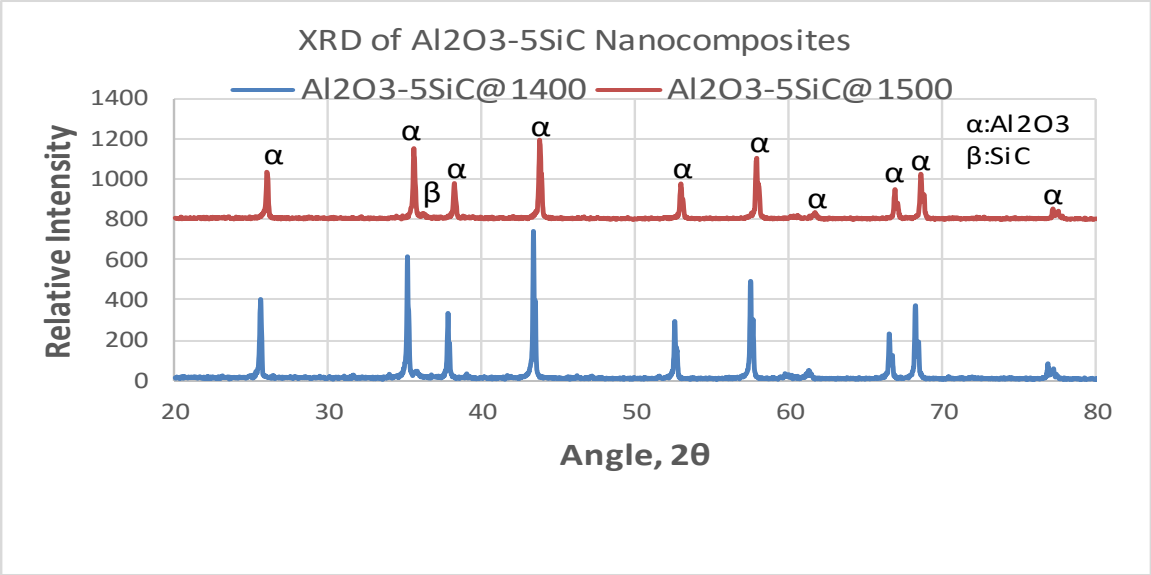

Figure 61 X-ray diffraction of Alumina-5wt%SiC nanocomposites sintered at 1400°C and 1500°C SPS temperature.

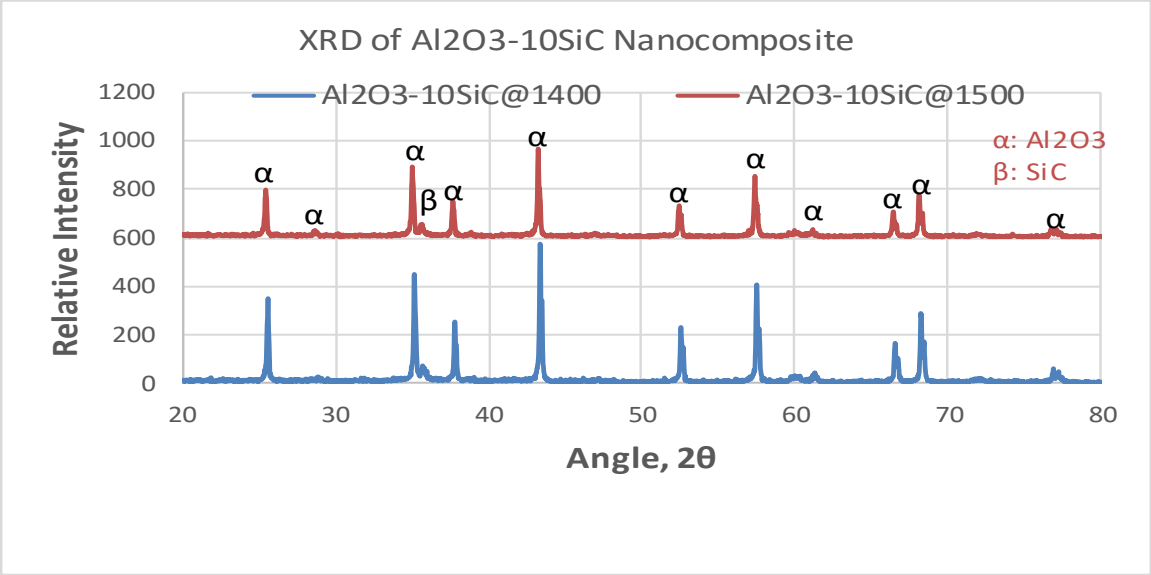

Figure 62 X-ray diffraction of Alumina-10wt%SiC nanocomposites sintered at 1400°C and 1500°C SPS temperature.

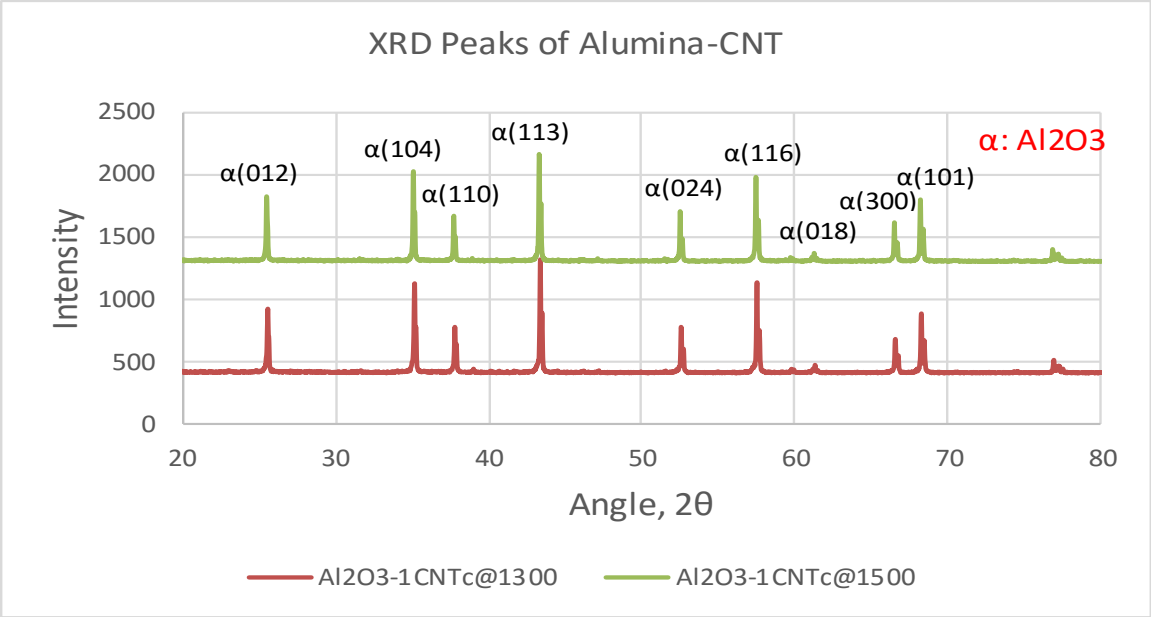

Figure 63 X-ray diffraction of Alumina-1wt%MWCNT nanocomposites sintered at 1300 and 1500°C.

CHAPTER 5

CONCLUSIONS AND RECOMMENDATIONS

5.1 Conclusions

Fabrication of Alumina-SiC and alumina-carbon nanotubes nanocomposites have been successfully developed by spark plasma consolidation of the nanopowders at various SPS conditions (1300°C, 1400°C, 1500°C, 50MPa, 100°C/min, and 10min holding time). Densification studies on the nanocomposites and the monolithic alumina were done using Archimedes' method. The relative density of pure alumina increase steadily with SPS temperature however, addition of SiC nanoparticles and functionalized MWCNT to alumina result in the reduction of the density and the degree of this reduction depends on the concentration of the nanophase. Thermal properties which include thermal diffusivity, specific heat capacity and thermal conductivity of the nanocomposites at all SPS temperature were all lower than the value of monolithic alumina. Maximum thermal conductivity (34.44W/mK) was achieved on monolithic alumina densified by SPS at 1400°C which reduced to about 42% and 17.2% on the addition of 5wt%SiC nanoparticles and 1wt%MWCNT respectively densified by SPS at 1500°C. This reduction in thermal properties of alumina with the inclusion of SiC nanoparticles and MWCNT was attributed to the microstructure refinement and agglomeration of CNT respectively. In addition, the influence of temperature on thermal properties was equally evaluated in the temperature range (25-250°C) and it was discovered that the thermal diffusivity and thermal conductivity decrease with the measuring temperature while the specific heat capacity increase with the increasing temperature.

The electrical conductivity studied on the nanocomposites showed significant enhancement in the electrical conductivity of alumina with the addition of secondary nanophase. The increasing electrical conductivity with addition of SiC and MWCNT was attributed to the additional interconnected network path created as the concentration of the nanophase increases. Besides concentration effect, the electrical conductivity also increases with SPS temperature although the influence of nanophase concentration is more significant than SPS temperature. Microstructural examination through FE-SEM images showed that the grains size of alumina was reduced with the addition of SiC and MWCNT nanophase. The small grain sizes were observed on the thermal etched images with large grain boundaries and this explained the reduction in the thermal properties of alumina with the addition of SiC and MWCNT. X-ray diffraction do not indicate extra peaks and this probably mean that the nanocomposites were stable even at high SPS temperature of 1500°C. However, the presence of SiC Were observed at 5wt% and 10wt% SiC concentration while CNT was no detected as the concentration is below the detection limit of XRD instrument.

5.2 Recommendations

The followings are the recommendations for the future work

1. Special drying techniques such as freeze drying should be adopted for drying of the slurry after wet dispersion. This prevents the re-agglomeration of the prepared powder during conventional drying that impairs the expected performance of the resulting nanocomposites.
2. The composition of MWCNT in the range of 0.6wt% to 0.8wt% should be tried as the percolation threshold exist within this range. This will prevent agglomeration of the MWCNT and thereby improve thermal properties of the resulting nanocomposites.
3. Other consolidation techniques such as HIP, CIP and HP should be used for the consolidation of the nanopowders and compare the results with the SPS results presented in this work.
4. Mechanical properties of the developed nanocomposites should be measured so as draw better conclusions on the performance application of the nanocomposites developed.

References

[1] O. Vasylkiv, Y. Sakka, V. V. Skorokhod, Low-Temperature Processing and Mechanical Properties of Zirconia and Zirconia–Alumina Nanoceramics, J. Am. Ceram. Soc. 86 (2003) 299–304. doi:10.1111/j.1151-2916.2003.tb00015.x.

[2] S.S. Samal, S. Bal, Carbon Nanotube Reinforced Ceramic Matrix Composites- A Review, J. Miner. Mater. Charact. Eng. 07 (2008) 355. http://www.scirp.org/journal/PaperInformation.aspx?PaperID=20571&#abstract.

[3] A. Aguilar-Elguézabal, M.H. Bocanegra-Bernal, Fracture behaviour of α-Al2O3 ceramics reinforced with a mixture of single-wall and multi-wall carbon nanotubes, Compos. Part B Eng. 60 (2014) 463–470. doi:10.1016/j.compositesb.2013.12.056.

[4] E. Zapata-Solvas, D. Gómez-García, a. Domínguez-Rodríguez, Towards physical properties tailoring of carbon nanotubes-reinforced ceramic matrix composites, J. Eur. Ceram. Soc. 32 (2012) 3001–3020. doi:10.1016/j.jeurceramsoc.2012.04.018.

[5] I. Ahmad, M. Fay, A. Kennedy, Y.Q. Zhu, Nanocomposites, Interfacial Investigations and Mechanical Properties of Carbon Nanotube Reinforcing Al2O3 Nanocomposites, J. Ceram. Soc. Japan. 99 (1992) 105-115.

[6] K. Niihara, New Design Concept of Structural Ceramics, J. Ceram. Soc. Japan. 99 (1991) 974–982. doi:10.2109/jcersj.99.974.

[7] P. Palmero, Structural Ceramic Nanocomposites: A Review of Properties and Powders' Synthesis Methods, Nanomaterials. 5 (2015) 656–696.

doi:10.3390/nano5020656.

[8] A. Rahimnejad Yazdi, H. Baharvandi, H. Abdizadeh, J. Purasad, A. Fathi, H. Ahmadi, Effect of sintering temperature and siliconcarbide fraction on density, mechanical properties and fracture mode of alumina-silicon carbide micro/nanocomposites, Mater. Des. 37 (2012) 251–255. doi:10.1016/j.matdes.2011.12.038.

[9] D. Jianxin, A. Xing, Wear behavior and mechanisms of alumina-based ceramic tools in machining of ferrous and non-ferrous alloys, Tribol. Int. 30 (1997) 807–813. doi:10.1016/S0301-679X(97)00062-5.

[10] P.F. Becher, G.C. Wei, Toughening Behavior in Sic-Whisker-Reinforced Alumina, J. Am. Ceram. Soc. 67 (1984) C–267–C–269. doi:10.1111/j.1151-2916.1984.tb19694.x.

[11] J. Sedláček, D. Galusek, P. Švančárek, R. Riedel, A. Atkinson, X. Wang, Abrasive wear of Al2O3-SiC and Al2O3-(SiC)-C composites with micrometer- and submicrometer-sized alumina matrix grains, J. Eur. Ceram. Soc. 28 (2008) 2983–2993. doi:10.1016/j.jeurceramsoc.2008.04.018.

[12] H. Reveron, O. Zaafrani, G. Fantozzi, Microstructure development, hardness, toughness and creep behaviour of pressureless sintered alumina/SiC micro-nanocomposites obtained by slip-casting, J. Eur. Ceram. Soc. 30 (2010) 1351–1357. doi:10.1016/j.jeurceramsoc.2009.12.008.

[13] S.T. Oh, K.I. Tajima, M. Ando, T. Ohji, Strengthening of porous alumina by pulse

electric current sintering and nanocomposite processing, J. Am. Ceram. Soc. 83 (2000) 1314–1316. http://www.scopus.com/inward/record.url?eid=2-s2.0-0033737713&partnerID=tZOtx3y1.

[14] Y.M. Ko, W.T. Kwon, Y.W. Kim, Development of Al2O3-SiC composite tool for machining application, Ceram. Int. 30 (2004) 2081–2086. doi:10.1016/j.ceramint.2003.11.011.

[15] A. Mukhopadhyay, R.I. Todd, Microstructure and mechanical properties of Al2O3 matrix nanocomposites produced by solid state precipitation, J. Eur. Ceram. Soc. 30 (2010) 1359–1372. doi:10.1016/j.jeurceramsoc.2009.12.007.

[16] J.H. Chae, K.H. Kim, Y.H. Choa, J.I. Matsushita, J.W. Yoon, K.B. Shim, Microstructural evolution of Al2O3-SiC nanocomposites during spark plasma sintering, J. Alloys Compd. 413 (2006) 259–264. doi:10.1016/j.jallcom.2005.05.049.

[17] M. Parchovianský, D. Galusek, P. Švančárek, J. Sedláček, P. Šajgalík, Thermal behavior, electrical conductivity and microstructure of hot pressed Al2O3/SiC nanocomposites, Ceram. Int. 40 (2014) 14421–14429. doi:10.1016/j.ceramint.2014.06.038.

[18] A. Borrell, I. Álvarez, R. Torrecillas, V.G. Rocha, A. Fernández, Microstructural design for mechanical and electrical properties of spark plasma sintered Al2O3–SiC nanocomposites, Mater. Sci. Eng. A. 534 (2012) 693–698. doi:10.1016/j.msea.2011.12.032.

[19] L. KUMARI, T. ZHANG, G. DU, W. LI, Q. WANG, A. DATYE, K. WU, Thermal properties of CNT-Alumina nanocomposites, Compos. Sci. Technol. 68 (2008) 2178–2183. doi:10.1016/j.compscitech.2008.04.001.

[20] J.F. Kahles, M. Field, D. Eylon, F.H. Froes, Machining of Titanium Alloys, Jom. 37 (1985) 27–35. doi:10.1007/BF03259441.

[21] M. Fitzsimmons, V.K. Sarin, Development of CVD WC-Co coatings, Surf. Coatings Technol. 137 (2001) 158–163. doi:10.1016/S0257-8972(00)01079-3.

[22] W. König, R. Komanduri, H.K. Tönshoff, G. Ackershott, Machining of Hard Materials, CIRP Ann. - Manuf. Technol. 33 (1984) 417–427. doi:10.1016/S0007-8506(16)30003-8.

[23] Z.A. Zoya, R. Krishnamurthy, Performance of CBN tools in the machining of titanium alloys, J. Mater. Process. Technol. 100 (2000) 80–86. doi:10.1016/S0924-0136(99)00464-1.

[24] S. Sun, M. Brandt, M.S. Dargusch, Characteristics of cutting forces and chip formation in machining of titanium alloys, Int. J. Mach. Tools Manuf. 49 (2009) 561–568. doi:10.1016/j.ijmachtools.2009.02.008.

[25] J. D H, Ceramic Cutting Tool Materials, Mater. Des. 7 (1986) 267–273.

[26] R.P. Feynman, Plenty of Room at the Bottom, Am. Phys. Soc. (1959).

[27] R.C. Cammarata, Nanomaterials : Synthesis , Properties and Applications Edited by A S Edelstein Institute of Physics Publishing Bristol and Philadelphia, Mater.

Sci. (1996).

[28] G. Cao, Nanostructures and Nanomaterials - Synthesis, Properties and Applications, 2004. doi:10.1142/9781860945960.

[29] N. Saheb, Z. Iqbal, A. Khalil, A.S. Hakeem, N. Al Aqeeli, T. Laoui, A. Al-Qutub, R. Kirchner, Spark plasma sintering of metals and metal matrix nanocomposites: a review, J. Nanomater. 2012 (2012) 1–13. doi:10.1155/2012/983470.

[30] C. Suryanarayana, Mechanical alloying and milling, Prog. Mater. Sci. 46 (2001) 1–184. doi:10.1016/S0079-6425(99)00010-9.

[31] C. Suryanarayana, N. Al-Aqeeli, Mechanically alloyed nanocomposites, Prog. Mater. Sci. 58 (2013) 383–502. doi:10.1016/j.pmatsci.2012.10.001.

[32] P.C. Ma, S.Q. Wang, J.-K. Kim, B.Z. Tang, <I>In-Situ</I> Amino Functionalization of Carbon Nanotubes Using Ball Milling, J. Nanosci. Nanotechnol. 9 (2009) 749–753. doi:10.1166/jnn.2009.C017.

[33] P.-C. Ma, N.A. Siddiqui, G. Marom, J.-K. Kim, Dispersion and functionalization of carbon nanotubes for polymer-based nanocomposites: A review, Compos. Part A Appl. Sci. Manuf. 41 (2010) 1345–1367. doi:10.1016/j.compositesa.2010.07.003.

[34] C. Park, Z. Ounaies, K.A. Watson, R.E. Crooks, J. Smith, S.E. Lowther, J.W. Connell, E.J. Siochi, J.S. Harrison, T.L. St Clair, Dispersion of single wall carbon nanotubes by in situ polymerization under sonication, Chem. Phys. Lett. 364 (2002) 303–308. doi:10.1016/S0009-2614(02)01326-X.

[35] P.G. Sanders, J. a. Eastman, J.R. Weertman, Elastic and tensile behavior of nanocrystalline copper and palladium, Acta Mater. 45 (1997) 4019–4025. doi:10.1016/S1359-6454(97)00092-X.

[36] T.R. Malow, C.C. Koch, Mechanical properties in tension of mechanically attrited nanocrystalline iron by the use of the miniaturized disk bend test, Acta Mater. 46 (1998) 6459–6473. doi:10.1016/S1359-6454(98)00294-8.

[37] K. Abdullahi, N. Al-Aqeeli, Mechanical Alloying and Spark Plasma Sintering of Nano-SiC Reinforced Al–12Si–0.3Mg Alloy, Arab. J. Sci. Eng. 39 (2014) 3161–3168. doi:10.1007/s13369-013-0780-1.

[38] D. Tiwari, B. Basu, K. Biswas, Simulation of thermal and electric field evolution during spark plasma sintering, Ceram. Int. 35 (2009) 699–708. doi:10.1016/j.ceramint.2008.02.013.

[39] D. Hardy, D.J. Green, Mechanical properties of a partially sintered alumina, J. Eur. Ceram. Soc. 15 (1995) 769–775. doi:10.1016/0955-2219(95)00045-V.

[40] K.-Y. Lee, L.C.G. Cropsey, B.R. Tyszka, E.D. Case, Grain size, density, and mechanical properties of alumina batch-processed in a single-mode microwave cavity, Mater. Res. Bull. 32 (1997) 287–295. doi:10.1016/S0025-5408(96)00196-1.

[41] O.L. Ighodaro, O.I. Okoli, Fracture toughness enhancement for alumina systems: A review, Int. J. Appl. Ceram. Technol. 5 (2008) 313–323. doi:10.1111/j.1744-7402.2008.02224.x.

[42] T. Ohji, A. Nakahira, T. Hirano, K. Niihara, Tensile creep behavior of alumind-silicon carbide nanocomposite, J. Eur. Ceram. Soc. 77 (1994) 3259–62.

[43] T. Ohji, Y.-K. Jeong, Y.-H. Choa, K. Niihara, Strengthening and Toughening Mechanisms of Ceramic Nanocomposites, J. Am. Ceram. Soc. 60 (1998) 1453–1460. doi:10.1111/j.1151-2916.1998.tb02503.x.

[44] J.L. Shi, High-temperature structural ceramics: Recent progress in China, Adv. Mater. 11 (1999) 1103–1109. doi:10.1002/(SICI)1521-4095(199909)11:13<1103::AID-ADMA1103>3.0.CO;2-C.

[45] R. Barea, M. Belmonte, M.I. Osendi, P. Miranzo, Thermal conductivity of Al2O3/SiC platelet composites, J. Eur. Ceram. Soc. 23 (2003) 1773–1778. doi:10.1016/S0955-2219(02)00449-1.

[46] X. Sun, W. Bao, Y. Lv, J. Deng, X. Wang, Synthesis of high quality single-walled carbon nanotubes by arc discharge method in large scale, Mater. Lett. 61 (2007) 3956–3958. doi:10.1016/j.matlet.2006.12.070.

[47] M.H. Rummeli, C. Kramberger, M. Loffler, O. Jost, M. Bystrzejewski, A. Gruneis, T. Gemming, W. Pompe, B. Buchner, T. Pichler, Catalyst volume to surface area constraints for nucleating carbon nanotubes, J. Phys. Chem. B. 111 (2007) 8234–8241. doi:10.1021/jp072556f.

[48] P. Ayala, A. Grüneis, D. Grimm, C. Kramberger, R. Engelhard, M. Rümmeli, J. Schumann, R. Kaltofen, B. Büchner, C. Schaman, H. Kuzmany, T. Gemming, A. Barreiro, T. Pichler, Cyclohexane triggers staged growth of pure and vertically

aligned single wall carbon nanotubes, Chem. Phys. Lett. 454 (2008) 332–336. doi:10.1016/j.cplett.2008.02.041.

[49] L. Meng, C. Fu, Q. Lu, Advanced technology for functionalization of carbon nanotubes, Prog. Nat. Sci. 19 (2009) 801–810. doi:10.1016/j.pnsc.2008.08.011.

[50] N. Rubio, C. Fabbro, M.A. Herrero, la H.A. de, M. Meneghetti, J.L.G. Fierro, M. Prato, E. Vazquez, Ball-milling modification of single-walled carbon nanotubes: purification, cutting, and functionalization, Small. 7 (2011) 665–674. doi:10.1002/smll.201001917.

[51] T. Saito, K. Matsushige, K. Tanaka, Chemical treatment and modification of multi-walled carbon nanotubes, Phys. B Condens. Matter. 323 (2002) 280–283. doi:10.1016/S0921-4526(02)00999-7.

[52] S. Gustafsson, L.K.L. Falk, E. Lidén, E. Carlström, Pressureless sintered Al2O3-SiC nanocomposites, Ceram. Int. 34 (2008) 1609–1615. doi:10.1016/j.ceramint.2007.05.005.

[53] M. Mansoor, M. Shahid, A. Habib, Strengthening of Bisphenol-A Epoxy Resin by the Addition of Multi-Wall Carbon Nanotubes, Arab. J. Sci. Eng. 39 (2014) 6411–6420. doi:10.1007/s13369-014-1290-5.

[54] P.-C. Ma, N.A. Siddiqui, G. Marom, J.-K. Kim, Dispersion and functionalization of carbon nanotubes for polymer-based nanocomposites: A review, Compos. Part A Appl. Sci. Manuf. 41 (2010) 1345–1367. doi:10.1016/j.compositesa.2010.07.003.

[55] L. Gao, H.. Wang, J.. Hong, H. Miyamoto, K. Miyamoto, Y. Nishikawa, S.D.D.. Torre, Mechanical Properties and Microstructure of Nano-SiC–Al2O3 Composites Densified by Spark Plasma Sintering, J. Eur. Ceram. Soc. 19 (1999) 609–613. doi:10.1016/S0955-2219(98)00232-5.

[56] H.Z. Wang, L. Gao, J.K. Guo, Effect of nanoscale SiC particles on the microstructure of Al2O3 ceramics, Ceram. Int. 26 (2000) 391–396. doi:10.1016/S0272-8842(99)00069-3.

[57] H. Qu, S. Zhu, Q. Li, C. Ouyang, Microstructure and mechanical properties of hot-pressing sintered WC – x vol .% Al 2 O 3 composites, Mater. Sci. Eng. A. 543 (2012) 96–103. doi:10.1016/j.msea.2012.02.053.

[58] M. Sternitzke, B. Derby, R.J. Brook, Alumina / Silicon Carbide Nanocomposites by Hybrid Polymer / Powder Processing : Microstructures and Mechanical Properties, Scanning. 48 (1998) 41–48.

[59] S. Maensiri, S.G. Roberts, Thermal Shock Resistance of Sintered Alumina/Silicon Carbide Nanocomposites Evaluated by Indentation Techniques, J. Am. Ceram. Soc. 85 (2002) 1971–1978. doi:10.1111/j.1151-2916.2002.tb00390.x.

[60] H. Kara, S.G. Roberts, Polishing behavior and surface quality of alumina and alumina/silicon carbide nanocomposites, J. Am. Ceram. Soc. 83 (2000) 1219–1225.

[61] K. Takahashi, M. Yokouchi, S. Lee, K. Ando, Crack-Healing Behavior of Al 2 O 3 Toughened by SiC Whiskers, Ceramics. 47 (2003) 2143–2147.

doi:10.1111/j.1151-2916.2003.tb03622.x.

[62] V.M. Sglavo, F. De Genua, A. Molinari, F. Casari, Alumina/silicon carbide laminated composites by spark plasma sintering, J. Am. Ceram. Soc. 92 (2009) 2693–2697. doi:10.1111/j.1551-2916.2009.03247.x.

[63] M.D. Unlu, G. Goller, O. Yucel, F.C. Sahin, The Spark Plasma Sintering of Silicon Carbide Ceramics Using Alumina, Acta Phys. Pol. A. 125 (2014) 257–259. doi:10.12693/APhysPolA.125.257.

[64] A. NAKAHIRA, Sintering Behaviors and Consolidation for Al2O3/SiC Nanocomposites, J. Ceram. Soc. Japan. 100 (1992) 448–453.

[65] J. Liu, Z. Li, H. Yan, K. Jiang, Spark plasma sintering of alumina composites with graphene platelets and silicon carbide nanoparticles, Adv. Eng. Mater. (2014) 1–8. doi:10.1002/adem.201300536.

[66] C. Society, Sintering and Mechanical Properties of SiC-Whisker / Al2O3 Composites with Two-Layered Structure Hidemi WATANABE and Osamu KIMURA * of Mechanical Engineering , Ashikaga of Technology , of Materials Science and Ceramic Technology of Technology , Kanagawa *f*, 592 (1992).

[67] D. Sciti, J. Vicens, a. Bellosi, Microstructure and properties of alumina-SiC nanocomposites prepared from ultrafine powders, J. Mater. Sci. 37 (2002) 3747–3758. doi:10.1023/A:1016577728915.

[68] T. Zhang, L. Kumari, G.H. Du, W.Z. Li, Q.W. Wang, K. Balani, a. Agarwal, Mechanical properties of carbon nanotube-alumina nanocomposites synthesized by

chemical vapor deposition and spark plasma sintering, Compos. Part A Appl. Sci. Manuf. 40 (2009) 86–93. doi:10.1016/j.compositesa.2008.10.003.

[69] F. Inam, H. Yan, T. Peijs, M.J. Reece, The sintering and grain growth behaviour of ceramic-carbon nanotube nanocomposites, Compos. Sci. Technol. 70 (2010) 947–952. doi:10.1016/j.compscitech.2010.02.010.

[70] F. Inam, H. Yan, D.D. Jayaseelan, T. Peijs, M.J. Reece, Electrically conductive alumina-carbon nanocomposites prepared by Spark Plasma Sintering, J. Eur. Ceram. Soc. 30 (2010) 153–157. doi:10.1016/j.jeurceramsoc.2009.05.045.

[71] Guo-Dong Zhan and Amiya K. Mukherjee, Carbon nanotube reinforced alumina-based ceramics with novel mechanical, electrical, and thermal properties, Int. J. Appl. Ceram. Technol. 1 (2004) 161–171. doi:10.1111/j.1744-7402.2004.tb00166.x.

[72] F. De Genua, V.M. Sglavo, High Strength Engineered Alumina-Silicon Carbide Laminated Composites by Spark Plasma Sintering, Procedia Eng. 10 (2011) 2621–2626. doi:10.1016/j.proeng.2011.04.437.

[73] O.T. Johnson, P. Rokebrand, I. Sigalas, Microstructure and Properties of Al2O3-SiC Nanomaterials, Proceedings of the World Congress on Engineering 2014 Vol II WCE 2014, July 2-4, 2014, London, U.K.

[74] J. Zhao, L.C. Steams, I. Martin, H.M. Chan, G.A. Miller, R.E. Cook, Mechanical Behavior of Alumina-Silicon Carbide “Nanocomposites,” (n.d.).

[75] J. Rodriguez, A. Martın, J.Y. Pastor, J. Llorca, J.F. Bartolome, S. Moya, Sliding

Wear of Alumina / Silicon Carbide Nanocomposites, J. Am. Ceram. Soc. 82 (1999) 2252–2254.

[76] M. Belmonte, M.I. Nieto, M.I. Osendi, P. Miranzo, Influence of the SiC grain size on the wear behaviour of Al2O3/SiC composites, J. Eur. Ceram. Soc. 26 (2006) 1273–1279. doi:10.1016/j.jeurceramsoc.2005.01.049.

[77] X. Sun, J.G. Li, S. Guo, Z. Xiu, K. Duan, X.Z. Hu, Intragranular particle residual stress strengthening of Al 2O3-SiC nanocomposites, J. Am. Ceram. Soc. 88 (2005) 1536–1543. doi:10.1111/j.1551-2916.2005.00309.x.

[78] Y. Sakka, T.S. Suzuki, T. Uchikoshi, Fabrication and some properties of textured alumina-related compounds by colloidal processing in high-magnetic field and sintering, J. Eur. Ceram. Soc. 28 (2008) 935–942. doi:10.1016/j.jeurceramsoc.2007.09.039.

[79] M.I. NIETO, P. MIRANZO, S. DE AZA, J.S. MOYA, Effect of atmosphere on microstructural evolution of pressureless sintered Al2O3/SiC composites, Nippon Seramikkusu Kyokai Gakujutsu Ronbunshi. 100 (n.d.) 459–462. http://cat.inist.fr/?aModele=afficheN&cpsidt=5495290 (accessed January 26, 2016).

[80] W.E. Lee, Ceramic processing and sintering, Int. Mater. Rev. 41 (1996) 36–37. doi:10.1179/095066096790151286.

[81] S. Rul, F. Lefèvre-Schlick, E. Capria, C. Laurent, A. Peigney, Percolation of single-walled carbon nanotubes in ceramic matrix nanocomposites, Acta Mater. 52

(2004) 1061–1067. doi:10.1016/j.actamat.2003.10.038.

[82] J. Sun, L. Gao, X. Jin, Reinforcement of alumina matrix with multi-walled carbon nanotubes, Ceram. Int. 31 (2005) 893–896. doi:10.1016/j.ceramint.2004.10.002.

[83] T. Wei, Z. Fan, G. Luo, F. Wei, D. Zhao, J. Fan, The effect of carbon nanotubes microstructures on reinforcing properties of SWNTs/alumina composite, Mater. Res. Bull. 43 (2008) 2806–2809. doi:10.1016/j.materresbull.2007.10.026.

[84] Z. Xia, W. a. Curtin, B.W. Sheldon, Fracture Toughness of Highly Ordered Carbon Nanotube/Alumina Nanocomposites, J. Eng. Mater. Technol. 126 (2004) 238. doi:10.1115/1.1751179.

[85] L. Kumari, T. Zhang, G.H. Du, W.Z. Li, Q.W. Wang, a. Datye, K.H. Wu, Synthesis, microstructure and electrical conductivity of carbon nanotube-alumina nanocomposites, Ceram. Int. 35 (2009) 1775–1781. doi:10.1016/j.ceramint.2008.10.005.

[86] O. Lourie, H.D. Wagner, Evidence of stress transfer and formation of fracture clusters in carbon nanotube-based composites, Compos. Sci. Technol. 59 (1999) 975–977. doi:10.1016/S0266-3538(98)00148-1.

[87] S. Sarkar, P.K. Das, Effect of sintering temperature and nanotube concentration on microstructure and properties of carbon nanotube/alumina nanocomposites, Ceram. Int. 40 (2014) 7449–7458. doi:10.1016/j.ceramint.2013.12.092.

[88] J. Silvestre, N. Silvestre, J. De Brito, An Overview on the Improvement of Mechanical Properties of Ceramics Nanocomposites, 2015 (2015).

[89] K.E. Thomson, D. Jiang, W. Yao, R.O. Ritchie, A.K. Mukherjee, Characterization and mechanical testing of alumina-based nanocomposites reinforced with niobium and/or carbon nanotubes fabricated by spark plasma sintering, Acta Mater. 60 (2012) 622–632. doi:10.1016/j.actamat.2011.10.002.

[90] L.C. Stearns, J. Zhao, M.P. Harmer, Processing and Microstructure Development in Al2O3-SiC Nanocomposites, Journal of the European Ceramic Society10 (1992) 473–477.

[91] Y. Jeong, A. Nakahira, K. Niihara, Effects of Additives on Microstructure and Properties of Alumina-SiC Carbide Nanocomposites, J. Am. Ceram. Soc., 82 [12] (1999) 3609–3612.

[92] J. Sedláček, D. Galusek, R. Riedel, M.J. Hoffmann, Sinter-HIP of polymer-derived Al2O3-SiC composites with high SiC contents, Mater. Lett. 65 (2011) 2462–2465. doi:10.1016/j.matlet.2011.04.094.

[93] I. Ahmad, M. Unwin, H. Cao, H. Chen, H. Zhao, a. Kennedy, Y.Q. Zhu, Multi-walled carbon nanotubes reinforced Al2O3 nanocomposites: Mechanical properties and interfacial investigations, Compos. Sci. Technol. 70 (2010) 1199–1206. doi:10.1016/j.compscitech.2010.03.007.

[94] L. Gao, L. Jiang, J. Sun, Carbon nanotube-ceramic composites, J. Electroceramics. 17 (2006) 51–55. doi:10.1007/s10832-006-9935-8.

[95] S.C. Zhang, W.G. Fahrenholtz, G.E. Hilmas, E.J. Yadlowsky, Pressureless sintering of carbon nanotube-Al2O3 composites, J. Eur. Ceram. Soc. 30 (2010)

1373–1380. doi:10.1016/j.jeurceramsoc.2009.12.005.

[96] A. Grain, P.P. Definitions, Introduction to Grain and Particle Effects on Ceramic and Ceramic Composite Properties I . GRAIN AND PARTICLE PARAMETER DEFINITIONS AND TREATMENT OUTLINE, (n.d.) 1–42.

[97] M. Parchovianský, D. Galusek, M. Michálek, P. Švančárek, M. Kašiarová, J. Dusza, M. Hnatko, Effect of the volume fraction of SiC on the microstructure and creep behavior of hot pressed Al2O3/SiC composites, Ceram. Int. 40 (2014) 1807–1814. doi:10.1016/j.ceramint.2013.07.081.

[98] J.-W. An, D.-H. You, D.-S. Lim, Tribological properties of hot-pressed alumina–CNT composites, Wear. 255 (2003) 677–681. doi:10.1016/S0043-1648(03)00216-3.

[99] G. Yamamoto, M. Omori, T. Hashida, H. Kimura, A novel structure for carbon nanotube reinforced alumina composites with improved mechanical properties., Nanotechnology. 19 (2008) 315708. doi:10.1088/0957-4484/19/31/315708.

[100] S. Sarkar, P. Das, Processing and properties of carbon nanotube/alumina nanocomposites: a review, Rev. Adv. Mater. Sci. 37 (2014) 53–82. http://mp.ipme.ru/e-journals/RAMS/no_13714/08_13714_das.pdf.

[101] S.I. Cha, K.T. Kim, K.H. Lee, C.B. Mo, S.H. Hong, Strengthening and toughening of carbon nanotube reinforced alumina nanocomposite fabricated by molecular level mixing process, Scr. Mater. 53 (2005) 793–797. doi:10.1016/j.scriptamat.2005.06.011.

[102] D.S. Lim, D.H. You, H.J. Choi, S.H. Lim, H. Jang, Effect of CNT distribution on tribological behavior of alumina-CNT composites, Wear. 259 (2005) 539–544. doi:10.1016/j.wear.2005.02.031.

[103] M. Mazaheri, D. Mari, Z.R. Hesabi, R. Schaller, G. Fantozzi, Multi-walled carbon nanotube/nanostructured zirconia composites: Outstanding mechanical properties in a wide range of temperature, Compos. Sci. Technol. 71 (2011) 939–945. doi:10.1016/j.compscitech.2011.01.017.

[104] I. Ahmad, H. Cao, H. Chen, H. Zhao, A. Kennedy, Y.Q. Zhu, Carbon nanotube toughened aluminium oxide nanocomposite, J. Eur. Ceram. Soc. 30 (2010) 865–873. doi:10.1016/j.jeurceramsoc.2009.09.032.

[105] L. Fabbri, E. Scafè, G. Dinelli, Thermal and elastic properties of alumina-silicon carbide whisker composites, J. Eur. Ceram. Soc. 14 (1994) 441–446. doi:10.1016/0955-2219(94)90082-5.

[106] S. Krukowski, A. Witek, J. Adamczyk, J. Jun, M. Bockowski, I. Grzegory, B. Lucznik, G. Nowak, M. Wróblewski, A. Presz, S. Gierlotka, S. Stelmach, B. Palosz, S. Porowski, P. Zinn, Thermal properties of indium nitride, J. Phys. Chem. Solids. 59 (1998) 289–295. doi:10.1016/S0022-3697(97)00222-9.

[107] N. Castle, Thermal Conductivity and Thermal Diffusivity, (n.d.).

[108] W.D. Callister, Fundamentals of Materials Science and Engineering: An Interactive E.Text, 2001. http://books.google.com/books?id=0TfIngEACAAJ&pgis=1.

[109] S.U.S. Choi, The role of interfacial layers in the enhanced thermal conductivity of nanofluids: A renovated Maxwell model, J. Nanoparticle Res. 5 (2003) 167–171.

[110] A.S. Composites, M.I.K. Collin, D.J. Rowcliffe, Influence of Thermal Conductivity and Fracture Toughness on the Thermal Shock Resistance of, 40 (2001) 1334–1340.

[111] P.H. Mccluskey, R.K. Williams, R.S. Graves, T.N. Tiegs, Thermal Diffusivity/Conductivity of Alumina-Silicon Carbide Composites, 64 (1990) 461–464.

[112] A.L. Geiger, D.P.H. Hasselman, K.Y. Donaldson, Effect of reinforcement particle size on the thermal conductivity of a particulate silicon carbide-reinforced aluminium-matrix composite, J. Mater. Sci. Lett. 12 (1993) 420–423. doi:10.1007/BF00609172.

[113] C. Kawai, Effect of Interfacial Reaction on the Thermal Conductivity of Al–SiC Composites with SiC Dispersions, J. Am. Ceram. Soc. 84 (2001) 896–898. doi:10.1111/j.1151-2916.2001.tb00764.x.

[114] C.-W. Nan, T. Physik, U. Saarlandes, D.- Saarbrucken, Inverse problem for composites with imperfect interface : determination of interfacial thermal resistance, thermal conductivity of constituents, and microstructural parameters, Am. Ceram. Soc. 54 (2000) 848–854. doi:10.1111/j.1151-2916.2000.tb01284.x.

[115] R. Sivakumar, S. Guo, T. Nishimura, Y. Kagawa, Thermal conductivity in multi-wall carbon nanotube/silica-based nanocomposites, Scr. Mater. 56 (2007) 265–

268. doi:10.1016/j.scriptamat.2006.10.025.

[116] T. Wei, Z. Fan, G. Luo, F. Wei, A new structure for multi-walled carbon nanotubes reinforced alumina nanocomposite with high strength and toughness, Mater. Lett. 62 (2008) 641–644. doi:10.1016/j.matlet.2007.06.025.

[117] J.J. Sparkes, Conduction in Semiconductors, (1966) 1–34. doi:10.1016/B978-0-08-011531-3.50005-7.

[118] F. Lux, Models proposed to explain the electrical conductivity of mixtures made of conductive and insulating materials, J. Mater. Sci. 28 (1993) 285–301. doi:10.1007/BF00357799.

[119] D.S. McLachlan, G. Sauti, The AC and DC conductivity of nanocomposites, J. Nanomater. 2007 (2007). doi:10.1155/2007/30389.

[120] K. Ahmad, W. Pan, Dramatic effect of multiwalled carbon nanotubes on the electrical properties of alumina based ceramic nanocomposites, Compos. Sci. Technol. 69 (2009) 1016–1021. doi:10.1016/j.compscitech.2009.01.015.

[121] K. Lee, C. Bin Mo, S. Bin Park, S.H. Hong, Mechanical and electrical properties of multiwalled CNT-alumina nanocomposites prepared by a sequential two-step processing of ultrasonic spray pyrolysis and spark plasma sintering, J. Am. Ceram. Soc. 94 (2011) 3774–3779. doi:10.1111/j.1551-2916.2011.04689.x.

[122] M.B. Heaney, Electrical Conductivity and Resistivity, Electr. Meas. Signal Process. Displays. (2004) 7–1–7–14. doi:10.1201/9780203009406.ch7.

[123] K.Y. Lim, T.Y. Cho, Y.W. Kim, S.J. Lee, Effect of Initial Alpha-SiC Content on Thermal Conductivity of Silicon Carbide Ceramics, Key Eng. Mater. 616 (2014) 23–26. doi:10.4028/www.scientific.net/KEM.616.23.

[124] D.P.H. Hasselman, L.F. Johnson, Effective Thermal Conductivity of Composites with Interfacial Thermal Barrier Resistance, J. Compos. Mater. 21 (1987) 508–515. doi:10.1177/002199838702100602.

[125] D.P.H. Hasselman, Comment on "Inverse Problem for Composites with Imperfect Interface: Determination of Interfacial Thermal Resistance, Thermal Conductivity of Constituents, and Microstructural Parameters," J. Am. Ceram. Soc. 85 (2002) 1643–1645. doi:10.1111/j.1151-2916.2002.tb00331.x.

[126] R. Kochetov, A. V. Korobko, T. Andritsch, P.H.F. Morshuis, S.J. Picken, J.J. Smit, Three-phase lewis-nielsen model for the thermal conductivity of polymer nanocomposites, Annu. Rep. - Conf. Electr. Insul. Dielectr. Phenomena, CEIDP. (2011) 338–341. doi:10.1109/CEIDP.2011.6232665.

[127] D.J. Yang, Q. Zhang, G. Chen, S.F. Yoon, J. Ahn, S.G. Wang, Q. Zhou, Q. Wang, J.Q. Li, Thermal conductivity of multiwalled carbon nanotubes, Phys. Rev. B. 66 (2002) 165440. doi:doi: 10.1103/physrevb.66.165440.

[128] P. Kim, L. Shi, a Majumdar, P.L. McEuen, Thermal transport measurements of individual multiwalled nanotubes., Phys. Rev. Lett. 87 (2001) 215502. doi:10.1103/PhysRevLett.87.215502.

[129] M. Zulkarnain, A.B. Muhamad Husaini, M. Mariatti, I.A. Azid, Particle Dispersion

Model for Predicting the Percolation Threshold of Nano-Silver Composite, Arab. J. Sci. Eng. (2015). doi:10.1007/s13369-015-1989-y.

[130] K.H. Ho, S.T. Newman, State of the art electrical discharge machining (EDM), Int. J. Mach. Tools Manuf. 43 (2003) 1287–1300. doi:10.1016/S0890-6955(03)00162-7.

Vitae

Name	IBRAHIM MOMOHJIMOH
Nationality	NIGERIAN
Date of Birth	5/3/1984
Email	momohjimoh_ibrahim@yahoo.com
Address	No 20, Adava Layout OTC, Check Point Okene Kogi State
Academic Background	BSc. Metallurgical and Materials Engineering (2011)
	University of Lagos, Akoka, Lagos Nigeria.

Research Publications

1. Muideen Adebayo Bodude, **Ibrahim Momohjimoh,** Ruth Nkiruka Nnaji, "Mechanical and microstructural evaluation of plastically deformed brass" Materials Sciences and Applications, 2015, 6, 1137-1144.
2. M.A. Bodude, **I.Momohjimoh** "Effects of welding parameters on the mechanical properties of welded low-carbon steel" Journal of Minerals and Materials Characterization and Engineering, 2015, 3, 142-153.
3. Bodude, M.A., Obidiegwu, E.O., Onovo, H.O., **Momohjimoh, I**. "Experimental studies on the use of sacrificial anode in oil and gas pipeline corrosion protection" Int. J. of Mechanical Computational and Manufacturing Research, Vol.1. No.3, (2012) 87 – 96, ISSN: 2301-4148.

4. Bodude, M.A., Oloyede, O.R., Esezobor, D.E., **Momohjimoh, I.** "Corrosion behavior in sea and waste water" European International Journal of Science and Technology ISSN: 2304-9693.
5. Mohammed Awwalu Usman, **Ibrahim Momohjimoh,** Abdullahi S.B. Gimba. "Effect of groundnut shell powder on the mechanical properties of recycled polyethylene and its biodegradability" Journal of Minerals and Materials Characterization and Engineering, 2016, 4, 228-240.